Vol. 23, no. 1, 2023 eISSN 2687-1653
PEER-REVIEWED SCIENTIFIC AND PRACTICAL JOURNAL

# Advanced Engineering Research (Rostov-on-Don)

Mechanics

Machine Buiding and Machine Science

Information Technology, Computer Science and Management

www.vestnik-donstu.ru
DOI 10.23947/2687-1653

# Advanced Engineering Research (Rostov-on-Don)

**Peer-reviewed scientific and practical journal (published since 2000)**

**eISSN 2687-1653**
**DOI: 10.23947/2687-1653**

## Vol. 23, no. 1, 2023

The journal is aimed at informing the readership about the latest achievements and prospects in the field of mechanics, mechanical engineering, computer science and computer technology. The publication is a forum for cooperation between Russian and foreign scientists, it contributes to the convergence of the Russian and world scientific and information space.

**The journal publishes articles in the following fields of science:**

– Theoretical Mechanics, Dynamics of Machines (Engineering Sciences)
– Deformable Solid Mechanics (Engineering, Physical and Mathematical Sciences)
– Mechanics of Liquid, Gas and Plasma (Engineering Sciences)
– Mathematical Simulation, Numerical Methods and Program Systems (Engineering Sciences)
– System Analysis, Information Management and Processing, Statistics (Engineering Sciences)
– Automation and Control of Technological Processes and Productions (Engineering Sciences)
– Software and Mathematical Support of Machines, Complexes and Computer Networks (Engineering Sciences)
– Computer Modeling and Design Automation (Engineering, Physical and Mathematical Sciences)
– Computer Science and Information Processes (Engineering Sciences)
– Machine Science (Engineering Sciences)
– Machine Friction and Wear (Engineering Sciences)
– Technology and Equipment of Mechanical and Physicotechnical Processing (Engineering Sciences)
– Engineering Technology (Engineering Sciences)
– Welding, Allied Processes and Technologies (Engineering Sciences)
– Methods and Devices for Monitoring and Diagnostics of Materials, Products, Substances and the Natural Environment (Engineering Sciences)
– Hydraulic Machines, Vacuum, Compressor Equipment, Hydraulic and Pneumatic Systems (Engineering Sciences)

| | |
|---|---|
| *Indexing:* | RSCI, CyberLeninka, EBSCO, Dimensions, DOAJ |
| *Name of the body that registered the publication* | Mass media registration certificate ЭЛ № ФС 77 – 78854 dated August 07, 2020, issued by the Federal Service for Supervision of Communications, Information Technology and Mass Media. |
| *Founder and publisher* | Federal State Budgetary Educational Institution of Higher Education Don State Technical University (DSTU). |
| *Periodicity* | Quarterly (4 issues per year) |
| *Address of the founder and publisher* | Gagarin Sq. 1, Rostov-on-Don, 344003, Russian Federation. |
| *E-mail* | vestnik@donstu.ru |
| *Telephone* | +7 (863) 2–738–372 |
| *Website* | http://vestnik-donstu.ru/ |
| *Date of publication* | 31.03.2023 |

# Advanced Engineering Research (Rostov-on-Don)

**Рецензируемый научно-практический журнал (издается с 2000 года)**

**eISSN 2687-1653**
**DOI: 10.23947/2687-1653**

## Том 23, № 1, 2023

Создан в целях информирования читательской аудитории о новейших достижениях и перспективах в области механики, машиностроения, информатики и вычислительной техники. Издание является форумом для сотрудничества российских и иностранных ученых, способствует сближению российского и мирового научно-информационного пространства.

**Журнал включен в перечень рецензируемых научных изданий, в котором должны быть опубликованы основные научные результаты диссертаций на соискание ученой степени кандидата наук, на соискание ученой степени доктора наук (Перечень ВАК) по следующим научным специальностям:**

1.1.7 – Теоретическая механика, динамика машин (технические науки)
1.1.8 – Механика деформируемого твердого тела (технические, физико-математические науки)
1.1.9 – Механика жидкости, газа и плазмы (технические науки)
1.2.2 – Математическое моделирование, численные методы и комплексы программ (технические науки)
2.3.1 – Системный анализ, управление и обработка информации, статистика (технические науки)
2.3.3 – Автоматизация и управление технологическими процессами и производствами (технические науки)
2.3.5 – Математическое и программное обеспечение вычислительных систем, комплексов и компьютерных сетей (технические науки)
2.3.7 – Компьютерное моделирование и автоматизация проектирования (технические, физико-математические науки)
2.3.8 – Информатика и информационные процессы (технические науки)
2.5.2 – Машиноведение (технические науки)
2.5.3 – Трение и износ в машинах (технические науки)
2.5.5 – Технология и оборудование механической и физико-технической обработки (технические науки)
2.5.6 – Технология машиностроения (технические науки)
2.5.8 – Сварка, родственные процессы и технологии (технические науки)
2.5.9 – Методы и приборы контроля и диагностики материалов, изделий, веществ и природной среды (технические науки)
2.5.10 – Гидравлические машины, вакуумная, компрессорная техника, гидро- и пневмосистемы (технические науки)

| | |
|---|---|
| *Индексация:* | РИНЦ, CyberLeninka, CrossRef, Dimensions, DOAJ, EBSCO |
| *Наименование органа, зарегистрировавшего издание* | Свидетельство о регистрации средства массовой информации ЭЛ № ФС 77 – 78854 от 07 августа 2020 г., выдано Федеральной службой по надзору в сфере связи, информационных технологий и массовых коммуникаций |
| *Учредитель и издатель* | Федеральное государственное бюджетное образовательное учреждение высшего образования «Донской государственный технический университет» (ДГТУ). |
| *Периодичность* | 4 выпуска в год |
| *Адрес учредителя и издателя* | 344003, Российская Федерация, г. Ростов-на-Дону, пл. Гагарина, 1. |
| *E-mail* | vestnik@donstu.ru |
| *Телефон* | +7 (863) 2–738–372 |
| *Сайт* | http://vestnik-donstu.ru/ |
| *Дата выхода в свет* | 31.03.2023 |

# Contents

# Содержание

## МЕХАНИКА



## МАШИНОСТРОЕНИЕ И МАШИНОВЕДЕНИЕ



## ИНФОРМАТИКА, ВЫЧИСЛИТЕЛЬНАЯ ТЕХНИКА И УПРАВЛЕНИЕ

**MECHANICS**
**МЕХАНИКА**



UDC 539.3
https://doi.org/10.23947/2687-1653-2023-23-1-7-16

*Original article*

# Construction of Forming Limit Diagram for Sheet Blanks from Aviation Aluminum Alloys

**Sergey I Feoktistov, Ivan K Andrianov** ✉
Komsomolsk-na-Amure State University, 27, Lenin Prospect, Komsomolsk-on-Amur, Russian Federation
✉ ivan_andrianov_90@mail.ru

**Abstract**

***Introduction.*** The modern development of stamping aircraft manufacturing is inextricably linked with the assessment of the limiting capabilities of sheet blanks. However, the issue of defect-free forming of blanks made of aviation aluminum alloys is understudied. The importance of this issue is due to the fact that aluminum alloys are often used in the manufacture of thin-walled products for aviation purposes. During the implementation of shaping processes, various defects may appear, specifically, corrugation or unacceptable thinning. In this regard, the objective of the work was to construct a diagram of the limit deformations of the base aviation alloys and to conduct a comparative analysis of the limit deformation curves for these materials.

***Materials and Methods.*** Logarithmic deformations with the property of additivity were used to account for large deformations. The construction of the diagram of the limit deformations was carried out in the formulation of the deformation theory of plasticity. The issue of constructing a diagram of limit deformations was considered on the basis of the positivity criterion of the loading force derivative. In the area of negative values of the smallest major deformations, the Hill criterion was used to construct the limit deformation curve, and in the area of positive values of the smallest major logarithmic deformations, the Swift criterion was used. When constructing the limit deformation diagram, a power approximation of the hardening rule was used.

***Results.*** The curves of limiting deformations for the following aviation alloys were obtained: AMg6, D16AT, AMg2M, 1201-T, AMcM. According to the comparative analysis of the areas of safe forming, the values of deformations of the beginning of necking and their influence on the change in the position of the curve of the limiting deformation of blanks were compared: the greater the deformation of the neck formation, the higher the position of the curve of the limiting deformations. The concept of the Keeler's limit deformation diagram was described. Approaches to the construction of the Hill-Swift criteria used on the basis of the results of tensile testing of sheet specimens were presented.

***Discussion and Conclusions.*** Based on the constructed curves of limiting deformations for aviation alloys, AMg-6, D16AT, AMg2M, 1201-T, AMcM, the following has been found. AMg2M alloy has the largest area of safe forming, 1201-T alloy has the smallest one. That is explained by the difference in relative deformations of the beginning of neck formation. The conducted research made it possible to evaluate the possibilities of defect-free forming of thin-walled blanks made of basic aviation aluminum alloys. The use of the constructed diagrams of limiting deformation will provide predicting the appearance of breaks in the process of forming sheet blanks.

**Keywords:** sheet stamping, forming limit diagram, logarithmic strains, Hill-Swift diagram.

**Acknowledgements.** Appreciation is expressed to the “Council for grants of the President of the Russian Federation for state support of young Russian scientists and for state support of leading scientific schools of the Russian Federation” for financial support of the research under scholarship project SP-2200.2022.5 “Development of models and algorithms for calculating the plastic shaping of blanks for stamping production”.

**For citation.** Feoktistov SI, Andrianov IK. Construction of Forming Limit Diagram for Sheet Blanks from Aviation Aluminum Alloys. *Advanced Engineering Research (Rostov-on-Don).* 2023;23(1):7–16. https://doi.org/10.23947/2687-1653-2023-23-1-7-16

*Научная статья*

# Построение диаграммы предельных деформаций формоизменения листовых заготовок из авиационных алюминиевых сплавов

**С.И. Феоктистов, И.К. Андрианов** ✉

Комсомольский-на-Амуре государственный университет, Российская Федерация, г. Комсомольск-на-Амуре, пр. Ленина, 27

✉ ivan_andrianov_90@mail.ru

**Аннотация**

***Введение.*** Современное развитие штамповочного авиастроительного производства неразрывно связано с оценкой предельных возможностей листовых заготовок. Однако малоизученным является вопрос бездефектного формоизменения заготовок из авиационных алюминиевых сплавов. Важность данного вопроса связана с тем, что алюминиевые сплавы достаточно часто используются при изготовлении тонкостенных изделий авиационного назначения. При реализации процессов формообразования возможно появление различных дефектов — гофрообразования или недопустимого утонения. В связи с этим целью работы являлось построение диаграммы предельных деформаций основных авиационных сплавов и проведение сравнительного анализа кривых предельного деформирования для данных материалов.

***Материалы и методы.*** Для учета больших деформаций были использованы логарифмические деформации, обладающие свойством аддитивности. Построение диаграммы предельных деформаций формоизменения проводилось в постановке деформационной теории пластичности. Вопрос построения диаграммы предельных деформаций рассмотрен на основании критерия положительности производной силы нагружения. В области отрицательных значений наименьших главных деформаций для построения кривой предельного деформирования использовался критерий Хилла, а в зоне положительных значений главных наименьших логарифмических деформаций — критерий Свифта. При построении диаграммы предельного деформирования использовалась степенная аппроксимация закона упрочнения.

***Результаты исследования.*** Получены кривые предельных деформаций для авиационных сплавов: АМг-6, Д16АТ, АМг2М, 1201-Т, АМцМ. Согласно проведенному сравнительному анализу областей безопасного формоизменения, сопоставлены значения деформаций начала шейкообразования и их влияние на изменение положения кривой предельного деформирования заготовок: чем больше деформация шейкообразования, тем выше положение кривой предельных деформаций. Описана концепция диаграммы предельных деформаций Килера. Представлены подходы к построению критериев Хилла и Свифта, используемых по результатам испытания листовых образцов на разрыв.

***Обсуждение и заключения.*** На основании построенных кривых предельных деформаций для авиационных сплавов АМг-6, Д16АТ, АМг2М, 1201-Т, АМцМ выяснили, что наибольшую область безопасного формоизменения имеет сплав АМг2М, наименьшую — сплав 1201-Т, что объясняется отличием относительных деформаций начала шейкообразования. Проведенное исследование позволило оценить возможности бездефектного формоизменения тонкостенных заготовок из основных авиационных алюминиевых сплавов. Применение построенных диаграмм предельного деформирования позволит прогнозировать появление разрывов в процессе формообразования листовых заготовок.

**Ключевые слова:** листовая штамповка, диаграмма предельных деформаций, логарифмические деформации, диаграмма Хилла-Свифта.

**Благодарности.** Авторы выражают благодарность «Совету по грантам Президента Российской Федерации для государственной поддержки молодых российских учёных и по государственной поддержке ведущих научных школ Российской Федерации» за финансовую поддержку для проведения исследования в рамках стипендии по проекту СП-2200.2022.5 «Разработка моделей и алгоритмов расчёта пластического формообразования заготовок штамповочного производства».

**Для цитирования:** Феоктистов С.И., Андрианов И.К. Построение диаграммы предельных деформаций формоизменения листовых заготовок из авиационных алюминиевых сплавов. *Advanced Engineering Research (Rostov-on-Don).* 2023;23(1):7–16. https://doi.org/10.23947/2687-1653-2023-23-1-7-16

**Introduction.** Modern development of the aviation production is inextricably linked with the study of sheet stamping processes. One of the key problems in the task of shaping is the defect prediction, in particular, thinning, ruptures, corrugation. These issues are related to the assessment of the limits of the blank. By forming limit of a sheet blank, we will mean the ability of the material to deform to the required geometry without necking or destruction.

To date, the problem of predicting defects of sheet blanks in the stamping process is solved using the following methods:

– empirical, based on mechanical tests for simple stretching of metal samples, thin sheets and tapes, bending tests, as well as pipe testing methods for flaring and broaching;

– theoretical and empirical, which are based on the use and dissemination of the test results of samples for uniaxial tension to other schemes of deformation of blanks;

– theoretical, which are based on the use of criteria for limit deformation, specifically, in the manufacture of thin-walled products. The founders of these methods were J. Sachs, R. Hill, A. D. Tomlenov, V. D. Golovlev, G. D. Del, Z. Marciniak, A. D. Matveev, J. D. Lubahn [1–20].

It should be noted that the disadvantage of empirical and theoretical-empirical methods is the limited use of the results.

The most important step in solving the problem of predicting defects of thin-walled products was the development of the concept of the forming limit diagram (FLD) proposed by S. P. Keeler [16–20], which today is generally accepted in solving sheet stamping problems. FLD diagrams are widely used in AUTOFORM and PAM-STAMP 2G CAE software systems.

Experimental methods for constructing deformation diagrams are based on the test methodology presented in the works of Marciniak and Nakazima. It should also be noted that the issues of plastic destruction of sheet blanks were considered in [17–19]. In the last decade, interest in the construction of FLD diagrams has grown significantly. Most foreign studies are aimed at experimental construction of diagrams for specific materials, as well as numerical modeling of shape-changing processes using finite element methods [20–30]. Theoretical aspects of the construction of DFD diagrams and deformation diagrams of the third kind are presented in [31, 32].

It is important to note that the diagram of limit deformations provides estimating the beginning of neck formation, which ends with the destruction of the sample in the process of deformation. The FLD diagram binds the values of the main logarithmic deformations acting in the plane of the sheet. Forming limit diagrams enable not only to predict the destruction of the blank, but also to assess the presence of other defects, in particular, wrinkling, thinning, which, in turn, reduce the quality of the stamped part. The main zones of the FLD diagram are the zones of destruction, possible ruptures, safe forming, probable formation of folds, and wrinkling (Fig. 1) [31].

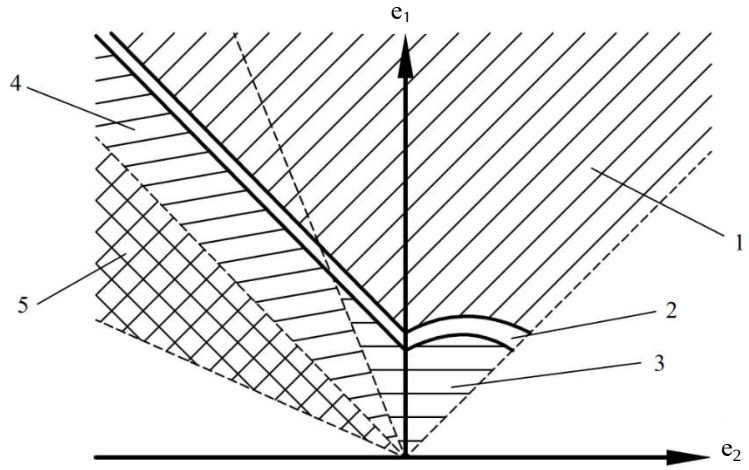


Fig. 1. Forming limit diagram: 1 — zone of destruction; 2 — zone of possible ruptures; 3 — zone of safe forming; 4 — zone of probable formation of folds; 5 — zone of wrinkling [31]

**Materials and Methods.** When describing the processes of forming thin-walled blanks, the moment of transition to the plasticity stage is determined in accordance with the Huber-von Mises criterion [33]:

$$\sigma_i = \sqrt{\sigma_1^2 + \sigma_2^2 - \sigma_1\sigma_2} = \sigma_\text{T},$$

where $\sigma_1$, $\sigma_2$ — primary true stresses, at $\sigma_3 = 0$ due to the light gauge of the blank; $\sigma_i$ — intensity of true stresses; $\sigma_\text{T}$ — yield strength.

According to the deformation theory of plasticity, the relationship between the intensity of stresses and the intensity of logarithmic deformations is defined as:

$$\left.\begin{aligned} e_1 &= \frac{e_i}{\sigma_i}\left(\sigma_1 - \frac{1}{2}\sigma_2\right), \\ e_2 &= \frac{e_i}{\sigma_i}\left(\sigma_2 - \frac{1}{2}\sigma_1\right), \end{aligned}\right\} \quad (1)$$

where $e_1, e_2,$ — principal deformations.

Since in sheet stamping tasks, the shaping processes can occur in several transitions, therefore, large deformations are considered. The use of relative deformations is unacceptable. In this regard, the deformed state in (1) is presented in true logarithmic deformations.

Intensity of the principal deformations:

$$e_i = \frac{2}{\sqrt{3}}\sqrt{e_1^2 + e_2^2 + e_1 e_2}.$$

The ratio of the principal deformations and the primary true stresses:

$$\alpha = \frac{e_2}{e_1}, \beta = \frac{\sigma_2}{\sigma_1}. \quad (2)$$

Based on ratio (1) and (2), the relationship between $\alpha$ and $\beta$ is determined by:

$$\beta = \frac{2\alpha+1}{2+\alpha}. \quad (3)$$

According to expression (2), the Huber-von Mises criterion has the form:

$$\sigma_i = \sigma_1\sqrt{1 - \beta + \beta^2} = \sigma_\text{T},$$

and the intensity of deformations:

$$e_i = \frac{2}{\sqrt{3}} e_1 \sqrt{1 + \alpha + \alpha^2}. \quad (4)$$

To assess the onset of necking, the criterion of positivity of the derivative of the loading force is currently used, the founders of which were G. Sachs and J. D. Lubahn [17]. According to the described criterion, the deformation of the sample is stable with a positive increment of the tensile force. The moment of unstable deformation with subsequent stretching starts at $\Delta P = 0$ and continues at $\Delta P < 0$ (Fig. 2).

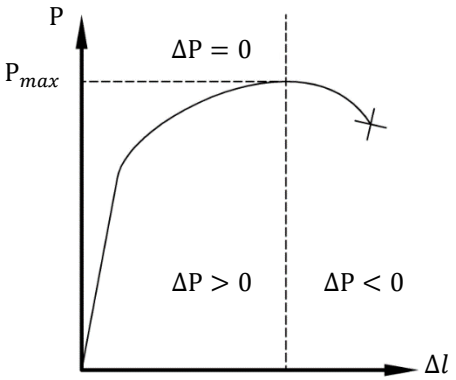


Fig. 2. Indicator diagram of uniaxial tension of the sample [33]

The deformation diagram of aluminum alloys obtained by the results of the uniaxial tensile test is approximated by a power function in the theoretical analysis of the diagrams of the limit deformations of the shape change [18, 19, 31, 32]:

$$\sigma_S = Ae^n \text{ или } \sigma_i = Ae_i^n,$$

where $\sigma_S = P/F$ — true stress; $P$ — tensile force; $F$— current cross-sectional area of the sample; $e = \ln(1 + \Delta l/l_0)$, while $A$ and $n$ — coefficients of the power approximation.

Using the criterion of positivity of the derivative of the loading force and the power approximation of the deformation diagram of the third kind, it is possible to obtain a relationship between the limit deformation of the sample at the time of the occurrence of the diffuse neck and the power approximation coefficient n under condition $\Delta P = 0$ (Fig. 3) [32]:

$$e_{\text{ш}} = e_{i\text{ш}} = n. \quad (5)$$

It is significant that relation (1) is performed using logarithmic deformations. In case of using relative deformations, only approximate equality is possible.

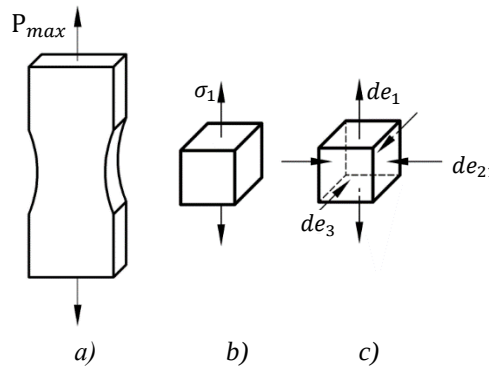


Fig. 3. Occurrence of a diffuse neck under uniaxial tension of a flat sample:
*a* — sample; *b* — stress state; *c* — deformed state [33]

Consider the stress state of a plate to which two tensile forces are applied at the edges, i.e., the blank experiences biaxial tension (Fig. 4).

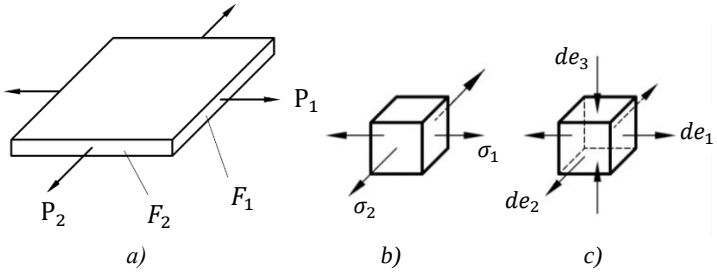


Fig. 4. Stress-strain state of the plate under biaxial tension: *a* — plate; *b* — stress state; *c* — deformed state [33]

Using the criterion of positivity of the derivative of the loading force, we determine the deformation limit value $e_{iш}$ at the moment when forces $P_1$ or $P_2$ are maximum. For the case when $F_2/F_1 = \text{const}$, $P_2/P_1 = \text{const}$, at the moment of maximum tensile forces $dP_1 = dP_2 = 0$. H. W. Swift [19] proposed the relation for the limit deformation:

$$e_{iш} = 4n\frac{(1-\beta+\beta^2)^{3/2}}{4-3\beta-3\beta^2+4\beta^3}.$$

According to expressions (2)–(4), the relation for describing the curve of limit deformations at various exponents of power approximation in the hardening zone has the form:

$$4(e_1-n)(e_2+2e_1)^3-3(e_1-2n)(e_1+2e_2)(e_2+2e_1)^2- \\ -3(e_1+2n)(e_2+2e_1)(e_1+2e_2)^2+2(2e_1+n)(e_1+2e_2)^3=0. \quad (6)$$

It is known from the experimental and theoretical studies that after the occurrence of a diffuse neck, plastic deformation of the sample continues. Thereafter, a localized neck may occur, which differs from the diffuse one not only in size, but also in that its occurrence and development are carried out under conditions of flat deformation with intensive thinning of the sample.

According to R. Hill [20], the limit deformation criterion is determined by the moment of formation of the local neck, at which the increment of the total force is zero. In this case, the relation for the limit deformation is determined by the expression:

$$e_{iш} = 2n\frac{(1-\beta+\beta^2)^{1/2}}{1+\beta}. \quad (7)$$

Taking into account expressions (2), (4), expression (7) for constructing a limit deformation diagram according to the Hill criterion has the form:

$$e_1+e_2-n=0. \quad (8)$$

It should also be noted that the described approach is consistent with the finite element method, which has been widely used to construct FLD diagrams of various materials in recent years [21–29].

**Research Results.** In practice, we will construct the FLD diagram using two criteria [31], namely: the Hill criterion, which is used for $e_2 \le 0$ according to (8); the Swift criterion, which is used for $e_2 \ge 0$ according to (6). Let us consider the application of these relations to construct the curve of the limit deformations of aluminum alloys widely used in the aviation industry at known values of deformation of necking: $\varepsilon_ш = 0.18$ (AMg6), $\varepsilon_ш = 0.16$ (D16AT), $\varepsilon_ш = 0.2$ (AMg2M), $\varepsilon_ш = 0.06$ (1201-T), $\varepsilon_ш = 0.1$ (AMcM) [34].

Determining $e_ш$ from formula $e_ш = \ln(1+\varepsilon_ш)$ and using expression (5), we obtain the value of the strain-hardening indices: $n = 0.17$ (AMg6), $n = 0.15$ (D16AT), $n = 0.18$ (AMg2M), $n = 0.06$ (1201-T), $n = 0.09$ (AMcM). Then, the Hill-Swift diagram, according to (6), (8), will take the form shown in Figure 5.

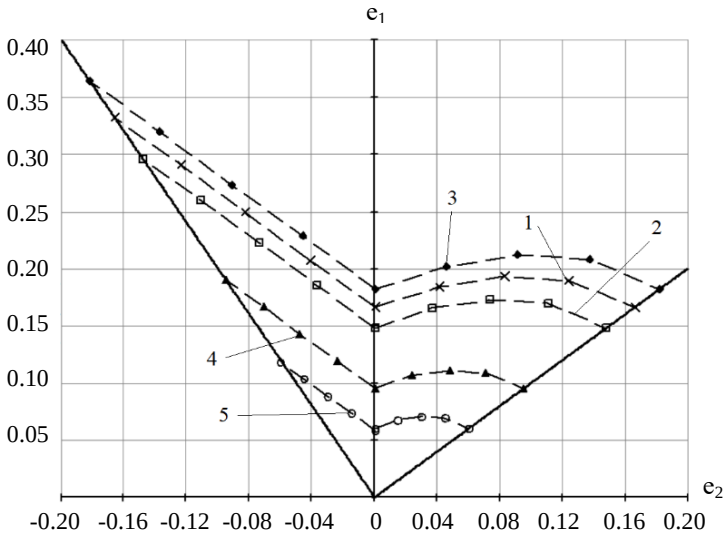


Fig. 5. FLD-Hill-Swift diagrams for various aviation alloys: 1 — AMg6 alloy; 2 — D16AT alloy; 3 — AMg2M alloy; 4 — 1201-T alloy; 5 — AMcM alloy

**Discussion and Conclusions.** According to the constructed curves of limit deformations, AMg2M alloy has the largest area of safe forming of the five alloys studied, 1201-T alloy has the smallest one. That is due to differences in the deformation properties of materials, specifically, the difference in the deformations of the necking onset. In AMg2M alloy, the relative deformation of the beginning of neck formation is 20 %, and in 1201-T alloy — 6 %.

Thus, on the basis of data on the hardening curves, power approximation and deformation of necking for aviation aluminum alloys AMg6, D16AT, AMg2M, 1201-T, AMcM, curves of limit deformations of forming have been constructed, providing for the determination of the zone of safe deformation of sheet blanks. The study results are of practical importance in solving sheet stamping problems for these materials to predict unacceptable thinning, raptures, and wrinkling of thin-walled blanks.

**References**

1. Narayanasamy R, Narayanan S. Forming Limit Diagram for Interstitial Free Steels Supplied by Ford India Motors. *Materials and Design*. 2007;28(1):16–35. https://doi.org/10.1016/j.matdes.2005.06.021

2. Krishnan E, Narayanan S, Narayanasamy R. Modelling of Forming Limit Diagram of Perforated Commercial Pure Aluminium Sheets Using Artificial Neural Network. *Computational Materials Science*. 2010;47:1072–1078. https://doi.org/10.1016/j.commatsci.2009.12.016

3. Li B, Nye TJ, Wu PD. Predicting the Forming Limit Diagram of AA 5182-O. *Journal of Strain Analysis for Engineering Design*. 2010;45(4):255–273. https://doi.org/10.1243/03093247JSA608

4. Hong Wei Liu, Peng Zhang. Forming Limit Diagram of Stainless Steel-Aluminum Alloy Clad. *Advanced Materials Research*. 2011;152–153:541–544. https://doi.org/10.4028/www.scientific.net/AMR.152-153.541

5. Chamos AN, Labeas GN, Setsika D. Tensile Behavior and Formability Evaluation of Titanium-40 Material Based on the Forming Limit Diagram Approach. *Journal of Materials Engineering and Performance*. 2013;22(8):2253–2260. https://doi.org/10.1007/s11665-013-0495-1

6. Feoktistov SI, Kyaw Zayar Soe. Method for Construction of Forming Limit Diagram by Using Reference Mechanical Characteristics of the Metal. *Materials Science Forum*. 2019;945:833–838. https://doi.org/10.4028/www.scientific.net/MSF.945.833

7. Zhiying Sun, Hong Zhuang. Experimental Study on Forming Limit Diagram Obtained by Bulging Uniformly in Thickness Direction. *The International Journal of Advanced Manufacturing Technology*. 2019;104:967–977. https://doi.org/10.1007/s00170-019-03887-9

8. Min-A Woo, Woo-Jin Song, Beom-Soo Kang, et al. Acquisition and Evaluation of Theoretical Forming Limit Diagram of Al 6061-T6 in Electrohydraulic Forming Process. *Metals*. 2019;9:401. https://doi.org/10.3390/met9040401

9. Glushchenkov VA, Chernikov DG, Tiabashvili AT. Method of Dynamic Test of Sheet Materials with Pulse Magnetic Loading. *Actual Problems in Machine Building*. 2017;4:94–99.

10. Davidenko M, Davidenko A, Matveev V, et al. Definition of the Limit Strain Fiber Concrete Deformations Based on the Energy Dependences of Concrete Deformation Diagrams. *Nauchnyi vestnik GOU LNR LGAU*. 2020;8(3):214–219.

11. Mamutov VS, Mamutov AV, Arsentyeva KS, et al. Ehksperimental'no-raschetnaya diagramma predel'nykh deformatsii dlya proektirovaniya ehlektrogidroimpul'snoi shtampovki. *Modern Mechanical Engineering. Science and Education*. 2021;10:611–622. (In Russ.).

12. Keller IE, Petukhov DS, Kazantsev AV, et al. The Limit Diagram under Hot Sheet Metal Forming. A Review of Constitutive Models of Material, Viscous Failure Criteria and Standard Tests. *Journal of Samara State Technical University, Ser. Physical and Mathematical Sciences*. 2018;22:447–486. http://doi.org/10.14498/vsgtu1608

13. Bezgodov IM, Dmitrenko EN. Improvement of Curvilinear Diagrams of Concrete Deformation. *Industrial and Civil Engineering*. 2019;8:99–104. https://doi.org/10.33622/0869-7019.2019.08.99-104

14. Eryshev VA. Numerical Methods of Strengthening Strength of Reinforced Concrete Elements on a Nonlinear Deformation Model with the Use of Diagrams of Material Breaking. *Bulletin NGIEI*. 2018;85(6):17–26.

15. Izosimova SV. Issledovanie vliyaniya formy zagotovki na tochnost' postroeniya diagrammy predel'nykh deformatsii. *Molodezhnyi nauchno-tekhnicheskii vestnik*. 2013;10:3. (In Russ.).

16. Feoktistov SI, Kyaw Zayar Soe. Determination of Technological Possibilities of Titanium and Aluminum Alloys at Distribution. *Scholarly Notes of KNASTU*. 2019;37(1):4–9.

17. Feoktistov SI, Zho Zayar So. Determination of the Limiting Expanding Ratio by FLD-Diagrams. *Forging and Stamping Production. Material Working by Pressure*. 2019;9:3–7.

18. Feoktistov SI, Zho Zayar So. Determination of the Limiting Drawing Ratio of Titanium and Aluminum Alloys by FLD-Diagrams. *Forging and Stamping Production. Material Working by Pressure*. 2019;5:27–34.

19. Swift HW. Plastic Instability under Plane Stress. *Journal of the Mechanical and Physics of Solids*. 1952;1:1–18. https://doi.org/10.1016/0022-5096(52)90002-1

20. Hill R. On Discontinuous Plastic States with Special Reference to Localized Necking in Thin Sheet. *Journal of the Mechanics and Physics of Solids*. 1952;1:19–30. https://doi.org/10.1016/0022-5096(52)90003-3

21. Petroušek P, Kočiško R, Kvackaj T, et al. Formability Evaluation of Aluminium Alloys by FLD Diagrams. *Acta Physica Polonica A*. 2017;131:1344–1347. http://dx.doi.org/10.12693/APhysPolA.131.1344

22. Lisiecka-Graca P, Kwiecień M, Madej Ł, et al. Application of the DIC System to Build a Forming Limit Diagram (FLD) of Multilayer Materials. *Key Engineering Materials*. 2022;926:963–969. http://dx.doi.org/10.4028/p-s33fqx

23. Rubešová K, Rund M, Rzepa S, et al. Determining Forming Limit Diagrams Using Sub-Sized Specimen Geometry and Comparing FLD Evaluation Methods. *Metals*. 2021;11:484. http://dx.doi.org/10.3390/met11030484

24. Marrapu B. Effect of Localization Criteria and Yield Criteria in Predicting the Forming Limit Diagram (FLD) of DP590 Steel Sheets. *Advances in Materials and Processing Technologies*. 2021;8(1):1739–1752. https://doi.org/10.1080/2374068X.2021.1874710

25. Guangyong Sun, Wenwu Zhang, Zhen Wang, et al. A Novel Specimen Design to Establish the Forming Limit Diagram (FLD) for GFRP through Stamping Test. *Applied Science and Manufacturing*. 2020;130:105737. http://dx.doi.org/10.1016/j.compositesa.2019.105737

26. Panahizadeh V, Hoseinpour M, Gholamzadeh E, et al. Theoretical and Experimental Study of FLDs of AA5083 Sheet and Investigation of Advanced Anisotropic Yield Criteria Coefficients. *Journal of the Brazilian Society of Mechanical Sciences and Engineering*. 2022;44:356. http://dx.doi.org/10.1007/s40430-022-03600-0

27. Godage O, Kakandikar G. Numerical and Analytical Investigation of Forming Limit Diagram of SS316L Foil. *International Journal for Research in Applied Science and Engineering Technology*. 2022;10:1544–1549. https://doi.org/10.22214/ijraset.2022.40899

28. Mahalle G, Takalkar P, Kotkunde N, et al. Strain and Stress-Based Forming Limit Diagrams for Inconel 718 Alloy. In book: *NUMISHEET 2022, Proc. 12th Int. Conference and Workshop on Numerical Simulation of 3D Sheet Metal Forming Processes.* 2022;1:549–556. http://dx.doi.org/10.1007/978-3-031-06212-4_50

29. Takalkar AS, Koteswara Rao JM, Mailan Chinnapandi LB. Numerical Simulation for Predicting Failure in Deep Drawing Process Using Forming Limit Diagram (FLD). *International Journal of Advances in Mechanical and Civil Engineering*. 2015;2:11–15.

30. Sekhara Reddy AC, Sandeep B, Sandeep Kumar J, et al. Experimental Determination of Anisotropic Properties and Evaluation of FLD for Sheet Metal Operations. *Advances in Science and Technology*. 2021;106:39–45. http://dx.doi.org/10.4028/www.scientific.net/AST.106.39

31. Lonardi C, Corallo L, Verleysen P. Prediction of Forming Limit Diagram Using the Marciniak-Kuczynski Method for Ti-6Al-4V Using Different Material Models. *Key Engineering Materials*. 2022;926:885–896. http://dx.doi.org/10.4028/p-10z13b

32. Paul SK. Theoretical Analysis of Strain- and Stress-Based Forming Limit Diagrams. *Strain Analysis*. 2013;48(3):177–188. http://dx.doi.org/10.1177/0309324712468524

33. Chumadin AS. *Teoriya i raschety protsessov listovoi shtampovki (dlya inzhenerov)*. Moscow: Ehksservis “VIP”; 2014. 216 p. (In Russ.).

34. Andrianov IK, Tun Lin Htet, Feoktistov SI. *Determination of Relative Strain Corresponding to the Beginning of Neck Formation When Testing Aluminum Alloys for Rapture*. In: Proc. V All-Russian National Sci. Conf. of young scientists. Komsomolsk-on-Amur; 2022. P. 157–160.

*About the Authors:*

**Sergey I Feoktistov,** professor of the Aircraft Engineering Department, Komsomolsk-na-Amure State University (27, Lenin Prospect, Komsomolsk-on-Amur, 681013, RF), Dr.Sci. (Eng.), ResearcherID, ORCID, serg_feo@mail.ru

**Ivan K Andrianov,** associate professor of the Aircraft Engineering Department, Komsomolsk-na-Amure State University (27, Lenin Prospect, Komsomolsk-on-Amur, 681013, RF), Cand.Sci. (Eng.), ScopusID, ORCID, ivan_andrianov_90@mail.ru

*Claimed contributorship:*

SI Feoktistov: description of the theoretical part of the study of limit deformation diagrams based on the Hill-Swift criteria. IK Andrianov: calculation of the construction of limit strain curves for aviation alloys; layout of the scientific paper.

**Received** 13.12.2022.
**Revised** 09.01.2023.
**Accepted** 09.01.2023.

*Conflict of interest statement*

The authors do not have any conflict of interest.

*All authors have read and approved the final manuscript.*

*Об авторах:*

**Сергей Иванович Феоктистов,** профессор кафедры «Авиастроение» Комсомольского-на-Амуре государственного университета (681013, РФ, г. Комсомольск-на-Амуре, пр. Ленина, 27), доктор технических наук, ResearcherID, ORCID, serg_feo@mail.ru

**Иван Константинович Андрианов,** доцент кафедры «Авиастроение» Комсомольского-на-Амуре государственного университета (681013, РФ, г. Комсомольск-на-Амуре, пр. Ленина, 27), кандидат технических наук, ScopusID, ORCID, ivan_andrianov_90@mail.ru

*Заявленный вклад соавторов:*

С.И. Феоктистов — описание теоретической части исследования диаграмм предельного деформирования на основании критериев Хилла-Свифта. И.К. Андрианов — проведение расчета построения кривых предельных деформаций для авиационных сплавов, оформление научной статьи.

**Поступила в редакцию** 13.12.2022.
**Поступила после рецензирования** 09.01.2023.
**Принята к публикации** 09.01.2023.

*Конфликт интересов*

Авторы заявляют об отсутствии конфликта интересов.

*Все авторы прочитали и одобрили окончательный вариант рукописи.*

MECHANICS
МЕХАНИКА





UDC 517.956.223
https://doi.org/10.23947/2687-1653-2023-23-1-17-25

*Original article*

# On the Construction of Mathematical Models of the Membrane Theory of Convex Shells

**Evgeniy V Tyurikov**
Don State Technical University, 1, Gagarin sq., Rostov-on-Don, Russian Federation
✉ etyurikov@hotmail.com

**Abstract**

***Introduction.*** The paper considers the issues of constructing mathematical models of the momentless equilibrium stress state of elastic convex shells using methods of the complex analysis. At the same time, shells with a piecewise smooth (ribbed) lateral surface were considered for the first time. The work objective was to find classes of shells for which it is possible to build meaningful mathematical models.

***Materials and Methods.*** Using the methods of the theory of the discontinuous Riemann-Hilbert problem for generalized analytic functions, a criterion for the unconditional solvability of the corresponding static problem for the equilibrium equation of a convex shell with a ribbed lateral surface has been obtained. This criterion, combined with the methods of the theory of generalized analytical functions, is a tool for constructing mathematical models of the state of momentless stress equilibrium of elastic convex shells.

***Results.*** A method has been developed for constructing mathematical models of the momentless equilibrium stress state of a convex shell under the action of a variable external load and the condition of stress concentration at the corner points of the median surface. The introduction of a vector parameter, as well as the concepts of "order of quasi-correctness" and "quasi-stability", into the boundary condition provided both quantitative and qualitative comparison of mathematical models. Classes of shells have been found for which the description of mathematical models is given in terms of the geometry of the boundary in the vicinity of the corner points of the median surface. The obtained result, when applied to shallow convex shells, provides a geometric criterion of quasi-stability. It is established that for a shallow shell, which is not quasi-stable, the only adequate mathematical model is a probabilistic one.

***Discussion and Conclusions.*** The proposed method for constructing a two-parameter family of problems with a modified boundary condition makes it possible to simulate the momentless equilibrium stress state for fairly wide classes of convex shells with a piecewise-smooth lateral surface under a sleeve connection. At the same time, the developed algorithm for calculating the boundary condition index allowed us to answer the question of the existence of an adequate mathematical model for a shell with a side surface of an arbitrary configuration, and for shells of a special type (specifically, shallow or shells of revolution), to formulate a geometric criterion for the existence of a mathematical model.

**Keywords:** thin elastic shell, generalized analytic function, Riemann-Hilbert problem, index of boundary value condition, mathematical model.

**Acknowledgements.** The author would like to thank the staff of the Theoretical and Applied Mechanics Department, Don State Technical University, for discussing the results of the work, and professor A. N. Solovyov, Dr.Sci. (Engineering), for professional support in writing the work.

**For citation.** Tyurikov EV. On the Construction of Mathematical Models of the Membrane Theory of Convex Shells. *Advanced Engineering Research (Rostov-on-Don).* 2023;23(1):17–25. https://doi.org/10.23947/2687-1653-2023-23-1-17-25

*Научная статья*

# К вопросу о построении математических моделей мембранной теории выпуклых оболочек

**Е.В. Тюриков**

Донской государственный технический университет, г. Ростов-на-Дону, Российская Федерация, пл. Гагарина, 1

✉ etyurikov@hotmail.com

**Аннотация**

***Введение.*** В работе рассмотрены вопросы построения математических моделей безмоментного состояния напряженного равновесия упругих выпуклых оболочек с использованием методов комплексного анализа. При этом впервые рассмотрены оболочки с кусочно-гладкой (ребристой) боковой поверхностью. Целью работы являлось отыскание классов оболочек, для которых возможно построение содержательных математических моделей.

***Материалы и методы.*** С помощью методов теории разрывной задачи Римана-Гильберта для обобщённых аналитических функций получен критерий безусловной разрешимости соответствующей статической задачи для уравнения равновесия выпуклой оболочки с ребристой боковой поверхностью. Этот критерий в сочетании с методами теории обобщённых аналитических функций представляет собой инструмент построения математических моделей состояния безмоментного напряжённого равновесия упругих выпуклых оболочек.

***Результаты исследования.*** Разработан метод построения математических моделей безмоментного состояния напряжённого равновесия выпуклой оболочки при действии переменной внешней нагрузки и условии концентрации напряжений в угловых точках срединной поверхности. Введение в граничное условие векторного параметра, а также понятий «порядок квазикорректности» и «квазиустойчивость» позволяют провести как количественное, так и качественное сравнение математических моделей. Найдены классы оболочек, для которых описание математических моделей дается в терминах геометрии границы в окрестности угловых точек срединной поверхности. Полученный результат в применении к пологим выпуклым оболочкам позволяет дать геометрический критерий квазиустойчивости. Установлено, что для пологой оболочки, не являющейся квазиустойчивой, единственной адекватной математической моделью является вероятностная.

***Обсуждение и заключения.*** Предлагаемый метод построения двухпараметрического семейства задач с модифицированным граничным условием позволяет моделировать состояние безмоментного напряженного равновесия для достаточно широких классов выпуклых оболочек с кусочно-гладкой боковой поверхностью при условии втулочной связи. При этом разработанный алгоритм вычисления индекса граничного условия позволяет ответить на вопрос о существовании адекватной математической модели для оболочки с боковой поверхностью произвольной конфигурации, а для оболочек специального вида (например, пологих или оболочек вращения) — сформулировать геометрический критерий существования математической модели.

***Ключевые слова:*** тонкая упругая оболочка, обобщенная аналитическая функция, задача Римана-Гильберта, индекс граничного условия, математическая модель.

**Благодарности.** Автор выражает признательность коллективу кафедры «Теоретическая и прикладная механика» Донского государственного технического университета за обсуждение результатов работы, также благодарность доктору технических наук, профессору А. Н. Соловьёву за профессиональную поддержку при написании работы.

**Для цитирования.** Тюриков Е.В. К вопросу о построении математических моделей мембранной теории выпуклых оболочек. *Advanced Engineering Research (Rostov-on-Don).* 2023;23(1):17–25. https://doi.org/10.23947/2687-1653-2023-23-1-17-25

**Introduction.** The issues considered in the paper were studied and described in the works of I. N. Vekua [1, 2] and A. L. Goldenveizer [3, 4], who initiated the application of methods of the theory of generalized analytical functions to the momentless (membrane) theory of thin elastic shells and the theory of surface bending. To date, the final results in this direction have been obtained for convex shells with a smooth edge (i.e., with a smooth boundary of its median surface). The most significant of them — the correctness and quasi-correctness of the key problem with a static boundary condition with simply connected and multiply connected median surfaces — are consequences of the fact that the index of the corresponding Riemann-Hilbert problem is an invariant of the connectivity of the surface. The author's application of I. N. Vekua's methods to the problems of the theory of convex shells with a piecewise smooth edge[1][5, 6] recognized a connection between the "geometry" of the median surface in the vicinity of its angular point and the picture of the solvability of the corresponding Riemann-Hilbert problems with a discontinuous coefficient of the boundary condition. The use of these methods in [7–9] allowed us to obtain an effective formula for the index under some additional geometric conditions on the angular points of the surface, and, as a consequence, the geometric criterion of quasi-correctness of the main boundary problem.

The purpose of this work is to construct mathematical models of the momentless equilibrium stress state of convex shells with ribbed side surfaces based on the geometric criterion of quasi-correctness of the main boundary problem.

**Materials and Methods.** Let $S$ be a simply connected surface of a given class of regularity [7] with a piecewise smooth edge $L=\bigcup_{j=1}^{n}L_j$ and angulat points $p_i$ $(i=1,...,n)$. Let us define on $S$ along $L$, piecewise continuous vector field $\mathrm{r}=\{\alpha(s),\beta(s)\}$, which admits discontinuities of the first kind at points $p_j$, where $\alpha(s)$, $\beta(s)$ ($\alpha^2+\beta^2=1$, $\beta\geq 0$) — tangential and normal components, $s$ — a natural parameter, and we denote by $J$ the homeomorphism of surface $S_0$ to complex plane $z=x+iy$ given in [9]. Let area $D=J(S)$ be the image of the surface when mapped to plane $z$ with boundary $\Gamma$ and angular points $q_i=J(p_i)$. Consider the following problem (task $R$): to find in domain $D$, complex-valued solution $w(z)$ of the equation:

$$w_{\bar{z}}(z)-B(z)\overline{w}(z)=F(z),\quad z\in D, \tag{1}$$

satisfying the Riemann–Hilbert condition

$$\mathrm{Re}\{\lambda(\zeta),w(\zeta)\}=\gamma(\zeta),\quad \zeta\in\Gamma, \tag{2}$$

where

$$\lambda(\zeta)=s(\zeta)\left[\beta(\zeta)t(\zeta)-\alpha(\zeta)s(\zeta)\right], \tag{3}$$

$s(\zeta)=s_1(\zeta)+is_2(\zeta)$, $t(\zeta)=t_1(\zeta)+it_2(\zeta)$, $i^2=-1$, $s_i$, $t_i$ $(i=1,2)$ — real-valued functions, complex-valued functions $\gamma(\zeta)$, $\lambda(\zeta)$ Hölder functions on each of the arcs $\Gamma_j=J(L_j)$, $w_{\bar{z}}=\frac{1}{2}(w_x+iw_y)$, $B(z)$, $F(z)$ — functions of class $L_r(D)$, $r>2$. Here, it is assumed that the solutions of class $W^{1,r}$ at the points of discontinuity $q_i$ admit "integrable infinity", i.e., they admit an estimate $|w(z)|<\mathrm{const}\cdot|z-q_i|^{-\alpha_j}$, $0<\alpha_j<1$. Following [10], the class of such solutions is denoted by $H^*$.

As is known [11], the static boundary value problem of the momentless theory for an elastic convex shell with a ribbed side surface in the mathematical formulation is problem $R$, where $w(z)$ — a complex stress function, $F(z)$ — a complex-valued function of the external load. In this case, the condition $w\in H^*$ is equivalent to the stress concentration condition at the corner points of the median surface. We will construct a mathematical model of the equilibrium state of the shell based on the results on the solvability of problem $R$ for a surface of a special type

[1] Tyurikov EV. Obobshchennaya granichnaya zadacha Goldenveizera dlya bezmomentnykh sfericheskikh kupolov. In: Proc. XIV Int. Conf. "Sovremennye problemy mekhaniki sploshnoi sredy. Rostov-on-Don. P. 290–293. (In Russ.)

(canonical dome [9]). To simplify the presentation, we assume that at each corner point, the direction of one of the arcs coincides with one of the main directions $\mathrm{k}_2$ ($\mathrm{k}_1$) and call the dome 2-canonical (1-canonical). Problem $R$ for canonical dome $K$ is called canonical if the direction of field $\mathrm{r}$ at each corner point $p$ is the direction of the generalized tangent [7, p. 46]. Let us introduce the notation: $\delta_i^2$ — ratio of the corresponding principal curvatures $k_1$, $k_2$ at point $p_i$ $(0<\delta_i<1)$, $p(\nu_i)$ — corner point $p_i$ with internal angle $\nu_i$, $T(\nu_i)$ — the set (*sector*) of directions of the *generalized* tangent at this point, $T$ — the set of continuous on $L$ vector fields $\mathrm{r}$, defining the direction of the generalized tangent at each corner point $p(\nu_j)$. As established in [7], canonical problem $R$ is quasi-correct for any field $\mathrm{r}\in T$, if $n\ge 2$. Problem $R$ is family $R^{\mathrm{r}}$ of problems (1)–(3), each of which is given by the selection of vector field $\mathrm{r}$. Following I. N. Vekua [1], we will call problem $R^{\mathrm{r}}$ $s$-quasi-correct in class $H^*$, if it is unconditionally solvable in this class, and its solution depends on $s$ real arbitrary constants ($s$ — *the order of quasi-correctness*).

*Definition 1. Canonical problem $R$ is called quasi-stable with respect to the field of directions of a generalized tangent if problem $R^{\mathrm{r}}$ is $s$-quasi-correct for any field $\mathrm{r}\in T$.*

*Remark 1.* Owing to the theorem on the solvability of the Riemann–Hilbert problem for generalized analytic functions [11], problem $R$ is quasi-stable if and only if index $\kappa$ of problem $R$ is an invariant of field $\mathrm{r}\in T$. Here, the index of the corresponding conjugation problem with coefficient $\Lambda(\zeta)=\overline{\lambda}(\zeta)\lambda^{-1}(\zeta)$ is called the index of the problem. In the case of $\kappa\ge -1$, the order of quasi-correctness is $s=\kappa+1$.

The technique [6, 8] of calculating the index of a boundary condition of form (2) is used below, as well as the concept [10] of *special node* $p_i$ of problem (1), (2) or *special point* $q_i=J(p_i)$ of discontinuity of the boundary condition (2). Following [6], the direction of the generalized tangent at a corner point is called *special* if the corresponding point of the discontinuity of boundary condition (2), (3) is *a special node* of problem *R*.

*Definition 2. Corner point $p(\nu)$ is called an instability point of problem $R$, if sector $T(\nu)$ contains a special direction.*

We introduce the notation: $\nu$, $\sigma$ — one-sided limits at corner point $p(\nu)$ of the unit vector tangent to $L$, where vector $\sigma$ sets main direction $\mathrm{k}_2$ on the surface at point $p$, and inside corner $\nu$ is given by pair $(-\nu,\sigma)$.

*Statement 1. If the direction of vector $\mathrm{r}$ at point $p(\nu)$ coincides with the direction of vector $\nu$, then point $q=J(p)$ is a special node of boundary condition (2) if and only if:*

$$\nu=\arccos\frac{1}{1+\delta}. \tag{4}$$

*If vector ν is replaced by vector $\sigma$, then:*

$$\nu=\operatorname{arcctg}\sqrt{t}, \tag{5}$$

*Where t — the only positive root of the equation:*

$$2\sqrt{\frac{1+\delta^2 t}{\delta^2+t}}+\frac{1+\delta^2 t}{\delta^2+t}-4\sqrt{\frac{E}{K\left(1+t^2\right)+4Et}}=\frac{1}{t}\ . \tag{6}$$

*Here* $E=\left(\frac{k_1-k_2}{2}\right)^2$, $K=k_1k_2$ [12, p.164]. *At that,* $\arccos\frac{1}{1+\delta}<\operatorname{arcctg}\sqrt{t}$.

We denote

$$\theta=\arccos\frac{1}{1+\delta},\ \mu=\operatorname{arcctg}\sqrt{t}\ . \tag{7}$$

The consequence of statement 1 is statement 2.

*Statement 2. Corner point $p(\nu)$ is a point of instability of problem $R$ if and only if:*

$$\theta\le\nu\le\mu\ . \tag{8}$$

Corner point $p(\nu)$ is a 1-type (2-type) point if condition $0<\nu<\theta$ $\left(\mu<\nu\le\frac{\pi}{2}\right)$ is met. As established in [8], $k$-type $(k=1,2)$ point is a point of stability. If $p(\nu)$ — is the point of instability, then the only *special* direction $\mathrm{r}_0$ of the generalized tangent divides sector $T(\nu)$ into two connected sets $T^1(\nu)$ and $T^2(\nu)$.

*Statement 3. The index of problem $R$ in class $H^*$ is calculated from the formula:*

$$\kappa=-4+\sum_{i=1}^{n}(4-\kappa_i), \tag{9}$$

*where $n$ — number of corner points of the boundary, $\kappa_i=m$ for point of stability $p(\nu)$ of $m$-type $(m=1,2)$, and $\kappa_i=s$ in case $\mathrm{r}\in T^{(s)}(\nu)$ $(s=1,2)$ for the point of instability $p(\nu)$.*

*Remark 2.* Formula (9) for the index of problem $R$ in class $H_0$ of bounded solutions, according to [10], takes the form:

$$\kappa=-4+\sum_{i=1}^{n}(3-\kappa_i). \tag{10}$$

The condition that the solution to problem $R$ belongs to class $H^*$ is the boundedness condition of the integral of the shell stretching energy [13, p. 83] in the vicinity of the corner point.

From formulas (9), (10), statement 4 follows.

*Statement 4. If boundary $L$ contains a single 1-type corner point, then problem $R$ is for sure solvable in class $H^*$ and has a unique solution $\forall\mathrm{r}\in T$; if $n\ge 2$, $n=n_1+n_2$, where $n_k$ — the number of corner points of $k$-type $(k=1,2)$, then, problem $R$ is quasi-stable with respect to $\mathrm{r}\in T$ with the order of quasi-correctness $s=2n_1+n_2-3$.*

If boundary $L$ contains instability points, then according to (9), problem $R$ in class $H^*$ is not quasi-stable with respect to field $\mathrm{r}\in T$. However, it is possible to distinguish such classes of fields with respect to which problem $R$ is quasi-stable with different orders of quasi-correctness. Classes of such fields can be set by choosing the direction of the generalized tangent in only one of the sectors $T^{(1)}(\nu)$, $T^{(2)}(\nu)$ at each point of instability $p(\nu)$.

*Remark 3.* As it is easy to see, formulas (9), (10) together with statement 4 are valid in the case:

$$\mu<\nu\le\frac{\pi}{2}+\omega^2, \tag{11}$$

where $\omega$ — a sufficiently small value given by surface $S$. At this, the condition of smallness $\omega$ is not mandatory. For example, for umbilical $(k_1=k_2)$ point $p(\nu)$, it is enough to put $\omega^2=\frac{\pi}{6}$.

Let us now consider 1-canonical dome $K$. In this case, the description of the special nodes of boundary condition (2) is also given by statement 2, with the only difference that in equality (4) and equation (6), value $\delta^2=\frac{k_2}{k_1}<1$ must be replaced by $\delta^2=\frac{k_1}{k_2}>1$. Here, for corner point $p(\nu)$ of instability of problem $R$, inequality (8) takes the form:

$$\mu\le\nu\le\arccos\frac{1}{1+\delta}. \tag{12}$$

Based on the obvious graphical analysis of equation (6), we conclude:

$1^\circ$ value $\mu=\operatorname{arcctg}\sqrt{t}$ is a function of two parameters, namely: $\mu=\mu(\delta,k_1)$, $k_1\in(0;+\infty)$, if $\delta^2=\frac{k_2}{k_1}<1$, and $\mu=\mu(\delta,k_2)$, $k_2\in(0;+\infty)$, if $\delta^2=\frac{k_1}{k_2}>1$;

$2^\circ$ $\lim\limits_{\delta\to 1-0}\mu(\delta,k_1)=\frac{\pi}{3}$, $\lim\limits_{\delta\to 0}\mu(\delta,k_1)=\frac{\pi}{2}$ $\forall k_1\in(0;+\infty)$, if $\delta^2=\frac{k_2}{k_1}$;

$3^\circ$ $\lim\limits_{\delta\to 1+0}\mu(\delta,k_2)=\frac{\pi}{3}$, $\lim\limits_{\delta\to+\infty}\mu(\delta,k_2)=0$ $\forall k_2\in(0;+\infty)$, if $\delta^2=\frac{k_1}{k_2}$;

$4^\circ$ for any fixed $\delta$ from the right (left) semineighborhood of the unit, function $\mu$ as a function of argument $k_2$ $(k_1)$ is a slowly changing function [14] in the sense that $\mu(\delta_0, k_j) \in \left(0, \frac{\pi}{2}\right)$ for any fixed $\delta = \delta_0$, $k_j \in (0; +\infty)$ $(j = 1,2)$.

**Research Results**. We submit for consideration a family of surfaces $S_\tau$, $\tau \in [0, \varepsilon)$, where $\tau$ — a small parameter, each of which is the median surface of a thin elastic shell $V_\tau$ from some family $\{V_\tau\}$, where $V_0$ and $S_0$ coincide with shell $V$ and surface $S$, respectively. We assume that for $\forall \tau \in [0, \varepsilon)$, the following conditions are met:

1) surface $S_\tau$ is a canonical dome of the regularity class $W^{3,r}$, $r > 2$, with internal angles of magnitude $\nu_j$ at corner points $p_i$ $(i = 1, ..., n)$ of boundary $L_\tau$, where surface $S_0$ is a 2-canonical (1-canonical) dome S with boundary L;

2) ratios of principal curvatures $k_1^{(\tau)}$, $k_2^{(\tau)}$ of surface $S_\tau$ at corner points, coincide with values $\delta^2$ at the corner points of surface $S$;

3) $k_j^{(\tau)} = k_j + \varepsilon_j(\tau)$, where $\lim\limits_{\tau \to 0} \varepsilon_j(\tau) = 0$, $k_j = k_j^{(0)}$ $(j = 1,2)$.

Let $J$ be the mapping of surface $S_\tau$ onto complex plane $z = x + iy$, given above, $D_\tau = J(S_\tau)$ — a family of simply connected regions with corresponding $\Gamma_\tau = J(L_\tau)$ and corner points $q_i = J(p_i)$, bounded in plane z. Consider a family of problems $R_\tau$, $\tau \in [0, \varepsilon)$,

$$w_{\bar{z}}(z) - B_\tau(z)\overline{w}(z) = F_\tau(z), \quad z \in D_\tau, \tag{13}$$

$$\operatorname{Re}\{\lambda_\tau(\zeta) w(\zeta)\} = \gamma_\tau(\zeta), \quad \zeta \in \Gamma_\tau, \tag{14}$$

where functions $B_\tau(z)$, $\lambda_\tau(\zeta)$, $\gamma_\tau(\zeta)$ are defined by the middle surface $S_\tau$ of shell $V_\tau$ according to [8], and $\lambda_\tau(\zeta)$ has form (3).

It is assumed that the lateral surfaces of shells $V_\tau$ have common edges containing points $p_i$ $(i = 1, ..., n)$. Note that problem (13), (14) $\forall \tau \in [0, \varepsilon)$ can be considered as a family of problems $R_\tau^{(r)}$, each of which is given by selecting a vector field on $S_\tau$ along $L_\tau$.

Consider 1-canonical dome S. Statement 4 is true.

*Statement 4. If in each of the corner points $p(\nu)$ of dome S, the following condition is met:*

$$\nu < \arccos \frac{1}{1+\delta}, \tag{15}$$

*then $\forall \tau \in [0, \varepsilon)$ problem $R_\tau$ is quasi-stable in class $H^*$ with respect to the field of directions of a generalized tangent with the order of quasi-correctness $s = 3n - 3$. If at each point $p(\nu)$, the following condition is met:*

$$\operatorname{arcctg} \sqrt{t + \omega_0^2} < \nu < \frac{\pi}{2} + \omega^2, \tag{16}$$

*where $\omega^2$ is determined by remark 3, value $\omega_0 = \omega_0(\varepsilon)$ is given by family $S_\tau$, $\tau \in [0, \varepsilon)$, then problem $R_\tau$ is quasi-stable in class $H^*$ with the order of quasi-correctness $s = 2n - 3$.*

For proof, it is enough to use statement 3, conditions 1–3 and the known properties [1, p. 97] of mapping $J$. Statement 4 remains valid for 2-canonical dome $S$, if conditions (15), (16) are replaced by the conditions:

$$\nu < \operatorname{arcctg} \sqrt{t - \omega_0^2}, \tag{17}$$

$$\arccos \frac{1}{1+\delta} < \nu < \frac{\pi}{2} + \omega^2 \tag{18}$$

respectively.

Now let us refine the concept of a corner point of $k$-type $(k = 1,2)$ of surface $S$. We say that point $p(\nu)$ of boundary $\Gamma$ is a 1-type (2-type) point relative to family $S_\tau$, $\tau \in [0, \varepsilon)$, if conditions (15) and (17) are met for 1-canonical and 2-canonical points, respectively, (conditions (16) and (18) for 1-canonical and 2-canonical points,

respectively). Consider canonical dome S, each corner point of which is a point of 1-type or 2-type relative to the specified family $S_\tau$. Then, the consequence of statement 4 is:

*Statement 5. If* $p$ *and* $q$ — the number of points of 1-type and 2-type, respectively $(p+q=n)$, *then* $\forall\tau\in[0,\varepsilon)$ *problem* $R_\tau$ *is for sure solvable in class* $H^*$ *and quasi-stable with respect to directions* r *of the generalized tangent with the order of quasi-correctness* $s=3p+2q-3$. *Specifically, if* $p=0$, *then* $q\geq 2$.

The statement remains valid if class $H^*$ is replaced by class $H_0$ of bounded in $D_\tau$ solutions, and order $s=3p+2q-3$ by order $s=2p+q-3$ provided $2p+q\geq 3$. Thus, problem $R_\tau$ is not unconditionally solvable in the following cases: $p=0$, $q\leq 2$ and $p=1$, $q=1$.

The case of an umbilical $(\delta=1)$ corner point $p(\nu)$, in which any direction is the main one, requires special consideration. In this case, according to[2] $\mu=\theta=\frac{\pi}{3}$, any direction of the generalized tangent is a special direction of problem $R$. However, even in this case, statement 4 remains valid if, for family $\{S_\tau\}$, we consider $\tau\neq 0$, and values ν, $\mu$ are replaced by value $\frac{\pi}{3}$.

**Discussion and Conclusions.** The results obtained can be used to construct mathematical models of thin and shallow shells of the positive Gaussian curvature with ribbed side surfaces. The most complete and advanced results of both linear and nonlinear elastic shell theory are obtained for thin shallow shells. A detailed discussion of the concept of "shallow shell", as well as a description of various versions of the theory is given in [15, p. 29]. The linear theory of flat convex curves was developed by I.N. Vekua [2, 16]. Within the framework of this theory, the issue of the realization of the equilibrium stress state of a shallow shell with a ribbed side surface, when a static boundary condition of a general form is met, is reduced to problem $R$ discussed above.

Let $P$ be a shallow shell [2, p. 164] with a ribbed side surface, $S$ — its median surface with a piecewise smooth edge. We assume that at each corner point of surface $S$, the condition of *strong shallowness* $k_1\approx k_2$ is satisfied, which is equivalent to the following:

$$\delta\approx 1, \tag{19}$$

where $\delta$ — any of the ratios $\frac{k_1}{k_2}$, $\frac{k_2}{k_1}$. Condition (19) means that any corner point $p(\nu)$ should be considered both a 1-canonical and a 2-canonical point. Consider corner point $p(\nu)$, at which $\nu\approx\frac{\pi}{3}$, and a family of surfaces $S_\tau$, $\tau\in[0,\varepsilon)$, given by conditions (1)–(3). According to properties 1°–4° of values $\theta$, $\mu$ and statement 2, the corresponding problem $R_\tau$ $\forall\tau\in(0,\varepsilon)$ is not quasi-stable in class $H^*$, i.e., point $p(\nu)$ at $\nu\approx\frac{\pi}{3}$ — the point of instability of problem $R_\tau$. In this case, the natural presumption is that in the right part of formula (10), value $\kappa_i$ $(1\leq i\leq n)$ corresponding to point $p(\nu)$ is a discrete random variable with possible values 1 and 2. Thus, if at each corner point $p(\nu)$ of the median surface, the condition $\nu\approx\frac{\pi}{3}$ is met, then, owing to formula (9), the order of quasi-correctness of problem $R$ is a discrete random variable taking values $m$, $m+1,\ldots$, $m+n$, where $n$ — the number of corner points, $m=2n-3$ for class of solutions $H^*$, and $m=n-3$ for class $H_0$.

[2] Tyurikov EV. Obobshchennaya granichnaya zadacha Goldenveizera dlya bezmomentnykh sfericheskikh kupolov.

The method proposed above can be used to construct mathematical models of the theory of thin shallow shells with ribbed side surfaces of any configuration. To do this, it is enough to use the results[3] on the solvability of problem $R$ for spherical domes with a piecewise smooth edge. Let us consider for definiteness, the median surface $S$ under the assumption that all the corner points $p(\gamma)$ of the boundary are "outgoing", that is, $\gamma < \pi$. In this case, a corner point on a spherical surface is a special node of the boundary condition if and only if $\gamma = \frac{\pi k}{3}$ $(k = 1,...,5)$. It follows that the "outgoing" corner point of the median surface of the shallow shell is an instability point if one of the following conditions is met: $\gamma \approx \frac{\pi k}{3}$ $(k = 1,2)$. Thus, formula (9) for the index can serve as validation for the following hypothesis:

*if problem $R$ for a shallow convex shell is unconditionally solvable in a given class of solutions, then its quasi-correctness order is a discrete random variable taking integer values $K$, $K+1,...,$ $K+N$, where $N$ — the number of instability points, $K$ — the number given by a set of corner points and a selection of continuous vector parameter* r.

In conclusion, we note that the same reasoning can serve as validation for this hypothesis, but carried out for regular convex surfaces satisfying the condition of *local symmetry* [17] at corner points.

**References**

1. Vekua IN. *Generalized analytical functions*. Moscow: Fizmatlit; 1988. 512 p. (In Russ.)

2. Vekua IN. *Nekotorye obshchie metody postroeniya razlichnykh variantov v teorii obolochek*. Moscow: Fizmatlit; 1982. 288 p. (In Russ.)

3. Goldenveizer AL. O primenenii reshenii zadachi Rimana–Gil'berta k raschetu bezmomentnykh obolochek. *Journal of Applied Mathematics and Mechanics*. 1951;15:149–166. (In Russ.)

4. Goldenveizer AL. *Teoriya tonkikh uprugikh obolochek*. Moscow: Nauka; 1976. 512 p. (In Russ.)

5. Tyurikov EV. Boundary Value Problems in the Theory of Infinitesimal Bendings of Surfaces of Positive Curvature with Piecewise Smooth Boundary. *Sbornik*: *Mathematics*. 1977;32:385–400.

6. Tyurikov EV. Obshchii sluchai smeshannoi granichnoi zadachi membrannoi teorii vypuklykh obolochek. *Issledovaniya po sovremennomu analizu i matematicheskomu modelirovaniyu*. 2011;5:225–229. (In Russ.)

7. Muskhelishvili NI. *Singulyarnye integral'nye uravneniya*. Moscow: Fizmatlit; 1968. 511 p. (In Russ.)

8. Vekua IN. Sistemy differentsial'nykh uravnenii pervogo poryadka ehllipticheskogo tipa i granichnye zadachi s primeneniem k teorii obolochek. *Sbornik: Mathematics*. 1952;31:217–314. (In Russ.)

9. Tyurikov EV. The Canonical Form of the Main Boundary Value Problem of the Membrane Theory of Convex Shells. *Global and Stochastic Analysis*. 2020;7:209–218.

10. Tyurikov EV. A Geometric Analogue of the Vekua–Goldenveizer Problem. *Doklady Mathematics.* 2009;79:83–86. https://doi.org/10.1134/S1064562409010256

11. Tyurikov EV. One Case of Quasi–Correctness of the Canonical Boundary Value Problem of the Membrane Theory of Convex Shells. *Global and Stochastics Analysis*. 2021;8:45–52.

12. Vekua IN. *Osnovy tenzornogo analiza i teorii kovariantov*. Moscow: Fizmatlit; 1978. 296 p. (In Russ.)

13. Landau LD, Lifshits EM. *Teoreticheskaya fizika*. *Teoriya uprugosti*. Moscow: Fizmatlit; 1965. 204 p. (In Russ.)

14. Tyurikov EV, Polyakov AS. On One Case of Quasi–Correctness of the Static Boundary Value Problem for Shells of Rotation. *Journal of Physics: Conference Series*. 2021;2131:022130. https://doi.org/10.1088/1742-6596/2131/2/022130

15. Voronich II. *Matematicheskie problemy nelineinoi teorii pologikh obolochek*. Moscow: Nauka; 1989. 376 p. (In Russ.)

16. Vekua IN. *Teoriya tonkikh pologikh obolochek peremennoi tolshchiny*. Tbilisi: Metsniereba; 1965. 101 p. (In Russ.)

17. Tyurikov EV. One Case of Extended Boundary Value Problem of the Membrane Theory of Convex Shells by I. N. Vekua. *Issues of Analysis*. 2021;7(S):153–162. https://doi.org/10.15393/j3.art.2018.5471

*About the Author:*

**Evgeniy V Tyurikov,** professor of the Advanced Mathematics Department, Don State Technical University (1, Gagarin sq., Rostov-on-Don, 344003, RF), Dr.Sci. (Phys.-Math.), associate professor, ORCID, etyurikov@hotmail.com

[3] Tyurikov EV. Obobshchennaya granichnaya zadacha Goldenveizera dlya bezmomentnykh sfericheskikh kupolov.

**Received** 10.01.2023.
**Revised** 06.02.2023.
**Accepted** 08.02.2023.

*Conflict of interest statement*
The author does not have any conflict of interest.

*The author has read and approved the final manuscript.*

*Об авторе:*
**Евгений Владимирович Тюриков**, профессор кафедры «Высшая математика» Донского государственного технического университета (344003, РФ, г. Ростов-на-Дону, пл. Гагарина, 1), доктор физико-математических наук, доцент, ORCID, etyurikov@hotmail.com

**Поступила в редакцию** 10.01.2023.
**Поступила после рецензирования** 06.02.2023.
**Принята к публикации** 08.02.2023.

*Конфликт интересов*
Автор заявляет об отсутствии конфликта интересов.

*Автор прочитал и одобрил окончательный вариант рукописи.*

MECHANICS
МЕХАНИКА





УДК 004.032.24
https://doi.org/10.23947/2687-1653-2023-23-1-26-33

*Original article*

# Validation of Reliability Indices during Experimental Development of a Complex Technical Series System

**Oleg Yu Tsarev** [1], **Yury A Tsarev** [2]

[1] "Business Solutions and Technologies" JSC, 5B, Lesnaya St., Moscow, Russian Federation

[2] Don State Technical University, 1, Gagarin sq., Rostov-on-Don, Russian Federation

✉ myaucha-pyt@yandex.ru

**Abstract**

***Introduction.*** The article studies the problem of validating the specified levels of reliability during experimental development of a complex technical series system. Such tasks arise when it is required to make a decision on testing the system as part of a larger one or on the completion of experimental development and the start of series production. The study is aimed at validating the reduction of the experimental development time. The task is to determine whether the hypothesis $H_o$ is accepted or rejected.

***Materials and Methods.*** To implement the research objective and task, a critical area described by the inequality was constructed based on the test results. The formulation of the requirements validation task was based on well-known approaches to testing statistical hypotheses. The conceptual apparatus of information theory, probability, and statistics was involved. The theoretical and applied literature on mathematical methods in reliability theory was studied. The particular tasks of the work were solved by known ways. Thus, the probability of obtaining the exact number of successful outcomes in a certain number of experiments was determined by the Bernoulli scheme. The exact confidence interval based on the binomial distribution was derived from the Clopper-Pearson relation. The theorem of A.D. Solovyov and R. A. Mirny made it possible to assess the system reliability based on the test results of its components.

***Results.*** Control rules adequate to the stage of experimental development (with insufficient data on the technical system) and the stage of series production were mathematically defined. The probability of a successful outcome when testing technical systems was represented by:

– the probability of event for a system element;

– confidence value;

– required scope of tests

In these terms, the null and alternative hypotheses and the corresponding reliability control procedures were investigated. Two provisions were considered. The first one provided using the null confidence hypothesis $H_o = \{P \geq P_T\}$ and an alternative $H = \{P < P_T\}$ to confirm the requirements $(\underline{P}_T, \gamma)$ for the reliability indicator of one parameter for any $(\underline{P}_T, \gamma)$. In this case, one trouble-free test was enough. The second provision considered a sequential technical system with independent elements that were tested separately from the system according to the Bernoulli scheme for one parameter. We considered the requirements for the system in the form of a set of values $(\underline{P}_T, \gamma)$ and the requirements for any of its elements $(\underline{P}_{Ti}, \gamma)$. They coincided when the planned outcome of the tests corresponded to the cases when the ratio $\underline{P} = \lim\limits_{1 \leq i \leq N} : \underline{P}_i = \underline{P}_m$ was fulfilled, and the null alternative hypothesis was selected from the theory of statistical hypothesis testing.

***Discussion and Conclusions.*** The experimental development strategy should be implemented in two stages: the search and validation of the reliability of the elements through a series of fail-safe tests. In this case, the planned scope of tests of each element is determined taking into account the confidence probability, the lower limit of the confidence interval, and the requirements for reliability indices of one parameter of the technical system. If the use of the null confidence hypothesis is acceptable, one fail-safe test is sufficient to confirm the requirements for the reliability index.

**Keywords:** experimental development, testing of statistical hypotheses, reliability of a technical system, null hypothesis, alternative hypothesis, hypothesis of distrust, confidence hypothesis, confidence probability, scope of fail-safe tests, binomial type test model, Bernoulli scheme, Clopper-Pearson equation, theorem of A. D. Solovyov and R. A. Mirny.

**Acknowledgements.** The authors would like to thank the reviewers, whose critical assessment of the submitted materials and suggestions contributed to a significant improvement in the quality of this article.

**For citation.** Tsarev OYu, Tsarev YuA. Validation of Reliability Indices during Experimental Development of a Complex Technical Series System. *Advanced Engineering Research (Rostov-on-Don).* 2023;23(1):26–33. https://doi.org/10.23947/2687-1653-2023-23-1-26-33

*Научная статья*

# Подтверждение показателей надежности при экспериментальной отработке сложной технической системы с последовательным соединением элементов

**О.Ю. Царев[1], Ю.А. Царев[2]**

[1] АО «Деловые решения и технологии», Российская Федерация, г. Москва, ул. Лесная, 5 б

[2] Донской государственный технический университет, Российская Федерация, г. Ростов-на-Дону, пл. Гагарина, 1

✉ myaucha-pyt@yandex.ru

**Аннотация**

***Введение.*** Статья посвящена проблеме подтверждения заданных уровней надежности при экспериментальной отработке сложной технической системы с последовательным соединением элементов. Такие задачи возникают, когда требуется принять решение об испытании системы в составе более крупной или об окончании экспериментальной отработки и запуске серийного производства. Цель исследования — обосновать сокращение сроков экспериментальной отработки. Задача — определить, принимается или отклоняется гипотеза $H_o$.

***Материалы и методы.*** Для реализации цели и задачи работы по результатам испытаний строится критическая область, описываемая неравенством. Формулировка задачи подтверждения требований базируется на известных подходах к проверке статистических гипотез. Задействуется понятийный аппарат теории информации, вероятности и статистики. Изучена теоретическая и прикладная литература о математических методах в теории надежности. Частные задачи работы решены известными способами. Так, вероятность получения точного числа успешных исходов в определенном количестве экспериментов определена по схеме Бернулли. Точный доверительный интервал, основанный на биномиальном распределении, получен из соотношения Клоппера — Пирсона. Теорема А. Д. Соловьева и Р. А. Мирного позволила оценить надежность системы по результатам испытаний ее компонент.

***Результаты исследования.*** Математически определены правила контроля, адекватные этапу экспериментальной отработки (при недостаточности данных о технической системе) и этапу серийного производства. Вероятность успешного исхода при испытании технических систем представлена через:

– вероятность события для элемента системы;

– значение доверительной вероятности;

– требуемый объем испытаний.

С этих позиций исследованы нулевая и альтернативная гипотезы и соответствующие им процедуры контроля надежности. Рассмотрены два положения. Первое допускает использование нулевой гипотезы доверия

$H_o = \{P \geq P_T\}$ с альтернативой $H = \{P < P_T\}$ для подтверждения требований $(\underline{P}_T, \gamma)$ к показателю надежности одного параметра при любых $(\underline{P}_T, \gamma)$. При этом достаточно одного безотказного испытания. Второе положение рассматривает последовательную техническую систему с $N$ независимыми элементами, которые испытываются отдельно от системы по схеме Бернулли для одного параметра. Рассмотрим требования к системе в виде совокупности величин $(\underline{P}_T, \gamma)$ и требования к любому ее элементу $(\underline{P}_{Ti}, \gamma)$. Они совпадают, если планируемый исход испытаний соответствует случаям выполнения соотношения $\underline{P} = \lim\limits_{1 \leq i \leq N} : \underline{P}_i = \underline{P}_m$, а нулевая альтернативная гипотеза выбирается из теории проверки статистических гипотез.

***Обсуждение и заключения.*** Стратегию экспериментальной отработки следует реализовать в два этап: поиск и подтверждение надежности элементов серией безотказных испытаний. В этом случае планируемый объем испытаний каждого элемента определяется с учетом доверительной вероятности, нижней границы доверительного интервала и требований к показателям надежности одного параметра технической системы. Если допустимо использование нулевой гипотезы доверия, для подтверждения требований к показателю надежности достаточно одного безотказного испытания.

***Ключевые слова*:** экспериментальная отработка, проверка статистических гипотез, надежность технической системы, нулевая гипотеза, альтернативная гипотеза, гипотеза недоверия, гипотеза доверия, доверительная вероятность, объем безотказных испытаний, модель испытаний биномиального типа, схема Бернулли, уравнение Клоппера — Пирсона, теорема А. Д. Соловьева и Р. А. Мирного.

**Благодарности.** Авторы выражают благодарность рецензентам, чья критическая оценка представленных материалов и высказанные предложения по их усовершенствованию способствовали значительному повышению качества настоящей статьи.

**Для цитирования:** Царев О.Ю., Царев Ю.А. Подтверждение показателей надежности при экспериментальной отработке сложной технической системы с последовательным соединением элементов. *Advanced Engineering Research (Rostov-on-Don).* 2023;23(1):26–33. https://doi.org/10.23947/2687-1653-2023-23-1-26-33

**Introduction.** Rational methods of validating the specified reliability levels are of current concern for experimental testing of a complex technical system when a decision is made on the possibility of testing it as part of a larger structure or on the completion of experimental development and the start of series production. The same tasks arise during series production, if it is required:

– to assess the readiness of the enterprise to produce series products based on the test data of the pilot batch;

– to make a conclusion about the compliance of the products with the requirements of technical documentation, taking into account the operating data.

The study objective was to obtain an acceptable solution for planning and reducing the scope of tests using methods of interval estimation of reliability indices of sequential technical systems. To achieve the stated goal, it was required to determine whether hypothesis $H_o$ was accepted or rejected.

**Materials and Methods.** It is reasonable to formulate the task of validating the requirements in terms of the theory of statistical hypothesis testing [1–4]. Let $P$ be the reliability of the technical system, $P_T$ — some fixed (required) level for $P$. Prior to testing about $P$, three initial assumptions can be made: $P = P_T$, $P \leq P_T$, $P > P_T$.

Each of them is called a null hypothesis if it is written as:

$$H_o = \{P = P_T\}, H_o = \{P \leq P_T\}, H_o = \{P > P_T\}.$$

Set $H_o = \{P = P_T\}$ contains only one element, therefore, hypothesis $H_o = \{P = P_T\}$ is called simple. Hypotheses of the form $H_o = \{P \leq P_T\}$ and $H_o = \{P > P_T\}$ are called complex. Along with the null hypothesis expressing a pre-formulated point of view, an alternative hypothesis $H$ is specified expressing the opposite statement $H_o(H_o \cap H = \Omega)$. We use the conceptual apparatus of the theory of information [1], probability and statistics, applicable to solving such problems. Consider two aggregates of sets $H_o$ and $H$:

$$H_o = \{P \leq P'_T\}, H = \{P > P'_T\}, \quad (1)$$

$$H_o = \{P \geq P_T\}, H = \{P < P_T\}. \quad (2)$$

Hypothesis $H_o$ in (1) will be called rigid, or the distrust hypothesis. Indeed, in case (1), initially (before the test), we proceed from a position of distrust of the quality level of the system. Reliability index $P$ is assumed to be no higher than a certain fixed level $P'_T$. Hypothesis $H_o$ in (2) will be called the confidence hypothesis, since in this case, it is initially assumed that reliability index $P$ is not less than some fixed value $P_T$.

The meaning of values $P'_T$ and $P_T$ is different. In (1), $P'_T$ — such a rejected value that at $P \le P'_T$, the system is considered unacceptable. In (2), $P_T$ — such a value that at $P \ge P_T$, the system is considered acceptable for use. Obviously, $P_T > P'_T$.

**Research Results.** Thus, it is required to determine whether hypothesis $H_o$ is accepted or rejected. In the theory of statistical hypotheses, a critical area is constructed for this purpose based on the test results. It is described by some inequality. Moreover, the null hypothesis (due to the initial confidence in it) is adhered to as long as it is reasonable from the point of view of the accepted level of significance α. Therefore, as is already clear that the reliability control procedure in case (1) will be significantly different compared to case (2).

Indeed, we will further make sure that to reject hypothesis $H_o$ in (1) and accept hypothesis $H = \{P > P'_T\}$ of meeting the requirement for reliability indices, a critical area (or condition) should be used

$$\underline{P} > \underline{P}'_T, \tag{3}$$

where $\underline{P}$ — the lower bound of the confidence interval for $P$ at the value of the confidence probability $\gamma = 1 - \alpha$; $\underline{P}'_T$ — the lower bound of the rejected interval for $P$ at the value of confidence probability $\gamma = 1 - \alpha$.

In case (2), the condition should be used to accept hypothesis $H_o$ about the compliance of the value of parameter $P$ to the requirement

$$\overline{P} \ge P_T, \tag{4}$$

where $\overline{P}$ — the upper bound of the confidence interval for $P$ at the value of the confidence probability $\gamma = 1 - \alpha$.

In (3) and (4), the requirement for the reliability index of one parameter $P$ is understood as a set of values $(\underline{P}'_T, \gamma)$ or $(\underline{P}_T, \gamma)$, given before testing.

Let one successful test be carried out under the conditions of the Bernoulli scheme. Then, using the Clopper-Pearson relations, we find the lower and upper bounds of one parameter with the value, for example, $\gamma = 0.95$:

$$\underline{P} = (1 - \gamma)^{1/1} = 1 - \gamma = 0.05;\ \overline{P} = 1.$$

Here, even for very moderate values $\underline{P}'_T \in [0.05;\ 0.95]$, condition (3) is not fulfilled, while (4) is fulfilled at any $P_T$. Let us show the validity of the accepted position.

First position. If it is permissible to use the null confidence hypothesis $H_o = \{P \ge P_T\}$ with alternative $H = \{P < P_T\}$, then one fail-safe test is sufficient to confirm the requirements $(\underline{P}_T, \gamma)$ for the reliability index of one parameter for any $(\underline{P}_T, \gamma)$.

If the initial hypothesis $H_o$ is the hypothesis of distrust from (1), then a significantly larger number of tests are needed. Thus, for $m = 0$, we get $n \ge log(1 - \gamma) / log \underline{P}_T >> 1$. This is quite fair, because, when testing hypotheses, they initially proceed from the validity of the null hypothesis $H_o$.

At the stage of experimental development, there are no sufficiently complete data, therefore, it is reasonable to use control rule (3). At the stage of series production, one can proceed from the confidence hypothesis and use a significantly easier control rule (4). This is acceptable if, according to the experimental testing, condition (3) was fulfilled.

Consider a system consisting of $N$ independent elements connected in series, which can be tested separately. Then, the probability of a successful outcome when testing technical systems:

$$P = \prod_i^N P_i. \tag{5}$$

Here, $P_i$ — probability of the same event for the *i*-th element. The requirements for value *P* are specified in the form of a set of values $(\underline{P}_T, \gamma)$. It is required to plan a procedure for monitoring the reliability of one parameter for each element of the system, i.e., to specify $\forall i \in [1, n]$ a pair $(\underline{P}_{Ti}, \gamma)$.

Due to the multiplication of $P_i$ in formula (5), ratio $\prod_i^N P_{Ti} = P$ must be fulfilled. Besides, $\gamma_i = \gamma$.

As a result, the required scope of tests $n_i$ of each element increases dramatically, and even with fail-safe results of all tests, it becomes unacceptable. At $\underline{P}_T = 0.9$ and $\gamma = 0.95$, $N = 100$ and $m = 0$, $\forall i = 1, N$:

$$P_{Ti} \sim \underline{P}_T^{1/100} = 0.999,\ n_{oi} = log(1 - \gamma) / logP_{Ti} \sim 3000.$$

This method of planning is logically contradicted by inequality $n_{oi} > n_o$, following from $P_{Ti} > \underline{P}_T$ when $m_i = 0$. It is clear that with fail-safe outcomes, the required scope of tests $n_{oi}$ of *i*-th element, conducted separately from the system, should be equal to the required scope of tests of system $n_o$. To avoid this contradiction, the theorems of A.D. Solovyov and R.A. Mirny should be used [5–7]. Thus, when $m = 0$, $\forall i = 1, N$:

$$\underline{P} = \min_{1 \le i \le N} : \underline{P}_i = f\ (n,\ 0,\ \gamma) = (1 - \gamma)^{1/n}. \quad (6)$$

Here, $\underline{P}$ — the lower bound of the confidence interval for the reliability index of a technical system by one parameter, at value $\gamma$ of the confidence probability; $\underline{P}_i$ — the value of the lower bound of the confidence interval for the reliability index of the *i*-th element of the system with the same confidence probability; *n* — minimum number of tests of system elements; $f(n, 0, \gamma)$ — the root of the Clopper-Pearson equation:

$$1 - \gamma = \sum_{k=0}^{m} \binom{n}{k} P^{n-k} q^k = B(n,\ P,\ m). \quad (7)$$

According to [8–12]:

$$f(n, n\bar{q}, \gamma) \le P \le f(n,\ [n\bar{q}], \gamma). \quad (8)$$

Here, $\bar{q} = 1 - P$; $P = \prod_{i=1}^{N} (1 - m_i / n_i)$; $n = \min_{1 \le i \le N} n_i$; $[n\bar{q}]$ — integral part of the product $n\bar{q}$; $f(n, n\bar{q}, \gamma)$ — root of equation $J_P(n, P, n\bar{q} + 1) = 1 - \gamma$.

From (8), it follows:

$$\underline{P} = \min_{1 \le i \le N} : \underline{P}_i = \underline{P}m, \quad (9)$$

where $\underline{P}_m$ — minimum of $\underline{P}_i$ at the value of confidence probability $\gamma$.

$$P_m = \min_{1 \le i \le N} : \underline{P}_i \ge P_T \Leftrightarrow (\underline{P}_1 \ge P_T) \cap (\underline{P}_2 \ge P_T) \ldots \cap (\underline{P}_N \ge P_T).$$

This is true not only for case (1), when $m = 0$, $\forall i = 1, N$, but also for case (2), i.e., for the outcome $n = (n_1, n_2, \ldots, n_N)$, $m = (m_1, 0, 0, \ldots, 0)$ of the tests, where *n* and *m* — the vector of tests and the vector of failures, if $n_1 = n$.

At this, only one element that has been tested a minimum number of times fails. Indeed, in this case, $n\bar{q} = m_1$ — an integer. Calculations allowed us to establish that (9) is also approximately performed at the outcome of tests *n, m*, i.e., in case (3), if for pair $(n_1, m_1)$, $\min_{1 \le i \le N} : \underline{P}_i = \underline{P}_m$ is possible.

In all the cases mentioned (9), the lower bounds are not multiplied, and the system degenerates into one weakest element. This provides validating the following position.

Second position. Consider a sequential system with *N* independent elements that are tested separately from the system according to the Bernoulli scheme for one parameter. The requirements specified for the system in the form of a set of values $(\underline{P}_T, \gamma)$, and the requirements for any of its elements $(\underline{P}_{Ti}, \gamma_i)$ coincide if the planned outcome of the tests corresponds to the mentioned cases of fulfillment of ratio (9), and the null alternative hypothesis is selected based on (1) and (2).

Consequence. In case of (3), execution of (9) — the planned scope of fail–safe tests $(N - 1)$ of elements, it is determined from:

$$n_i \ge n_0 = log\ (1 - \gamma)\ /\ log \underline{P}_T. \quad (10)$$

The volume of failures of the conditionally first element at $m_1$ is from the ratio:

$$\underline{P}_1 = f(n_1, m_1, \gamma) = \underline{P}_T . \quad (11)$$

Proof (11) is based on the fact that the condition $\underline{P} = P_H \geq \underline{P}_T$ is fulfilled if $P_H = \underline{P}_1 = \underline{P}_T$ and $\underline{P}_1 \leq \forall i \in [2, N]$. The latter relation is satisfied if (10) is satisfied, because:

$$n_i \geq n_0 \Leftrightarrow \underline{P}_i = (1 - \gamma)^{1/ni} \geq \underline{P}_T .$$

In all the cases considered, it was assumed that there was no information about $P$ before the tests, except for the obvious fact $P \in [0, 1]$. However, it may be known that $P \geq P_H$, where $P_H = 0$. Hence, $P = \dot{P} \in [P_H, 1]$. Value $P_H$ can be found from test data or calculations at the time of planning reliability tests. There is no method for determining $P_H$ yet, and its development is the task of future research. But if value $P_H$ is known, according to the full probability formula, you can find:

$$\dot{P} = P + \bar{q}\underline{P} .$$

From here:

$$P = (\dot{P} - P_H)/(1 - P_H), \ \underline{P} = (\underline{\dot{P}} - P_H)/(1 - P_H) . \quad (12)$$

The latter relation is fulfilled due to monotonicity of dependence $P = (\underline{\dot{P}} - P_H)$ in $\dot{P}$:

Taking into account (12), ratio (2) will take the form:

$$P_H + (1 + P_H) f(n, n\bar{q}, \gamma) \leq \underline{\dot{P}} \leq P_H + (1 - P_H) f(n, [n\bar{q}], \gamma) . \quad (13)$$

Let the condition for making a decision on the compliance of the technical system with the requirements $(\underline{P}_T, \gamma)$ still be (3), where the lower bound of the confidence interval is determined from (13), taking into account $P = \underline{\dot{P}} \in [P_H, 1]$. Then, from the ratio:

$$\underline{\dot{P}} \geq \underline{P}_T \quad (14)$$

we find the planned scope of trouble-free tests by one parameter for each of $N$ elements:

$$n_i \geq n'_0 = log(1 - \gamma) \ log(\underline{P}_T - P_H) \ / \ (1 - P_H) . \quad (15)$$

Value $n'_0$ decreases in $P_H$. It means, $n_0$ (10) at $P_H = 0$ and $n'_0 = 0$ at $P_H = \underline{P}_T$.

Example. The requirements for the reliability indices $P = \prod_i^N P_i$ of the system are specified for one parameter in the form of a set of values ($\underline{P}_T = 0.90$; $\gamma = 0.95$). Number of elements of the technical system is $N = 100$. According to available data, $\underline{P}_T > P_H = 0.70$. It is required to find the planned scope of tests for each of $N$ elements, if the fulfillment of reliability requirements is checked by condition (14). From (15), we find:

$$n_i \geq n'_0 = log\ (0.05) / log\ (0.90 - 0.70) / (1 - 0.70) = 7.$$

Note that at $P_H = 0$ $n_i \geq n'_0 = 29$.

Ratios (10) and (15) make it possible to plan the required scope of testing of the $i$-th element of the technical system with a certain sequence of experimental development of the system. The whole process of experimental development is divided conditionally into two periods: the search and validation of reliability requirements for a decision on the transition to the next stage of testing or on the acceptance of a technical system for series production. In the first period, improvements are possible, and it is reasonable to use models with a variable probability $P$ of a successful outcome of the system test.

The data obtained in the first period can be used to calculate value $P_H$.

In the second period, we deal with an established version of the design of the technical system and technological process. This makes it possible to use the binomial type test models discussed above with constant probability $P$.

Let the first period of developing $N$ elements of the technical system be completed, then, the question is raised about validating the requirements for the reliability index of the system by one parameter. It is reasonable to validate reliability if a positive decision is made only in case of a fail-safe outcome of the last series of tests for each of $N$ elements. This strategy is convenient because it is based on the minimum possible number of tests of elements of the technical system and provides simple analytical solutions (10) and (15).

In general, it makes sense to investigate a strategy that allows for failures of elements during testing and is based on optimization of some objective function. But here, we restrict ourselves to considering only the mentioned strategy with fail-safe final series.

**Discussion and Conclusions.** The results of scientific research allowed us to formulate the following conclusions.

1. Even with a large number of *N* elements of the system, it is possible to plan the scope of their tests. In this case, the methods of interval estimation of reliability indices of sequential technical systems provide obtaining an acceptable solution, but only for one parameter.

2. The strategy of experimental development of technical systems is closely related to the method of validating the reliability of elements. The rational strategy of experimental development provides for confirmation of the reliability of the elements after the search period through a final series of fail-safe tests. In this case, the planned scope of tests of each of *N* elements does not depend on *N* and is determined by ratio (15), which includes the requirements ($\underline{P}_T$, γ) for the reliability indices of one parameter of the technical system as a whole and $P_H$. The scope of tests obtained by (15) for each element of the technical system, for any number of them, is small if moderate requirements ($\underline{P}_T$ = 0.80 …0.95; γ = 0.90 … 0.95) are specified for a system of *N* elements, but only for one parameter. At the same time, the scope decreases with increasing value $P_H$.

3. In series production, when testing upgraded technical systems, it is possible to use a control method with null and alternative hypothesis change. If the use of the null confidence hypothesis is acceptable, then one fail-safe test is sufficient to validate the requirements for the reliability index.

**References**

1. Belov VM, Novikov SN, Solonskaya OI. *Teoriya informatsii*. Moscow: GLT; 2012. 143 p. (In Russ.)

2. Godin AM. *Statistika*. Moscow: Dashkov i K°; 2016. 451 p. (In Russ.)

3. Müller K. The New Science of Cybernetics: A Primer. *Journal of Systemics, Cybernetics and Informatics*. 2013;11:32–46.

4. Hamdy A Taha. *Operations Research*: *An Introduction*, 9th ed. New York: Prentice Hall; 2011. 813 p.

5. Pavlov IV. Confidence Limits for System Reliability Indices with Increasing Function of Failure Intensity. *Journal of Machinery Manufacture and Reliability*. 2017;2:70–75.

6. Gnedenko BV, Belyaev YuK, Solovyev AD. *Matematicheskie metody v teorii nadezhnosti*. Moscow: Librokom; 2013. 584 p. (In Russ.)

7. Betsch S, Ebner B. Fixed Point Characterizations of Continuous Univariate Probability Distributions and their Applications. *Annals of the Institute of Statistical Mathematics*. 2021;73:31–59. https://doi.org/10.48550/arXiv.1810.06226

8. Nakakita SH, Kaino Y, Uchida M. Quasi-Likelihood Analysis and Bayes-Type Estimators of an Ergodic Diffusion Plus Noise. *Annals of the Institute of Statistical Mathematics*. 2021;73:177–225. https://doi.org/10.1007/s10463-020-00746-3

9. Pavlov IV, Razgulyaev SV. Lower Confidence Limit for Mean Time between Failures in a System Featuring Repairable Components. *Herald of the Bauman Moscow State Technical University, Series: Natural Sciences*. 2018;5:37–44. http://dx.doi.org/10.18698/1812-3368-2018-5-37-44

10. Fishwick P. (ed.) *Handbook of Dynamic Systems Modeling*. New York: CRC Press; 2007. 760 p. https://doi.org/10.1201/9781420010855

11. Antonov AV, Malovik KN, Chumakov IA. Interval Estimation of the Reliability Characteristics for Unique Equipment. *Fundamental Research*. 2011;12(1):71–76.

12. Gvozdev VE, Abdrafikov MA, Akhunyanova KB. Interval Estimation of Reliability Parameters Based on Methodology FMEA. *Vestnik UGATU*. 2014;65:91–98.

*About the Authors:*

**Oleg Yu Tsarev,** consultant, “Business Solutions and Technologies” JSC (5B, Lesnaya St., Moscow, 127055, RF), ORCID, myaucha-pyt@yandex.ru

**Yury A Tsarev,** professor of the Engineering and Maintenance of Transporting and Manufacturing Systems Department, Don State Technical University (1, Gagarin sq., Rostov-on-Don, 344003, RF), Dr.Sci. (Eng.), professor, ycarev@donstu.ru

*Claimed contributorship:*

OYu Tsarev: basic concept formulation; research objectives and tasks; computational analysis; text preparation; drawing conclusions. YuA Tsarev: academic advising; analysis of the research results; revision of the text; correction of the conclusions.

**Received** 09.01.2023.
**Revised** 01.02.2023.
**Accepted** 06.02.2023.

*Conflict of interest statement*

The authors do not have any conflict of interest.

*All authors have read and approved the final manuscript.*

*Об авторах:*

**Олег Юрьевич Царев,** консультант АО «Деловые решения и технологии» (127055, Российская Федерация, г. Москва, ул. Лесная, 5 б), ORCID, myaucha-pyt@yandex.ru

**Юрий Александрович Царев,** профессор кафедры «Проектирование и технический сервис транспортно-технологических систем» Донского государственного технического университета (344003, Российская Федерация, г. Ростов-на-Дону, пл. Гагарина, 1), доктор технических наук, профессор, ycarev@donstu.ru

*Заявленный вклад соавторов*

О.Ю. Царев — формирование основной концепции, цели и задачи исследования, проведение расчетов, подготовка текста, формулирование выводов. Ю.А. Царев — научное руководство, анализ результатов исследований, доработка текста, корректировка выводов.

**Поступила в редакцию** 09.01.2023.
**Поступила после рецензирования** 01.02.2023.
**Принята к публикации** 06.02.2023.

*Конфликт интересов*

Авторы заявляют об отсутствии конфликта интересов.

*Все авторы прочитали и одобрили окончательный вариант рукописи.*

MECHANICS
МЕХАНИКА





UDC 539.3
https://doi.org/10.23947/2687-1653-2023-23-1-34-40

*Original article*

# Method for Solving the Problem of Load Movement over the Ice Cover of a Reservoir along a Complex Trajectory

**Alexander V Galaburdin**
Don State Technical University, 1, Gagarin sq., Rostov-on-Don, Russian Federation
✉ galaburdin@mail.ru

**Abstract**

***Introduction.*** The development of the polar regions of the World Ocean contributed to an increased interest in studying wave processes in water bodies with ice cover caused by the action of a mobile load. In most papers of domestic and foreign scientists, the ice sheet was considered as an elastic or viscoelastic plate loaded with a rectilinearly moving vertical force. However, when modeling the impact of vehicles on the ice cover, it is of interest to investigate problems in which the force moves along a more complex trajectory. Therefore, this study aims at developing a method for studying the behavior of the ice cover under the action of a force moving along a trajectory of a complex shape, obeying an arbitrary law of motion.

***Materials and Methods.*** A method for solving problems of the action of an arbitrarily moving force on the ice cover of a reservoir of finite depth filled with an inviscid incompressible fluid is proposed. The ice cover was considered as a viscoelastic plate lying on the surface of a liquid in a state of potential flow. A concentrated force moving along an arbitrary closed trajectory and being periodic in time was applied to the upper surface of the plate. Hydrodynamic pressure acted on the lower surface of the plate from the liquid side. Due to the periodicity of the load applied to the plate, an integral time transformation was used to solve differential equations describing the behavior of this system. Further, using traditional methods, formulas were obtained for calculating stresses and displacements in the plate and components of the velocity vector of liquid particles. These formulas were presented in the form of an iterated integral. Numerical methods were used to calculate integrals.

**Results.** Calculations showed that the deflection of the ice cover increased markedly with the growth of speed and tangential acceleration of the load movement. An increase in the relaxation time of ice and a decrease in the radius of the trajectory of the load also caused an increase in deflection. The distribution of the fluid particle velocity vector over the depth of the reservoir was calculated.

***Discussion and Conclusions.*** The proposed method has shown its efficiency in solving problems about the impact of a moving load on the ice cover of a reservoir. With its help, the influence of the curvature of the trajectory of motion and the mechanical properties of ice, the kinematic characteristics of the movement of the load on the deflection of the ice cover was investigated. The method simulates the impact of vehicles on the ice cover of a reservoir. The results of its application can be used under the construction of ice roads or airdromes on ice.

**Keywords:** infinite ice cover, moving load, arbitrary closed trajectory, variable speed.

**Acknowledgements.** The author would like to thank the reviewers for the specified comments that improved the quality of the article.

**For citation.** Galaburdin AV. Method for Solving the Problem of Load Movement over the Ice Cover of a Reservoir along a Complex Trajectory. *Advanced Engineering Research (Rostov-on-Don).* 2023;23(1):34–40. https://doi.org/10.23947/2687-1653-2023-23-1-34-40

*Научная статья*

# Метод решения задачи о движении нагрузки по ледяному покрову водоема по сложной траектории

**А.В. Галабурдин**

Донской государственный технический университет, Российская Федерация, г. Ростов-на-Дону, пл. Гагарина, 1

✉ galaburdin@mail.ru

**Аннотация**

***Введение.*** Освоение полярных районов Мирового океана способствовало повышению интереса к изучению волновых процессов в водоемах с ледяным покровом, обусловленных действием подвижной нагрузки. В большинстве работ отечественных и зарубежных ученых ледяной покров рассматривался как упругая или вязкоупругая пластина, нагруженная прямолинейно движущейся вертикальной силой. Однако при моделировании воздействия транспортных средств на ледяной покров представляет интерес рассмотрение задач, в которых сила движется по более сложной траектории. Поэтому целью данного исследования является разработка метода исследования поведения ледяного покрова под действием силы, движущейся по траектории сложной формы, подчиняясь произвольному закону движения.

***Материалы и методы.*** Предложен метод решения задач о действии движущейся произвольным образом силы по ледяному покрову водоема конечной глубины, заполненного невязкой несжимаемой жидкостью. Ледяной покров рассматривался как вязкоупругая пластина, лежащая на поверхности жидкости, находящейся в состоянии потенциального течения. На верхнюю поверхность пластины приложена сосредоточенная сила, движущаяся по произвольной замкнутой траектории и являющаяся периодической по времени. На нижнюю поверхность пластины со стороны жидкости действует гидродинамическое давление. В силу периодичности приложенной к пластине нагрузки при решении дифференциальных уравнений, описывающих поведение данной системы, использовали интегральное преобразование по времени. Далее, применяя традиционные методы, получили формулы для вычисления напряжений и перемещений в пластине и компонент вектора скорости частиц жидкости. Эти формулы представили в виде повторного интеграла. Для вычисления интегралов использовали численные методы.

***Результаты исследования.*** Расчеты показали, что прогиб ледяного покрова заметно увеличивается с ростом скорости и касательного ускорения движения нагрузки. К росту прогиба также приводят увеличение времени релаксации льда и уменьшение радиуса траектории движения нагрузки. Рассчитано распределение вектора скорости частиц жидкости по глубине водоема.

***Обсуждение и заключения.*** Предложенный метод показал свою эффективность при решении задач о действии подвижной нагрузки на ледяной покров водоема. С его помощью исследовано влияние на прогиб ледяного покрова кривизны траектории движения и механических свойств льда, кинематических характеристик движения нагрузки. Метод моделирует воздействие транспортных средств на ледяной покров водоема. Результаты его применения могут быть использованы при строительстве ледовых дорог или аэродромов на льду.

**Ключевые слова:** бесконечный ледяной покров, движущаяся нагрузка, произвольная замкнутая траектория, переменная скорость.

**Благодарности.** Автор выражает благодарность рецензентам за указанные замечания, которые позволили повысить качество статьи.

**Для цитирования.** Галабурдин А.В. Метод решения задачи о движении нагрузки по ледяному покрову водоема по сложной траектории. *Advanced Engineering Research (Rostov-on-Don).* 2023;23(1):34–40. https://doi.org/10.23947/2687-1653-2023-23-1-34-40

**Introduction.** Recently, in connection with the development of the northern territories and areas of the World Ocean, great attention has been paid to the studying the behavior of the ice cover under the action of external load. A large number of works by domestic and foreign scientists are devoted to these issues. The impact of a pulsed moving load on a viscoelastic floating plate was considered in [1]. The effect of a moving load on the ice cover frozen to the channel walls was presented in [2, 3]. The fluctuations of the ice cover caused by a load moving at a constant speed

were considered in [4]. The behavior of a semi-infinite ice sheet under the action of a uniformly moving load on it was studied in [5]. The propagation of waves excited along a channel with an ice cover was discussed in [6]. In [7], nonlinear models were used in simulation. The monograph [8] presented the results of studies of surface waves in a sea with a floating broken and solid ice cover. The ice failure under the action of a moving load was considered in [9]. In the above works, the rectilinear load movement was mainly considered. The objective of this study was to develop a method for solving the problem of the impact of a force moving across the ice cover in an arbitrary way. Achieving this goal makes it possible to more accurately simulate the impact on the ice cover of vehicles, whose movement often occurs along rather complex trajectories and according to a complex law.

**Problem Statement.** The oscillations of an infinite ice cover lying on the surface of a reservoir of finite depth under the action of a force moving arbitrarily along a closed trajectory were considered. The ice cover was modeled by a thin viscoelastic plate, whose mechanical properties were described by the Kelvin-Voigt model. The reservoir was filled with an incompressible liquid.

**Materials and Methods.** The ice cover bending was described by the differential equation [7]:

$$(1+\tau_o\partial_t)\Delta^2 W + c^{-2}\partial_t^2 W + kW + b\partial_t\Phi|_{z=0} = \frac{P(x,y,t)}{D}, \quad (1)$$

where $W(x,y,t)$ — ice cover deflection; $D=Eh^3/(12(1-\mu^2))$; $E$ — Young's modulus; $\mu$ — Poisson's ratio; $h$ — thickness of the ice cover; $\tau_o$ — relaxation time of deformations; $\Delta^2=\partial_x^4+2\partial_x^2\partial_y^2+\partial_y^4$; $\rho_л$ — ice density; $\rho_в$ — water density; $c^{-2}=\rho_л h/D$, $k=\rho_в g/D$, $b=\rho_в/D$; $P(x,y,t)$ — load acting on the ice surface; $\Phi(x,y,z,t)$ — potential of fluid movement. The fluid behavior was subject to the equation:

$$\Delta\Phi=0.$$

Boundary conditions at the ice-water interface at $z=0$ and at the bottom of the reservoir $z=-H$ ($H$ — reservoir depth) had the form:

$$\partial_t W=\partial_z\Phi|_{z=0},\ \partial_z\Phi|_{z=-H}=0.$$

It was supposed that force $P(x, y, t)$ moved along an arbitrary closed trajectory $\gamma$ in an arbitrary way. It was assumed that $P=P(s(t))$, where $s$ — arc coordinate measured from some fixed point of the curve $\gamma$. If function $s(t)$ was periodic with period $T$, then it was quite obvious that value $P(s(t))$, would also be periodic, and also with period $T$. The parametric assignment of the trajectory was taken as:

$$\begin{cases} x = x_o(t) \\ y = y_o(t) \end{cases},$$

where $t$ — time.

Considering the steady-state process and applying the integral transformation with respect to variables $x$ and $y$ as well as the final integral transformation with respect to $t$ on the interval $[0; T]$, we obtained:

$$(1-i\omega_n\tau_o)\,p^4 W_0 - c^{-2}\omega_n^2 W_0 + kW_0 + bi\omega_k\Phi_0|_{z=0} = P_0/D,$$
$$\partial_z^2\Phi_0 - p^2\Phi_0 = 0,$$

where $W_0$, $\Phi_0$ — images of unknown functions $W$ and $\Phi$, $p^2=\lambda^2+\alpha^2$; $\lambda$; $\alpha$ — parameters of integral transformations, respectively, by variables $x$ and $y$; $\omega_n=2\pi n/T$, $n=0, 1, 2, 3, \ldots$ . Solving the second equation allowing for the boundary conditions, we obtained:

$$\Phi_0=-i\omega_n W_0 ch(p(z+H))/psh(pH).$$

Then, the first equation followed:

$$W_0=P_0/((c^{-2}+bcth(pH)/p)\,\omega_n^2-p^4-k+i\,\omega_n\tau_o p^4).$$

The moving concentrated force was approximated by the function:

$$P(x,y,t)=\varepsilon^2 exp(-\varepsilon^2((x-x_o(t))^2+(y-y_o(t))^2))/\pi,$$

where $\varepsilon$ — parameter.

Further, by performing quite obvious transformations, we got:

$$W = \frac{1}{2\pi D}\int_0^T\int_0^\infty \left[\frac{p}{p^4+k} + 2p\sum_{n=1}^{\infty}\left(\frac{r_{1n}\cos(\omega_n(t-\tau))}{r_n} + \frac{r_{2n}\sin(\omega_n(t-\tau))}{r_n}\right) J_o(pR)\,e^{-p^2/4\varepsilon^2}\right] d\tau dp$$

$$r_{1n}=(c^{-2}+bcth\,(pH)/p)\,\omega_n^2-p^4-k,\ r_{2n}=\omega_n\tau_o p^4,\ R^2=\delta^2+\beta^2,$$
$$\delta=x_o(\tau)-x,\ \beta=y_o(\tau)-y.$$

Knowing *W*, it was possible to determine formulas for calculating the components of the displacement vector and the stress tensor at any point of the ice cover using available ratios.

In the numerical implementation of the proposed method, a problem arose related to the need to calculate integrals. One of them as a subintegral function had a strongly oscillating function for sufficiently large *n*, and the second was improper with an infinite upper limit.

To calculate integrals from strongly oscillating functions, a quadrature formula was used, obtained by the cubic spline method [11]:

$$\int_a^b e^{i\omega x} f(x)dx \approx -\frac{1}{\omega^4}\sum_{j=1}^{N-1}\frac{e^{i\omega x_{j+1}}-e^{i\omega x_j}}{h_j}\left(M_{j+1}-M_j\right),$$

where $h_j$ — lengths of elementary segments into which the interval was divided [a; b]; S(*x*) — approximation of *f(x)* by cubic spline, $M_j = S''(x_j)$.

When calculating the improper integral, approximate ratio $\int_0^\infty f(p)dp \approx \int_0^A f(p)dp$ was used for a sufficiently large A. Value A was chosen so that the estimate of the allowable error $\left|\int_A^\infty f(p)dp\right|$ was small enough.

Using traditional methods, it was possible to obtain the required estimates for the calculated quantities. For example, for deflection value of the ice cover, this estimate had the form:

$$\left|\int_A^\infty w(p)dp\right| \le 4\varepsilon^2 e^{-A^2/4\varepsilon^2}\frac{\left(c^{-2}+bcth(AH)/A\right)\omega_n^2+A^4\left(1+\omega_n\tau_o\right)+k}{\left[\left(c^{-2}+bcth(AH)/A\right)\omega_n^2-A^4-k\right]^2+\left[\omega_n\tau_o A^4\right]^2}$$

$$W=\int_0^A w(p)dp+\int_A^\infty w(p)dp.$$

When calculating the sum of a series, the Lanczos sigma multiplier method was used to accelerate its convergence.

**Research Results.** The calculations were carried out for the case of the action of a single concentrated force that moved along a closed curve, shown in Figure 1:

$$s(t)=\frac{L\cdot\sin(\alpha(t-T/2))}{2\sin(\alpha T/2)}+\frac{L}{2},\ \alpha=\frac{\pi}{T},\ t\in[0:T].$$

It was assumed that the thickness of the ice cover was h=0.25 m, Young's modulus of the plate material $E$=500,000,000 N/m$^2$, Poisson's ratio μ=1/3, ice density ρ=900kg/m$^3$, water density ρ=1,000 kg/m$^3$, reservoir depth $H$=5 m, ε=2.5. The radii determining the shape of the force trajectory were assumed to be $R_1$=15 m, $R_2$=9 m, $R_3$=3 m (Fig. 1).

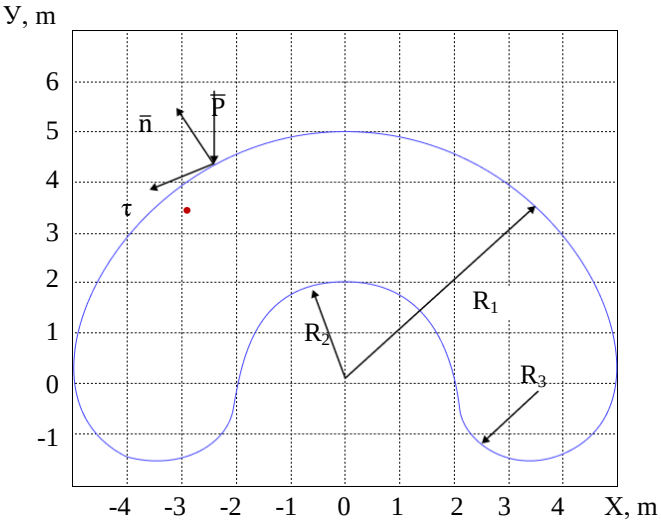


Fig. 1. Trajectory of the concentrated force

Figure 2 shows the change in the deflection of the ice cover (*a*), as well as the maximum values of normal stresses (at z=±h) Sx and Sy (*b* and *c*) and at the movement speed of single concentrated force v =7.4022 m/s and tangential acceleration $w_t$=0.

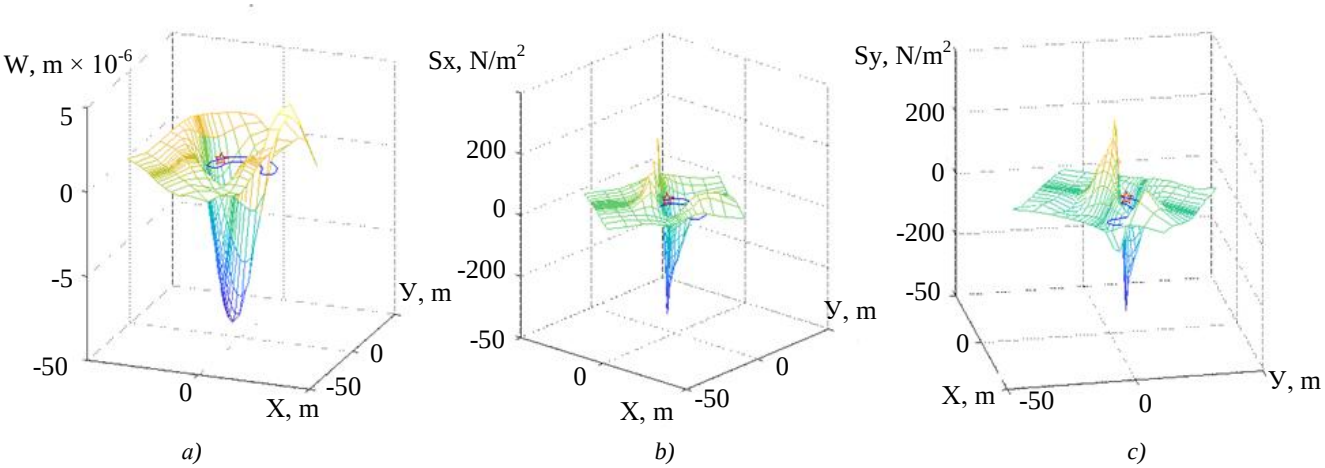


Fig. 2. Change in deflection and stresses of the ice cover: *a* — change in deflection; *b* — change in stress $S_x$; *c* — change in stress $S_y$

On these graphs, the red dot indicates the place of application of force, and the blue color indicates the trajectory of movement.

Figure 3 shows the dependence of the change in the maximum value of the deflection of the ice cover on the force speed rate (*a*) at the moment t=T/2. The position of the force on the trajectory at the moment is marked by a red dot (Fig. 1), while the tangential acceleration $w_t$=0. Two graphs are given, one of which corresponds to the radius of the trajectory $R_1$=15 m (solid line), and the second — to radius $R_1$=5 m (dotted line). Graph *b* in Figure 3 shows the dependence of the maximum value of the ice cover deflection on the tangential acceleration rate at moment t=T at the point of the trajectory (2; 0) in Figure 1 at speed v=0. The graph in Figure 3 shows the dependence of the maximum deflection value on the value of the strain relaxation time.

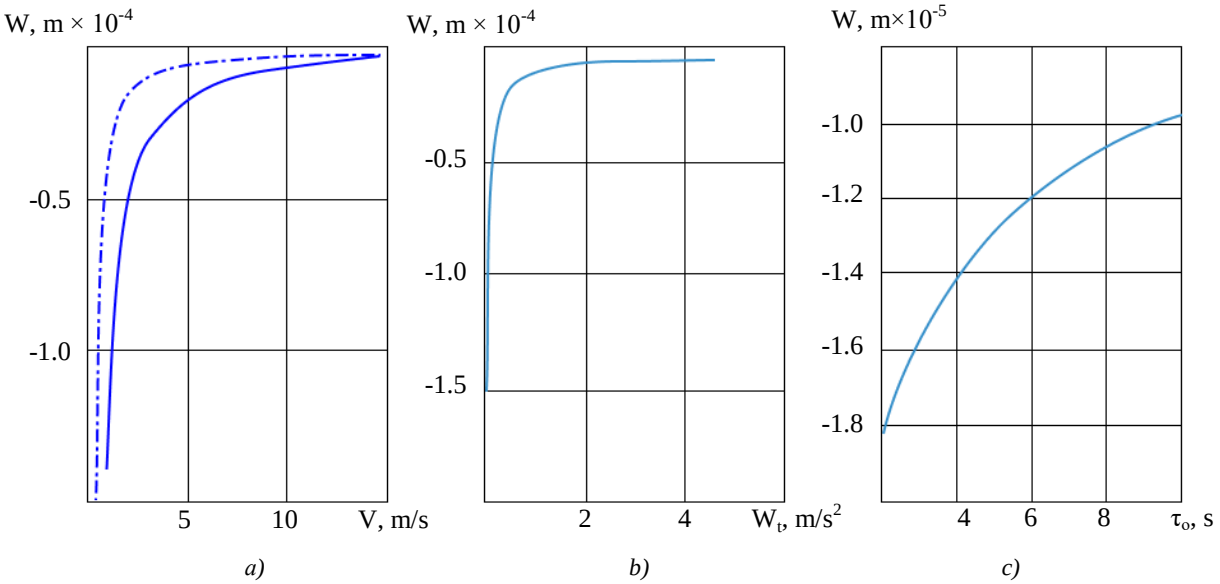


Fig. 3. Dependences of the ice cover deflection on: *a* — speed; *b* — tangential acceleration; *c* — relaxation time

The liquid behavior is shown in Figure 4. It illustrates the distribution of the speed vector of liquid particles over the depth of the reservoir at t=T/2, force speed v=3.7011 m/s and acceleration $w_t$=0.

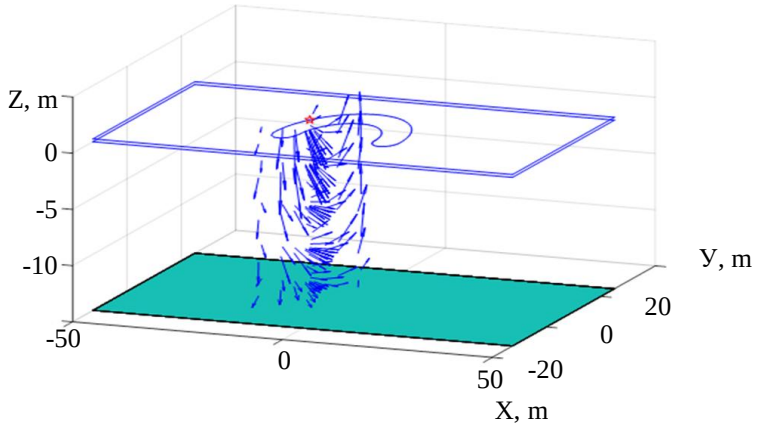


Fig. 4. Distribution of the speed vector of liquid particles over the reservoir depth

**Discussion and Conclusions.** The influence of the movement trajectory curvature and the mechanical properties of ice on the ice cover deflection, speed and acceleration of the load movement was investigated. Calculations have shown that the deflection of the ice cover depends significantly on the movement speed of the force and acceleration of movement.

However, the nature of qualitative changes in displacements and stresses in the ice cover caused by the action of a moving force with a change in speed and acceleration of movement changed slightly.

Mechanical properties of ice, specifically, the relaxation time, had a noticeable effect on the deflection of the ice cover.

The results obtained and the proposed method for solving such problems can be used in the construction of ice roads or airfields on ice. Moreover, the proposed solution method has shown its effectiveness and can be used to solve other similar problems.

**References**

1. Wang K, Hosking RJ, Milinazzo F. Time-Dependent Response of a Floating Viscoelastic Plate to an Impulsively Started Moving Load. *Journal of Fluid Mechanics*. 2004;521:295–317. https://doi.org/10.1017/S002211200400179X

2. Shishmarev K, Khabakhpasheva T, Korobkin A. The Response of Ice Cover to a Load Moving along a Frozen Channel. *Applied Ocean Research*. 2016;59:313–326. https://doi.org/10.1016/j.apor.2016.06.008

3. Shishmarev KA. Problem Formulation of Ice Plate Viscoelastic Oscillations in a Channel Caused by a Moving Load. *Izvestiya of Altai State University*. 2015;1–2:189–194.

4. Kozin VM, Zemlyak VL, Kozhaev AV. Influence of Physical and Mechanical Properties of Ice on the Parameters of Resonant Flexural-Gravity Waves. *Scholarly Notes of KNASTU*. 2019;37:36–45.

5. Tkacheva LA. Behavior of a Semi-Infinite Ice Cover under a Uniformly Moving Load. *Journal of Applied Mechanics and Technical Physics*. 2018;59:258–272. https://doi.org/10.15372/PMTF20180109

6. Korobkin A Khabakhpasheva T, Papin A. Waves Propagating along a Channel with Ice Cover. *European Journal of Mechanics – B/Fluids*. 2014;47:166–175. https://doi.org/10.1016/j.euromechflu.2014.01.007

7. Guyenne P, Părău EI. Computations of Fully Nonlinear Hydroelastic Solitary Waves on Deep Water. *Journal of Fluid Mechanics*. 2012;713:307–329. https://doi.org/10.1017/jfm.2012.458

8. Bukatov AE, Bukatov AA, Zharkov VV, et al. *Rasprostranenie poverkhnostnykh voln v ledovykh usloviyakh*. Sevastopol: FGBUN FITS MGI; 2019. 204 p. (In Russ.)

9. Malenko ZhB, Yaroshenko AA. Bending-Gravity Waves in the Sea with an Ice Cover from Moving Disturbances. *Marine Intellectual Technologies*. 2021;4:157–161. https://doi.org/10.37220/MIT.2021.52.2.086

10. Galaburdin AV. Infinite Plate Loaded with Normal Force Moving along a Complex Path. *Advanced Engineering Research (Russia)*. 2020;20:370−381. https://doi.org/10.23947/2687-1653-2020-20-4-370-381

*About the Author:*

**Alexander V Galaburdin,** associate professor of the Mathematics and Computer Sciences Department, Don State Technical University (1, Gagarin sq., Rostov-on-Don, 344003, RF), Cand.Sci. (Phys.-Math.), associate professor, ORCID, Galaburdin@mail.ru

**Received** 25.01.2023.
**Revised** 06.02.2023.
**Accepted** 06.02.2023.

*Conflict of interest statement*

The author does not have any conflict of interest.

*The author has read and approved the final manuscript.*

*Об авторе:*

**Александр Васильевич Галабурдин,** доцент кафедры «Математика и информатика» Донского государственного технического университета (РФ, 344003, г. Ростов-на-Дону, пл. Гагарина, 1), кандидат физико-математических наук, доцент, ORCID, Galaburdin@mail.ru

**Поступила в редакцию** 25.01.2023.
**Поступила после рецензирования** 06.02.2023.
**Принята к публикации** 06.02.2023.

*Конфликт интересов*

Автор заявляет об отсутствии конфликта интересов.

*Автор прочитал и одобрил окончательный вариант рукописи.*

# MACHINE BUILDING AND MACHINE SCIENCE
# МАШИНОСТРОЕНИЕ И МАШИНОВЕДЕНИЕ



UDC 621.791.052:539.4.014.11
https://doi.org/10.23947/2687-1653-2023-23-1-41-54

*Original article*

## Evaluation of the Occurrence of Initial Failures from Stress Concentrators in Welded Joints and Structural Elements

**Konstantin A Molokov[1,2], Valery V Novikov[1], Mohammad Dabalez[1]**
[1]Far Eastern Federal University, 8, Sukhanova St., Vladivostok, Russian Federation
[2]Vladivostok State University, 41, Gogoleva St., Vladivostok, Russian Federation
✉ Spektrum011277@gmail.com

**Abstract**

***Introduction.*** Data on the occurrence of initial failures obtained through testing on standard samples cannot always be extrapolated to real welded joints and structures. This is due to the difference between the concentrators in the joints, because after welding there is a significant structural and mechanical heterogeneity of the heat-affected and stress concentrator zone. Extended, deep concentrators are considered as crack-like defects, at whose vertices a volumetric, multiaxial stress state is formed. The paper addresses the issue of constructing critical diagrams of the onset of the limiting state at the concentrator vertex, which depends on the level of external load and the theoretical concentration coefficient.

***Materials and Methods.*** Analytical methods were used to study the stress state. The literature on the topic was analyzed. The features of proven physical models and patterns of behavior of materials were taken into account. The characteristics of steel alloys were taken from open sources and summarized in a tabulated form. Nonlinear equations were solved in MATLAB applications. The diagrams constructed by the authors enable to track the correlation of the dangerous level of the theoretical stress concentration factor and the level of external load. Curve Fitting Toolbox MATLAB was used to design the graphic part of the work.

***Results.*** The characteristic of damage from stress concentrators in welded joints was given. The crack propagation in the fusion zone was shown. The conditions stimulating and inhibiting destruction were indicated. The theoretical stress concentration factor $\alpha_T$ was specified. It was shown how this indicator depended on the width, the height of the seam and the thickness of the welded part. Acute stress concentrators with theoretical concentration factor $\alpha_т = 5 \ldots 14$ and more were studied. For this case, an approximating formula was given that took into account the maximum stress in the concentrator in the first half cycle, the initial deformation, and the load ratio. Through those elements, an indicator of an increase in maximum stresses was set depending on the number of loading cycles. The flow condition, the stress state, and the overvoltage factor, which took into account the increase in the first principal voltage for a combined stress state, were analytically shown. A model of the critical state at the apex of an acute stress macro concentrator was described. It was presented as the dependence of the relative stresses of the initiation of destruction $\sigma_{н}^{bc}/\sigma_{0.2}$ on the concentrator. Possible variations of this model were analyzed. The dependences of relative values $\sigma_{H}^{bc}/\sigma_{0.2}$ on the theoretical concentration factor $\alpha_T^{bc} = \alpha_T$ were presented. To check the physical adequacy of this model, graphs were constructed that reflected changes in the relative stress of the external load at a critical state at the stress concentrator apex. The inevitability of bifurcation as a result of the studied processes was validated. Two directions of further development of events were indicated: brittle destruction and loss of stability of the stressed state with the transition to an increase in plastic deformations. The moment of bifurcation was defined as a critical state in the focus of the concentrator.

***Discussion and Conclusion.*** The analysis and calculations performed within the framework of the presented scientific work enabled, in particular, to draw conclusions about the role of key factors of the processes under study. It was established, for example, that the operation of a steel alloy at a high theoretical stress concentration factor depended on the characteristics of the stress state. In a rigid state, it was possible to inhibit shear deformation and the onset of the limiting state at a lower value of the theoretical stress concentration factor. With the usual strength of steel (in comparison to high), a greater impact of the volume of the stress state on the value of the theoretical stress concentration factor was recorded. The probability of failure depended on the resistance of the material to the growth of a macrocrack. In future research, it is possible to refine analytical models and results, evaluate effective stress concentration factors.

**Keywords:** welded joint, theoretical concentration factor, defects of welded joints, volumetric stress state, stress concentration, yield strength, macrocrack.

**Acknowledgements.** The authors would like to thank the staff of the Department of Marine Engineering and Transport, FEFU, for their advisory assistance in the research into the topic, as well as to the reviewers for valuable comments on the structure of the manuscript.

**For citation.** Molokov KA, Novikov VV, Dabalez M. Evaluation of the Occurrence of Initial Failures from Stress Concentrators in Welded Joints and Structural Elements. *Advanced Engineering Research (Rostov-on-Don).* 2023;23(1):41–54. https://doi.org/10.23947/2687-1653-2023-23-1-41-54

*Научная статья*

## Оценка появления начальных разрушений от концентраторов напряжений в сварных соединениях и элементах конструкций

**К.А. Молоков[1, 2] ✉, В.В. Новиков[1], М. Дабалез[1]**

[1] Дальневосточный федеральный университет, Российская Федерация, г. Владивосток, ул. Суханова, 8

[2] Владивостокский государственный университет, Российская Федерация, г. Владивосток, ул. Гоголя, 41

✉ Spektrum011277@gmail.com

**Аннотация**

***Введение.*** Данные о возникновении начальных разрушений, полученные испытаниями на стандартных образцах, не всегда можно экстраполировать на реальные сварные соединения и конструкции. Это обусловлено отличиями концентраторов в соединениях, т. к. после сварки возникает значительная структурно-механическая неоднородность зоны термического влияния и концентраторов напряжений. Протяженные, глубокие концентраторы рассматриваются как трещиноподобные дефекты, в вершинах которых образуется объемное, сложное напряженное состояние. Решается вопрос построения критических диаграмм начала возникновения предельного состояния в вершине концентратора, которое зависит от уровня внешней нагрузки и теоретического коэффициента концентрации.

***Материалы и методы.*** Для исследования напряженного состояния задействовали аналитические методы. Проанализирована литература по теме. Учтены особенности проверенных физических моделей и закономерности поведения материалов. Характеристики сплавов стали взяты из открытых источников и обобщены в виде таблицы. Нелинейные уравнения решались в прикладных программах Matlab. Построенные авторами диаграммы позволяют отследить корреляцию опасного уровня теоретического коэффициента концентрации напряжений и уровня внешней нагрузки. Для оформления графической части работы использовали Curve Fitting Toolbox Matlab.

***Результаты исследования.*** Дана характеристика разрушений от концентраторов напряжений в сварных соединениях. Наглядно показано развитие трещин в зоне сплавления. Указаны условия, стимулирующие и тормозящие разрушение. Определен теоретический коэффициент концентрации напряжений $\alpha_T$. Показано, каким образом данный показатель зависит от ширины, высоты шва и от толщины свариваемой детали. Рассмотрены острые концентраторы напряжений с теоретическим коэффициентом концентрации $\alpha_т = 5 \ldots 14$ и более. Для этого случая приводится аппроксимирующая формула, которая учитывает максимальное

напряжение в концентраторе в первом полуцикле, исходную деформацию и коэффициент асимметрии цикла нагружения. Через эти элементы задается показатель повышения максимальных напряжений в зависимости от числа циклов нагружения. Аналитически показаны условие текучести, напряженное состояние и коэффициент перенапряжения, учитывающий повышение первого главного напряжения для сложного напряженного состояния. Описана модель критического состояния в вершине острого макроконцентратора напряжений. Она представлена как зависимость относительных напряжений зарождения разрушения $\sigma_{н}^{bc}/\sigma_{0,2}$ от концентратора. Проанализированы возможные вариации этой модели. Представлены зависимости относительных значений $\sigma_{H}^{bc}/\sigma_{0,2}$ от теоретического коэффициента концентрации $\alpha_{T}^{bc} = \alpha_{T}$. Для проверки физической адекватности данной модели построены графики, которые отражают изменения относительного напряжения внешней нагрузки при критическом состоянии в вершине концентратора напряжений. Обоснована неизбежность бифуркации как результата исследуемых процессов. Указаны два направления дальнейшего развития событий: хрупкое разрушение и потеря устойчивости напряженного состояния с переходом к росту пластических деформаций. Момент бифуркации определен как критическое состояние в очаге концентратора.

***Обсуждение и заключения.*** Анализ и расчеты, выполненные в рамках представленной научной работы, позволили, в частности, сделать выводы о роли ключевых факторов исследуемых процессов. Установлено, например, что работа сплава стали при высоком теоретическом коэффициенте концентрации напряжений зависит от характеристик напряженного состояния. При жестком состоянии возможно сдерживание сдвиговой деформации и наступление предельного состояния при меньшем значении теоретического коэффициента концентрации напряжений. При обычной прочности стали (в сравнении с высокой) фиксируется большее влияние объемности напряженного состояния на значение теоретического коэффициента концентрации напряжений. Вероятность разрушения зависит от сопротивляемости материала росту макротрещины. В будущих изысканиях возможно уточнение аналитических моделей и результатов, оценка эффективных коэффициентов концентрации напряжений.

**Ключевые слова:** сварное соединение, теоретический коэффициент концентрации, дефекты сварных соединений, объемное напряженное состояние, концентрация напряжений, предел текучести, макротрещина.

**Благодарности.** Авторы выражают признательность сотрудникам департамента морской техники и транспорта ДВФУ за консультативную помощь в разработке темы, а также рецензентам за ценные замечания по структуре рукописи.

**Для цитирования.** Молоков К.А., Новиков В.В., Дабалез М. Оценка появления начальных разрушений от концентраторов напряжений в сварных соединениях и элементах конструкций. *Advanced Engineering Research (Rostov-on-Don).* 2023;23(1):41–54. https://doi.org/10.23947/2687-1653-2023-23-1-41-54

**Introduction.** Static and fatigue strength is reduced due to defects in welded joints. These can be:

– cracks formed during or after welding;

– stress concentrators (undercuts, incomplete fusion, pores, welding craters, high rippling, abrupt change in the shape of the weld, rolls, etc.)

In the latter case, the determining factors will be:

– shape, size of the concentrator and the position in the welded joint;

– stress state indicator at the top [1].

Under cyclic loads, cracks often occur and develop in welded joints, provoked by stress concentrators [2]. The risk also depends on how close the stress state of the welded joint with the concentrator is to the occurrence of a macrocrack and its spread at operating $\sigma_H$ and cyclic loads $\sigma_{-1}$. Obviously, the latter depends significantly on the size, shape of the macrodefect and the stress state at its top. For example, an oblong and narrow macro stress concentrator is more dangerous than a rounded one. Probably, a crack is immediately formed at its top, and together with it, the initial concentrator will represent one long macrocrack [3]. The size of such a “total” macrocrack may be critical, which will

reduce the static strength [4]. It depends on its length and mechanical characteristics of the material at the top of the initial concentrator.

The study objective is to develop an analytical model for assessing the dangerous level of stress concentration. The case in hand is about the formation of a crack in the top of the concentrator, a sharp decrease in the bearing capacity of welded joints and structural parts.

**Materials and Methods.** Scientific research within the framework of the stated topic was based on known physical models and patterns of behavior of materials. The theoretical and applied literature was analyzed. Illustrative and reference materials were extracted from the sources.

The stress state was studied by analytical methods. The relationship between the rigidity of the stress state and the value of the theoretical stress concentration factor was established. The results were presented in the form of diagrams. This visualization method made it possible to track the correlation of the dangerous level of external load and the theoretical stress concentration factor.

To check the results of calculations based on the physical adequacy of the authors' model, dependency graphs for the critical state were constructed. The paper used information about widespread structural steels of ferrite-perlite class in the state of delivery (steel 10, 22K, 50, St3sp, 37KHN3A, 30KHGSA, etc.). Their mechanical characteristics were obtained from open sources[1] and summarized in Table 1. The data was visualized in the Curve Fitting Toolbox MATLAB.

Table 1

Characteristics of steels

| Steel grade | $\sigma_в$, MPa | $\sigma_т$, MPa | $m$ | $\varphi_k$ |
|---|---|---|---|---|
| 10 | 320 | 190 | 0.17 | 0.73 |
| 15G | 410 | 245 | 0.148 | 0.55 |
| St3sp | 450 | 270 | 0.16 | 0.71 |
| 22K | 540 | 310 | 0.16 | 0.69 |
| 50 | 680 | 350 | 0.16 | 0.62 |
| 10KHSND | 540 | 390 | 0.132 | 0.71 |
| 37KHN3A | 1014 | 743 | 0.12 | 0.6 |
| 30KHGSA | 1750 | 1360 | 0.09 | 0.44 |

Mathematical apparatus was applied to derive formulas. When solving nonlinear equations, the MATLAB application software package was used.

**Research Results**

**Characteristics of damage from stress concentrators in welded joints.** Since early 2000s, stress concentrations in welded joints and structures have been studied in relation to industrial tasks [2–3, 5–9].

Figure 1 shows examples of destruction of welded joints due to stress concentration.

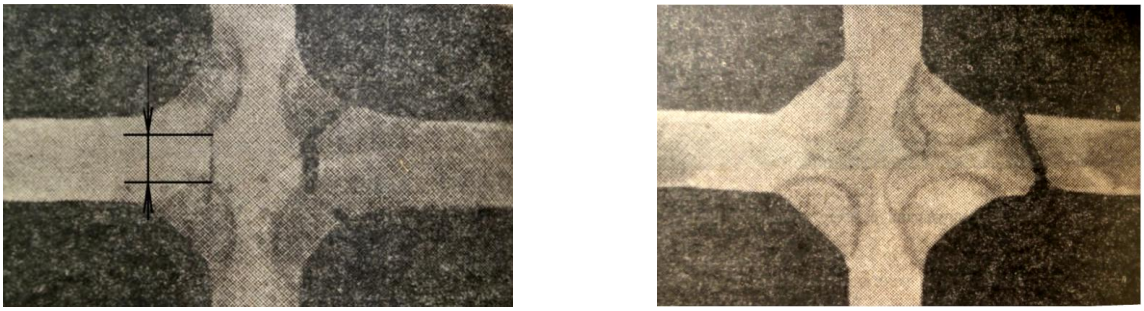

*a*) *b*)

[1] Sergeev NN, Sergeev AN. Mekhanicheskie svoistva i vnutrennee trenie vysokoprochnykh stalei v korrozionnykh sredakh**.** Vologda: Infra-Inzheneriya; 2020. 431 p. (In Russ.)

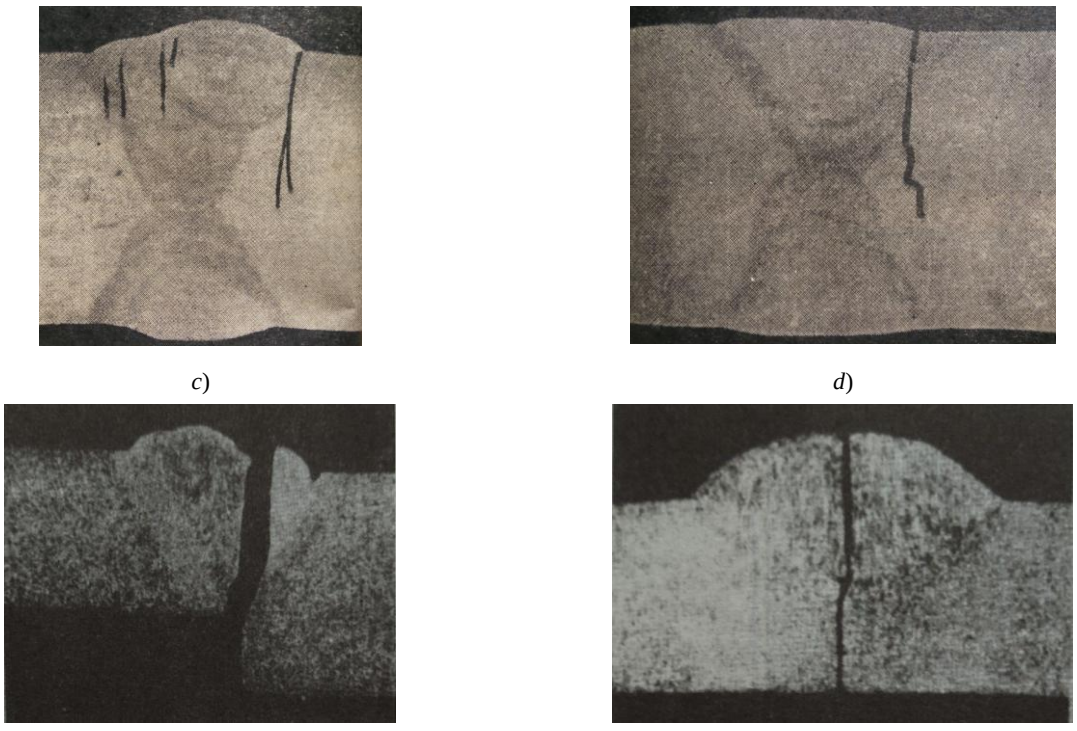

*c*) *d*)

*e*) *f*)

Fig. 1. Destruction of cross and butt joints[2] from stress concentrators:
*a, f* — from the incomplete fusion zone, square butt joint; *b* — from undercutting, V-weld; *c* — from a sharp transition in the fusion zone; *d* — undercut; *e* — from the concentrator formed by a step transition at the edge junction [10]

The destruction of cross joints with large non-fusion of the edges (indicated by arrows in Fig. 1*a*) is possible under the following loads:

– static (as a result of embrittlement of the fusion zone);

– cyclic (cause cracking at the tops of the concentrator).

In [5], the stress distribution for butt, corner, cross joints and intermittent connections of ship structures is analyzed. In butt and cross welded joints, the area of the base metal adjacent to the weld is of particular importance. This is the weakest cross-section that determines the strength of the joint at variable stresses. It should be noted that the welds are always quite long compared to the thickness of the metal and the stress concentrator (undercut in the butt or cross joint). This prevents a shift in the area of the concentrator and creates a biaxial, and more often a multiaxial stress state [11, 12]. When considering the destruction of welds with concentrators (see Fig. 1 *a*, *e*, *f*), we take into account the concept of the occurrence of plastic deformation in the top region [5, 7]. In addition, it should be noted that the concentrators are adjacent to the fusion zone, which, after welding, experiences longitudinal residual tensile stresses. They affect the degree of rigidity of the stress state in the concentrator focus [1, 13–14]. All this prevents the passage of shear in the concentrator focus and can contribute to the occurrence of a minimal brittle macrocrack with a high theoretical stress concentration factor $\alpha_т$ even from static load.

In [9], indicative failures from welded defects in large-diameter pipelines are described. It is established that with long-term operation (more than 20 years), fatigue cracks appear in the undercuts of longitudinal welded pipe joints. Cracks in undercuts in the fusion zone, as a rule, branch out and spread in two directions (fig. 2): one moves away from the fusion zone, the other develops along the fusion zone (along the weld). This indicates a strong impact of the

[2] Molokov KA, Novikov VV, Turmov GP. Osnovy raschetnogo proektirovaniya svarnykh konstruktsii. Vladivostok, 2019. T. 1. 204 p. (In Russ.)

mechanical, structural characteristics of the material[3]and mechanochemical heterogeneity on the propagation of initial destruction [13, 14]. On the other hand, the crack branching can complicate the process of further destruction and the transition of the crack into the main one.

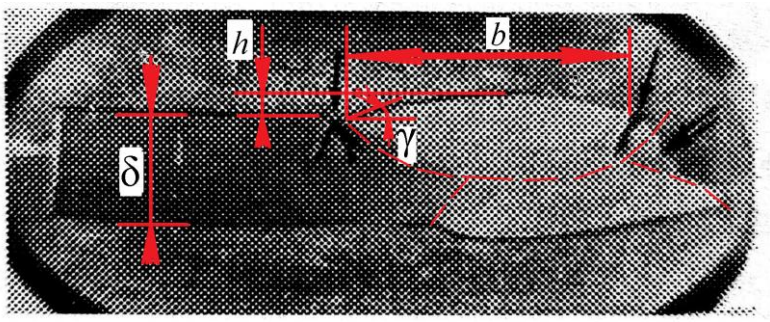


Fig. 2. Destruction in the pipe welded joint from the stress concentration in the fusion zone. Steel 14HGS. Single arrow shows fatigue cracks; double arrow — pipe burst edge; strokes — weld outlines. Here, *b* — weld width; *h* — weld height; δ — weldment thickness; γ — angle of transition from base metal to weld [9]

The theoretical stress concentration factor in the fusion zone can be determined from the formula that takes into account the concentration effect of a non-melting transition in this zone [5]:

$$\alpha_т = 1 + 1.1h\frac{(b/\delta)^2+1}{\delta}\sqrt{h/\ln(90°/\gamma)}, \quad (1)$$

where $\gamma = A[90\exp(-\rho/\rho_0) + B]$ — angle of transition from base metal to weld; ρ — radius of transition from base metal to weld; $\rho_0 = 1$ mm; $A = 0.94 \ldots 0.17$; $B = 0.8$; $b$ — weld width; $h$ — weld height; δ — weldment thickness (fig. 2).

However, this dependence does not take into account the changed mechanical characteristics of the material. In these zones, hardening structures are usually present, whose mechanical characteristics can differ significantly (up to 30 %) from the characteristics of the weld and the base metal.

It is possible to indirectly control crack formation and the stress state in the region of the top of the stress concentrator through the concentration factor of their intensity. Accordingly, when a sample fails due to fatigue, one macrocrack is formed at the concentrator top, and in a corrosive medium — a group (fig. 3).

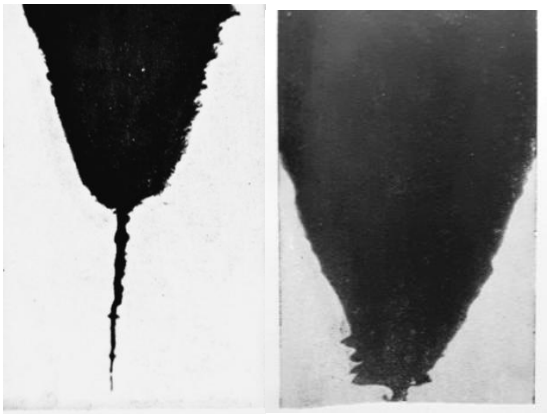

*a*) *b*)

Fig. 3. Fatigue failure of steel 45 from a V-shaped stress concentrator: *a* — in air; *b* — in water — in a corrosive environment. An increase of 134 times[4]

After the formation of a group of macrocracks (fig. 3 *b*), the role of the macro-concentrator decreases, and further development of destruction can be suspended or inhibited. This was validated by experiments that indicated an increase

[3] Molokov KA. Otsenka povrezhdennosti ferrito-perlitnykh stalei v usloviyakh malotsiklovogo nagruzheniya. In: Proc. Conf. "Nauka. Innovatsii. Tekhnika i tekhnologii: problemy, dostizheniya i perspektivy". URL: https://elibrary.ru/item.asp?id=23752241&selid=46181945 (accessed: 31.10.2022). (In Russ.)

[4] Molokov KA. Otsenka povrezhdennosti ferrito-perlitnykh stalei v usloviyakh malotsiklovogo nagruzheniya.

in fatigue strength in samples with stress concentration in a corrosive environment[5]. Such a group of cracks loosens the material, changes the stress state above and below the surface at the top of the macro-concentrator, which prevents the formation of a leading crack that can develop further at a lower level of cyclic loads.

Consider the situation on the surface or in the thickness of metal in massive bodies under stresses $\sigma_H$ at infinity in a plane-stressed state. In this case, it is reasonable to use the Kolosov and Inglis's solution for an elliptical shape concentrator:

$$\alpha_T = \frac{\sigma_{max}}{\sigma_H} = 1 + 2\sqrt{a/\rho}, \quad (2)$$

where $\rho$ и $\sigma_{max}$ — radius of curvature and maximum component of stresses on the surface, respectively, at the top of the notch; $a$ — semi-major axis, or half of the longest area perpendicular to the direction of the external load field.

Dependence (2) is well consistent with engineering practice. In accordance with the accepted concept, the theoretical stress concentration factor at the notch is determined by the depth of the notch and the contour curvature radius at its top, but does not depend on the shape of the contour.

Due to the development of information technologies, the evaluation of the theoretical stress concentration factor presents no great difficulty. The results of calculations of stress and strain concentrations in elastic and elastoplastic formulation of the problem can be obtained through the CAE finite element analysis [16–18, 12].

The experiments showed that at a certain stress concentration, external static load, and elastic-plastic stage of the material, an initial fracture crack appeared at the concentrator top at a certain distance from the surface. It rapidly propagated to an axis perpendicular to the direction of tension of the notched plates. The propagation is visible in the pictures (fig. 4). The process was fixed in the plates under a plane stress state and under a plane deformation. In the latter case, the appearance of a crack in the thickness of the metal under the surface was detected using an ultrasonic flaw detector.

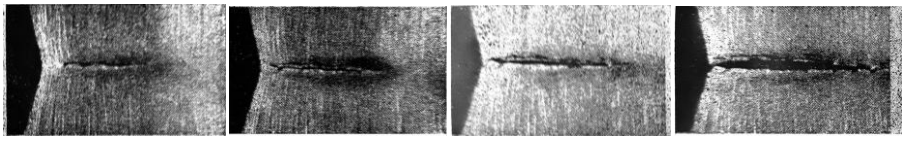

*a*) *b*) *c*) *d*)

Fig. 4. Initiation of a subsurface crack at the top of the concentrator under static tension: *a* — macrocrack initiation; *b, c* — size increase in depth and towards the surface; *d* — crack exit to the surface [19]

Thus, under the given conditions and a sufficiently acute stress concentrator, a zone of a multiaxial stress state was formed, in which the continuity violation was possible. There would be a higher level of the onset of fluidity, and the tensile strength in a weakened place due to the concentrator could increase to 20-60 % (it depends on the material) [11].

**Stress concentration and stress state conditions.** Consider rather sharp stress concentrators with theoretical concentration factor $\alpha_т = 5 \ldots 14$ and more. As a rule, the defects mentioned above act as such concentrators. At the top of the concentrator, the stress state can be considered the same as in plane deformation. In [18], the results of the analytical solution and experimental data for sharp concentrators under plane deformation were presented, the region of admissible values $[\alpha_T]$ and the radius at the top $[\rho]$ for steel 09G2S were established. However, the impact of its mechanical characteristics was not described. Moreover, it is not clear whether the analytical solutions are based on such initial parameters of 09G2S as the hardening coefficient $m$, yield strength $\sigma_{0.2}$, ultimate strength $\sigma_B$, critical fracture narrowing $\varphi_k$, etc. It is known that ductility and strength affect significantly the level of allowable stress concentration and the occurrence of brittle fracture at the top.

For hardening materials, cyclic stresses at the top of an acute concentrator aggravate the possibility of brittle

[5] Sergeev NN, Sergeev AN. Mekhanicheskie svoistva i vnutrennee trenie vysokoprochnykh stalei v korrozionnykh sredakh. Vologda: Infra-Inzheneriya; 2020. 432 p. (In Russ.)

fracture, therefore, we will take such $\alpha_T$ as a hazard criterion, at which brittle fracture is likely to occur under static load conditions. The increase in maximum stresses depending on the number of loading cycles $N$ is given by the approximating formula:

$$\sigma_{\max} = \sigma'_{\max} + A \cdot \lg(N), \quad (3)$$

where $\sigma'_{\max}$ — maximum stress in the concentrator in the first half cycle; $A$ —coefficient depending on the level of initial deformation and the asymmetry coefficient of the loading cycle at the top of the concentrator.

We accept the obvious assumption that the appearance of brittle fracture may be due to the following reasons:

– an increase in the intensity of three-dimensional stretching in close proximity to the top of the concentrator;

– an increase in the resistance to plastic deformation of the material near the top as a consequence of shear resistance in acute stress concentrators.

The latter circumstance turns out to be the stronger the higher the loading speed and the sharper the stress concentrator.

Consider the elastic-plastic plane stress at the top of the concentrator and the elastic state in the gross section: $\sigma_{max} = \alpha_T \sigma_H \gg \sigma_{0.2}$, $\sigma_H \approx \sigma_{0.2}$ and $\sigma_H < \sigma_{0.2}$. Here, $\sigma_{0.2}$ — conditional yield strength of the material under uniaxial tension. At $\alpha_T = 7.3$, stiffness of the stressed state is close to the state for a crack. Safety coefficient $m_{FAD}$ for a crack-like defect with a plane deformation differs slightly (within 10 %) from $\overline{m_{FAD}}$ for a crack, i.e., for a state where there is an approximate equality $m_{FAD} \approx \overline{m_{FAD}}$:

$$\frac{\sqrt{1-(\sigma_0/\sigma_T)^2/\alpha_T^2}\cdot\sqrt{1-(\sigma_{0.2}/n_T/\sigma_0)^2}}{\sqrt{1-(\sigma_0 n_T/\sigma_T)^2/\alpha_T^2}\cdot\sqrt{1-(\sigma_{0.2}/\sigma_0)^2}} \approx \frac{\sqrt{1-(\sigma_{0.2}/n_T/\sigma_0)^2}}{\sqrt{1-(\sigma_{0.2}/\sigma_0)^2}}. \quad (4)$$

Here, $n_T$ — yield strength margin coefficient, $\sigma_0$ — local strength of the material at the top of the crack or sharp concentrator.

In [11], the term “local yield strength” is applied to acute stress concentrators when the area of the concentrator adjacent to the top, experiences a complex stress state (CSS). Obviously, this term denotes the material flow stress on the concentrator circuit. There is plane stress state on the surface at its top, and a triaxial CSS appears under the surface. There, stiffness of the stress state increases sharply, therefore, the initial destruction of continuity is formed at some distance from the surface (fig. 4). It is established that the onset of local fluidity in the stress concentrator zone does not coincide with the level determined by the calculations based on strength criteria, particularly, according to von Mises–Huber–Hencky. As the stress concentration increases, the difference increases between:

– yield strength $\sigma_{0,2}$, theoretically calculated according to this criterion;

– experimentally determined stress value of the local flow of material $\sigma^*_{0.2}$ in the region adjacent to the top of the concentrator.

The results of experiments on plane samples of various steels and alloys [11, 16] show that ratio $\sigma^*_{0.2}/\sigma_{0.2}$ is well approximated by linear dependence on $\alpha_T$. Then, the yield condition can be written as:

$$\sigma_i = \sigma_{0.2}(0.9 + 0.1\alpha_T), \quad (5)$$

where $\sigma_i$ — von Mises stress intensity.

The authors limited their experimental studies to values $\alpha_T = 10$, and the tests were carried out only on plane samples with centrally located concentrators. In case of plane deformation, stiffness of the stressed state turns out to be slightly higher. Therefore, it is logical to assume that fluidity at some values $\alpha_T$ would occur no earlier than at the plane stressed state. And it is likely that the slope of the straight line according to equation (5) could be somewhat different [11]. However, we focus on this dependence.

For the moment of the beginning of yield, assume that with the transition from elastic deformations to elastoplastic, the ratio of the second and third main stresses to the first $\sigma_1 = \sigma_{\max}$ does not change. This has been proven

experimentally.

We equate to (5), the intensity of the stresses of the beginning of von Mises yield according to the fourth (energy) theory of strength, and introduce the coefficients of the relationship between the main stresses under plane deformation: $\sigma_1 = \sigma_i/D;\ \sigma_2 = q\sigma_1;\ \sigma_3 = \mu_T(1+q)\sigma_1$ [15]. Here, $\mu_T = 0.5$ — Poisson's ratio in the plastic region, and $D$ — overvoltage coefficient, which takes into account the increase in the first main voltage in the case of CSS. The equation obtained with respect to $q$ has two solutions. The first is for tensile $\sigma_2$ component, the second — for the compressive one. Tensile component $\sigma_2$ increases stiffness of the stress state in the case of CSS. After transformations and compressions, we can express it like this:

$$q = 1 - \frac{\sqrt{3}\sigma_{0.2}}{15\sigma_H}\left(1 + \frac{9}{\alpha_T}\right). \quad (6)$$

For the limiting case $\sigma_H = \sigma_{0.2}$, it is possible to neglect the change in the radius at the top of the concentrator and the onset of some initial global fluidity for the net cross section. Then, the only value $\alpha_T$, satisfying the stiffness of the stress state equivalent to the crack is 7.33. This validates approximate equality (4) obtained earlier. For other values, as can be seen from (6), proportionality $q$ will vary depending on value $\alpha_T$ and $\sigma_H$.

For a crack, coefficient $D$ is determined from the equilibrium condition in the elastoplastic region and is calculated for plane deformation from the formula:

$$D = \frac{(1+m)(1-2\mu)}{2}, \quad (7)$$

where $m$ — power hardening coefficient; $\mu$ — Poisson's ratio in the elastic region.

For ferritic-pearlitic steels, this coefficient takes values from 0.22 to 0.26.

Multiplier before $D$ in formula $q = 1 - 2D/\sqrt{3}$ for a crack is 1.156, and $q$ for ferrite-pearlite steels is 0.73. Indeed, when substituting $\alpha_T = 7.3$ (6) for $\sigma_H = \sigma_{0.2}$, we get $q \cong 0.73$. Next, we find $\alpha_T$, if $\sigma_{0.2}/\sigma_H > 1$, at which the same stress state is realized as at $\alpha_T = 7.3$ and $\sigma_{0.2}/\sigma_H \to 1$.

In [20], the impact of $\alpha_T$ on the effective stress concentration coefficient $K_э$ is investigated, and for a typical aluminum alloy, it is shown that, in the range $\alpha_T$ from 7 to 13, global extremum of the value $K_э$ is observed. It is quite probable that such a significant maximum value may indicate brittle fracture at the initial stages of cyclic loading or discontinuity at the top of the concentrator. In this case, the resource will depend only on the further ability of the material to prevent the propagation of macrocracks.

**Model of critical state at the top of an acute macro-stress concentrator.** Almost all defects in the welded connection of pipelines, hull ship structures, etc., create a stress concentration. An analytical model developed on the basis of the concept of "local stress concentration factor" is presented in [9]. In addition, a simple dependence was obtained based on the Neuber formula linking the theoretical generalized concentration factor and the concentration factors of the intensity of elastic stresses and deformations. As a result, for the critical value of plasticity in the concentrator focus, the following dependence was obtained:

$$\varepsilon_c = \frac{\sigma_B \alpha_C^{2/(1+m)}}{E}, \quad (8)$$

where $\alpha_c$ — critical value of the theoretical stress concentration factor; $\sigma_B$ — modulus of rupture; $E$ — modulus of elasticity; $m$ — exponent of power hardening.

Dependence (8) gives such high values that are rarely found in practice. For example, with critical logarithmic deformation for steel 50, the critical concentration factor is 26, and for high-strength steel 37KHN3A with $\sigma_B = 1.014$ MPa — more than 18. It can be concluded that such plasticity is unattainable until continuity is broken in the first loading cycles. This is not surprising, since it is known that the maximum plasticity value for samples with stress concentrators is significantly lower than for samples without stress concentration. In addition, $\varepsilon_c$ should be determined not only by the properties of the material, but also by the conditions for the development of plastic

deformation before destruction. Similar results are given by the dependence used in [9]:

$$\alpha_T = \frac{\sqrt{E \cdot \varepsilon_{\text{разр}} \cdot \sigma_{\text{разр}}}}{\sigma_H}. \quad (9)$$

S.A. Kurkin used it for a comparative assessment of the material sensitivity to stress concentration. Here, $\alpha_T$ characterizes the concentrator in which the crack occurs at specific load $\sigma_H$. Next, we will use the concept of "the most probable initiation of a macrocrack in the concentrator" (born crack) $\alpha_T^{bc}$ for this case. The true deformation and stress at the moment of occurrence of the discontinuity at the top of the concentrator are denoted respectively by $\varepsilon_{\text{разр}}$ and $\sigma_{\text{разр}}$. They can be determined from the generally accepted formulas $\varepsilon_{\text{разр}} \cong \varepsilon_{\text{кр}} = \ln[1/(1-\varphi_{\text{к}})]$ and $\sigma_{\text{разр}} \cong S_{\text{отр}} = \sigma_{\text{в}}(1 + 1.4\varphi_{\text{к}})$. Here, $S_{\text{отр}}$ — true stresses of destruction at uniaxial stress state. Note that the fluidity in the concentrator occurs according to (5). Replace $\sigma_H = \sigma_{0.2}$ and $\sigma_{0.2}$ with $\sigma_{0.2}^*$. As a result, we obtain for the critical states ($\alpha_T = \alpha_T^{bc}$) relative stresses of the nucleation of destruction $\sigma_{\text{н}}^{bc}/\sigma_{0.2}$ from the concentrator:

$$\frac{\sigma_H^{bc}}{\sigma_{0.2}} = \frac{\sqrt{E \cdot \varepsilon_{\text{разр}} \cdot \sigma_{\text{разр}}}}{\alpha_T^{bc}(0.9+0.1\alpha_T^{bc})\sigma_{0.2}}. \quad (10)$$

Note that for a very small radius of the concentrator top ($\rho < 10d_z$, where $d_z$ — average grain diameter), crack propagation is limited at constant $\alpha_T$. As shown in [6], it depends on $d_z$ of steel. Formulas (8) and (9) are attractive to an engineer because they provide comparing the material sensitivity to stress concentration and using the initial data of the mechanical characteristics of steel.

We can get a slightly different model that takes into account the CSS in the area of the top of the macro-concentrator. The author [12] uses the strength criterion of brittle fracture in the structural material $\sigma_1 > S_{\text{отр}}$, where $S_{\text{отр}}$ — stress of normal fracture in the approximation to a uniaxial stress state. Significantly, this characteristic of the material does not depend on the temperature of its test. We use this criterion in a slightly different way — for the moment of occurrence of a discontinuity in the area of the top of the stress concentrator. Suppose that $S_{\text{отр}}$ is achievable in the case of constant energy equality at CSS and uniaxial stress state, i.e., with loss of plastic stability and transition from a volumetric stress state (when $\sigma_i$ is small) to a uniaxial stress state with an inevitable increase in deformations.

We use power approximation of the deformation diagram within the framework of the deformation theory of plasticity. We equate true stresses $\sigma_i$ of the deformation diagram in the elastic solution function of the problem m $\sigma_i = F(\sigma_i^{(y)})$ to $S_{\text{отр}}$. As a result, we get:

$$\sigma_i = \sqrt[\frac{1}{m}+1]{\sigma_{0.2}^{\frac{1}{m}-1}\left(\sigma_i^{(y)}\right)^2} = S_{\text{отр}} = \sigma_B(1 + 1.4\varphi_K), \quad (11)$$

where $\sigma_i^{(y)}$ — uniaxial stresses in the elastic solution to the problem.

Writing (11) with respect to $\sigma_i^{(y)}$, we obtain an expression for the elastic solution to the stress concentration problem on the other hand: $\sigma_i^{(y)} = \alpha_T \cdot \sigma_H$. Thus:

$$\alpha_T \cdot \sigma_H = \sqrt{\frac{[\sigma_B(1+1.4\varphi_K)]^{\frac{1}{m}+1}}{\sigma_{0.2}^{\frac{1}{m}-1}}}. \quad (12)$$

Here, $\sigma_H$ — nominal workload on the welded joint. In hard points of welded structures, joints or under overloads, it can reach the value of the yield strength of the material. Let us imagine a special case under conditions of cyclic loading with hardening of the material for the moment of formation of the born crack discontinuity — failure initiation. After transformations (12), we write down a simplified formula:

$$\alpha_T^{bc} = \left[\frac{\sigma_B(1+1.4\varphi_K)}{\sigma_{0.2}^*}\right]^{\frac{1+m}{2m}}, \quad (13)$$

where $\alpha_T^{bc}$ — value of the theoretical stress concentration factor at which the nucleation of destruction occurs in the region of the top of the macro-concentrator; $\sigma_{0.2}^*$ — yield strength of the material at the top of the concentrator, which can be increased according to (5) in the case of CSS.

At the moment of equality $\alpha_T = \alpha_T^{bc}$, the nominal stresses must be equivalent to the nucleation (destruction) stresses $\sigma_H^{bc}$. For this situation (13), we can write in relative values $\sigma_H^{bc}/\sigma_{0.2}$ and construct the dependences of the relative values of the stresses of fracture formation on the theoretical concentration factor $\alpha_T^{bc} = \alpha_T$:

$$\sigma_H^{bc} = \frac{2\cdot\left(\alpha_T^{bc}\right)^{\frac{-2m}{m+1}}\cdot\sigma_B\cdot(7\varphi_K+5)}{\alpha_T^{bc}+9}. \quad (14)$$

Unfortunately, it is not possible to write (14) with respect to $\alpha_T^{bc}$ at $\sigma_H^{bc}/\sigma_{0.2} = 1$. However, $\alpha_T^{bc}$ can be found numerically for specific load $\sigma_H^{bc}$, or diagrams of the danger of discontinuities in the form of a macrocrack in the focus of the concentrator can be constructed.

Dependences are analytically obtained for calculating critical theoretical stress concentration factors related to the mechanical characteristics of the material and a given external static load under the condition of a volumetric stress state for concentrators in welded joints. It is shown that the volume of the stress state in the concentrator focus affects significantly the value of the critical theoretical stress concentration factor. It is established that the complex stress state in the concentrator focus can be controlled by the geometric characteristics of the concentrator itself and its location relative to the external stress field.

Experimental data of steels (see Table 1) are obtained from literary sources. These are ferrite-perlite materials for which formula (14) has shown good agreement. Dependence (14) is attractive because standard mechanical characteristics are used as initial data. It can also be used to assess the risk of defects in the fusion zone (fig. 1,fig. 2), where hardening structures are formed, whose properties differ significantly from the initial characteristics of the welded steel.

Solutions for (9) and (14) are used more often for the most brittle steels at low $\alpha_T^{bc}$. However, in the area of high stress concentration, critical ratios $\sigma_H^{bc}/\sigma_{0.2}$ for different steels will be very close in values. This can be explained by the fact that with the CSS, a stress state similar to a dangerous case is created for all steels in the top region. In the region of small stress concentrations, solutions to model (9) show higher critical stress values $\sigma_H^{bc}$. Note that the average value $\alpha_T^{bc}$ at $\sigma_H^{bc} \approx \sigma_{0.2}$ is ~8.5. For steels with different mechanical characteristics, it does not change as much as according to the calculated results of model (9).

Figure 5 is constructed to validate the calculation results based on the physical adequacy of model (14). These are graphs of critical state dependences $\sigma_H^{bc}/\sigma_{0.2}$ from $\alpha_T^{bc}$.

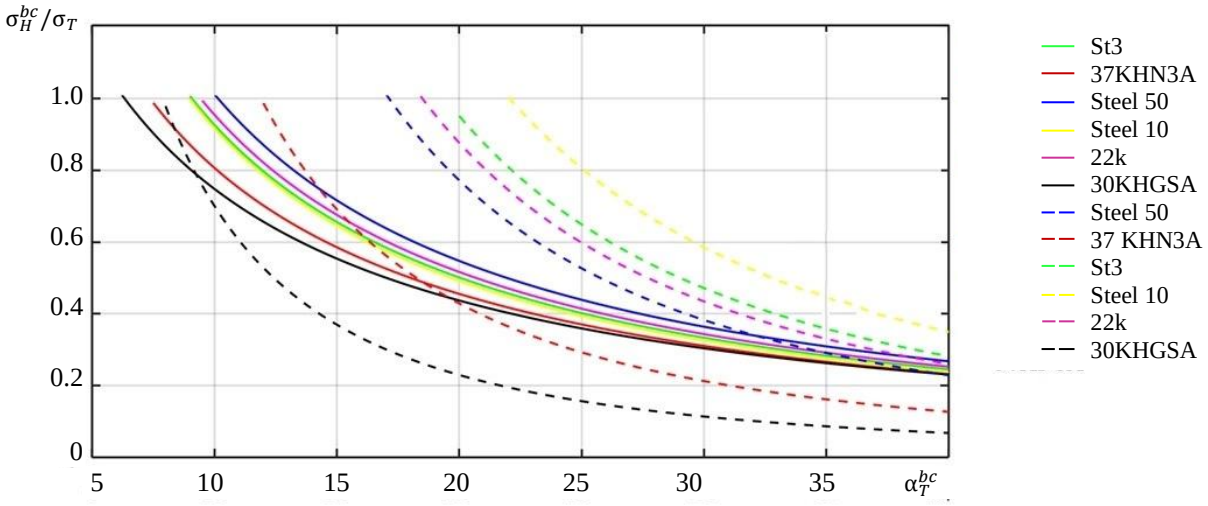


Fig. 5. Dependences of changes in the relative voltage of the external load $\sigma_H^{bc}/\sigma_{0.2}$ from $\alpha_T^{bc}$ for the critical state at the top of the stress concentrator. Solid curves — formula (14); dotted curves — formula (10)

Model (9), which does not take into account the volume and increase in yield stresses at the top of the concentrator, gives $\alpha_T^{bc} = 91$ at stresses $\sigma_H^{bc} = 0.5\sigma_{0.2}$ for steel 10, which is unlikely. If we take into account the volume in this

model, then $\alpha_T^{bc} = 33$, which is significantly less. Taking into account the volume of the stressed state, the critical plastic deformation is reduced to the occurrence of destruction during static tensile of the samples. This was validated by experiments with various steels and alloys[6]. Moreover, the researchers obtained less ductility of the steels on corroded samples. Here, it was shown that a volumetric stress state was created at the tops, and the volume prevented the free flow of plasticity. The plasticity before the destruction of these samples was 40 %, and the yield strength increased to 27 % [21]. It can be concluded that deeper concentrators cause a greater increase in the yield strength. The results of indirect experiments allowed us to assert that under hydrostatic load, the fluidity is not fixed, in this case the material only embrittles. However, in the focus of the concentrator, with an increase in the external load, the volumetric stress state cannot remain stable enough for the development of a higher volume level. Therefore, bifurcation is inevitable. Further, the development can go in two directions:

– fragile destruction or its beginnings in the focus;

– loss of stability of the stress state and, as a consequence, the transition to a sharp increase in plastic deformations.

Probably, the moment of bifurcation should be considered a critical state in the focus of the concentrator. Perhaps, this moment depends significantly on the depth of the concentrator, its relative length and depth to the thickness of the part, orientation to the external stress field, as well as on the mechanical characteristics and extent of the concentrator focus. All this requires additional research and more precise solutions.

**Discussion and Conclusions.** Defects and design features of welded joints (weld groove geometry, incomplete penetration, undercuts, pores, hardening structures, etc.) reduce static and fatigue strength. Stress concentrators are typical for welded joints, having a long and shallow shape relative to the thickness of the parts being connected (undercuts) or long and deep (incomplete penetration, etc.). All of them reduce fatigue strength. The analytical models obtained in the presented work allowed us to draw a number of conclusions.

1. The operation of the material at high values of the theoretical stress concentration factor depends on the stress state and its rigidity, as well as on mechanical and structural characteristics. The latter may differ from the parameters of the source material, since the tops of the concentrators may be located in the fusion zones of welded joints.

2. A rigid stress state in the stress concentrator focus can cause an increase in the yield strength. In this case, the passage of shear deformation is restrained, and the onset of the limiting state is achieved at a lower value of the theoretical stress concentration factor and is characterized by discontinuity at a constant value of the external load.

3. Comparison of high-strength steels with ductile and ordinary strength steels at the same level $\sigma_H^{bc}/\sigma_{0.2}$ . In the second case, the formation of the volume of the stress state will have a more significant effect on the change in the critical value of the theoretical stress concentration factor, at which the nucleation of destruction occurs in the region of the top of the macro-concentrator $\alpha_T^{bc}$ (fig. 5).

4. Comparison of models (14) and (10) allows us to draw a certain conclusion. Taking into account the rigidity of the stress state and the increase in the yield strength at $\sigma_H^{bc}/\sigma_{0.2} \to 1$ from below, $(10)$ gives estimate $\alpha_T^{bc}$ with a margin of safety, if we are talking about $\sigma_H^{bc}/\sigma_{0.2} = 0.8$ (30KHGSA). For less durable steel (14), the margin of strength at $\sigma_H^{bc}/\sigma_{0.2} = 0.5$ (37KHN3A), etc. Thus, it is preferable to take into account the volume and use model (14).

5. The dependences on the diagram of the theoretical stress factors are more densely grouped in (14), than in $(10)$ due to very similar stress states in the region of the tops of acute stress concentrators. Therefore, the mechanical characteristics of steels have a secondary effect on $\alpha_T^{bc}$.

6. With an increase in the theoretical stress concentration factor and a decrease in $\alpha_T^{bc}$ at the same level $\sigma_H^{bc}/\sigma_{0.2}$ of the external load, the influence of the structural factor in steel on the occurrence of initial destruction (formation of discontinuity) reduces. However, for further destruction, the resistance of the material to macrocrack growth is essential. After its occurrence, other criteria of mechanics and kinetics of destruction are triggered.

The presented study can serve as a prerequisite for the development of analytical models to assess the residual life of welded joints and structures exposed to cyclic loads. Further research will presumably refine the analytical models. The authors will check and test the results through CAE modeling and proceed to the evaluation of effective stress concentration factors.

[6] Krokha VA. Uprochnenie metallov pri kholodnoi plasticheskoi deformatsii. Moscow: Mashinostroenie: 1980. 157 p. (In Russ.)

**References**

1. Molokov KA, Novikov VV, Turmov GP, et al. Estimation of Reliability of Ship Structures with Microcracks and Residual Welding Stresses. *Marine Intellectual Technologies*. 2018;41:45–54.

2. Novikov VV, Turmov GP, Surov OE, et al. *Povrezhdeniya i raschetnyi analiz prochnosti korabel'nykh konstruktsii*. Vladivostok: Far Eastern Federal University; 2020. 266 p. (In Russ.)

3. Erofeev VV, Ignatiev AG, Oleinik NI, et al. Mathematical Model for Assessing Stress Concentration Factors in T-Shaped Welded Joints. *Information Technology*. 2021;17:28–36.

4. Molokov K, Sakharova A, Mikhalev M. Crack Propagation-Based Assessment of the Endurance Limits of Welded Joints. *FEFU: School of Engineering Bulletin*. 2017;30:42–51. https://doi.org/10.5281/zenodo.399005

5. Kazanov GT, Novikov VV, Turmov GP. *Kontsentratsiya napryazhenii i drugie osobennosti napryazhennogo sostoyaniya sudovykh korpusnykh konstruktsii*. Vladivostok: Far Eastern Federal University; 2014. 178 p. (In Russ.)

6. Molokov KA, Novikov VV, Turmov GP, et al. *Matematicheskie modeli otsenki ehkspluatatsionnogo resursa i rabotosposobnosti sudovykh svarnykh konstruktsii*. Vladivostok: Far Eastern Federal University; 2021. 240 p. (In Russ.)

7. Emelianov OV, Shapovalov EL, Gavrilov VB. The Level of Concentration of Elastic Stresses in Butt Welded Connections Depending on Design Parameters. *BST: Byulleten' stroitel'noi tekhniki*. 2017;999:26–28.

8. Makhutov NA, Albagachiev AYu, Alekseeva SI, et al. *Prochnost', resurs, zhivuchest' i bezopasnost' mashin*. Moscow: Librokom; 2008. 576 p. (In Russ.)

9. Yamaleev KM, Gumerova LR. *Strukturnye aspekty razrusheniya metalla nefteprovodov*. Ufa: Gilem; 2011. 144 p. (In Russ.)

10. Khazhinskiy GM. *Deformirovanie. Razrushenie. Nadezhnost': Zadachi deformirovaniya i razrusheniya stali. Metody otsenki prochnosti ehnergeticheskogo oborudovaniya i truboprovodov*. Moscow: Lenand; 2014. 544 p. (In Russ.)

11. Larionov VP, Filippov VV. *Khladostoikost' materialov i ehlementov konstruktsii: rezul'taty i perspektivy*. Novosibirsk: Nauka; 2005. 290 p. (In Russ.)

12. Kryzhevich GB. Limit and Fatigue Strength Calculation Methods for Arctic Marine Structures. *Transactions of the Krylov State Research Centre*. 2019;388:41–54. http://doi.org/10.24937/2542-2324-2019-2-388-41-54.

13. Smirnov AN, Muravyev VV, Ababkov NV. *Razrushenie i diagnostika metallov*. Moscow: Innovatsionnoe mashinostroenie; 2016. 479 p. (In Russ.)

14. Negoda EN. Fatigue of Welded Joints of Large Diameter Pipes. *FEFU: School of Engineering Bulletin*. 2015;25:62–74.

15. Matokhin GV, Gorbachev KP. *Inzheneru o soprotivlenii materialov razrusheniyu*. Vladivostok: Dal'nauka; 2010. 281 p. (In Russ.)

16. Mitenkov FM, Volkov IA, Igumnov LA, et al. *Prikladnaya teoriya plastichnosti*. Moscow: Fizmatlit; 2015. 284 p. (In Russ.)

17. Levin VA, Vershinin AV. *Nelineinaya vychislitel'naya mekhanika prochnosti*. Vol. 2. *Chislennye metody*. Moscow: Fizmatlit; 2015. 544 p. (In Russ.)

18. Matvienko YuG. *Dvukhparametricheskaya mekhanika razrusheniya*. Moscow: Fizmatlit; 2021. 208 p. (In Russ.)

19. Panferov VM. Kontsentratsiya napryazhenii pri uprugoplasticheskikh deformatsiyakh. *Izvestiya akademii nauk SSSR. Otdelenie tekhnicheskikh nauk. Mekhanika i mashinostroenie*. 1954;4:47–65. (In Russ.)

20. Huy Duong Bui. *Fracture Mechanics: Inverse Problems and Solutions*. Moscow: Fizmatlit; 2011. 412 p. (In Russ.)

21. Petrova NE, Baeva LS. Biokorroziya korpusov sudov. *Vestnik of MSTU. Proceedings of MSTU*. 2006;9:890–892. (In Russ.)

*About the Authors:*

**Konstantin A Molokov,** associate professor of the Department of Industrial Safety, Polytechnic Institute, Far Eastern Federal University (8, Sukhanova St., Vladivostok, 690091, RF), associate professor of the Information Technologies and Systems, Vladivostok State University (41, Gogoleva St., Vladivostok, 690014, RF), Cand.Sci. (Eng.), ScopusID, ORCID, Spektrum011277@gmail.com

**Valery V Novikov,** associate professor of the Department of Marine Engineering and Transport, Polytechnic Institute, Far Eastern Federal University (8, Sukhanova St., Vladivostok, 690091, RF), Cand.Sci. (Eng.), ScopusID, ORCID.

**Mohammad Dabalez,** graduate student of the Department of Industrial Safety, Polytechnic Institute, Far Eastern Federal University (8, Sukhanova St., Vladivostok, 690091, RF), ORCID, dabalez.mo@students.dvfu.ru.

*Claimed contributorship:*

KA Molokov: basic concept formulation; research objectives and tasks; computational analysis; initial version of the body text; formulation of conclusions. VV Novikov: academic advising; analysis of research results; revision of conclusions and the body text. M Dabalez: work with sources; design of graphic materials.

**Received** 30.12.2022.
**Revised** 16.01.2023.
**Accepted** 18.01.2023.

*Conflict of interest statement*

The authors do not have any conflict of interest.

*All authors have read and approved the final manuscript.*

*Об авторах:*

**Константин Александрович Молоков,** доцент Департамента промышленной безопасности, Политехнический институт Дальневосточного федерального университета (690091, РФ, г. Владивосток, ул. Суханова, 8), доцент кафедры «Информационные технологии и системы» Владивостокского государственного университета (690014, РФ, г. Владивосток, ул. Гоголя, 41), кандидат технических наук, ScopusID, ORCID, Spektrum011277@gmail.com

**Валерий Васильевич Новиков,** доцент Департамента морской техники и транспорта, Политехнический институт Дальневосточного федерального университета (690091, РФ, Владивосток, ул. Суханова, 8), кандидат технических наук, ScopusID, ORCID

**Мохаммад Дабалез,** магистрант Департамента промышленной безопасности, Политехнический институт, Дальневосточного федерального университета (690091, РФ, Владивосток, ул. Суханова, 8), ORCID, dabalez.mo@students.dvfu.ru

*Заявленный вклад соавторов*

К.А. Молоков — формирование основной концепции, цели и задачи исследования, проведение расчетов, начальная версия основного текста, формулирование выводов. В.В. Новиков — научное руководство, анализ результатов исследований, доработка выводов и основного текста. М. Дабалез — работа с источниками, оформление графических материалов.

**Поступила в редакцию** 30.12.2022.
**Поступила после рецензирования** 16.01.2023.
**Принята к публикации** 18.01.2023.

*Конфликт интересов*

Авторы заявляют об отсутствии конфликта интересов.

*Все авторы прочитали и одобрили окончательный вариант рукописи.*

# MACHINE BUILDING AND MACHINE SCIENCE
# МАШИНОСТРОЕНИЕ И МАШИНОВЕДЕНИЕ



UDC 673.7
https://doi.org/10.23947/2687-1653-2023-23-1-55-65

*Original article*

## Polyethylene Resistance to Oil and Associated Water

**Imad Rizakalla Antipas**
Don State Technical University, 1, Gagarin sq., Rostov-on-Don, Russian Federation
✉ Imad.antypas@mail.ru

**Abstract**

***Introduction.*** Polyethylene is the most widely used material in various fields of the national economy, and products made of it have essential advantages, such as lightness, insolubility in organic solutions with quite satisfactory strength. However, the mechanism of its destruction is quite complex and depends on the working conditions and substances, which are in contact with it. The research purpose was to study the polyethylene resistance to oil and associated water under the static and dynamic conditions and at room temperature.

***Methods and Materials.*** The research was carried out on a laboratory device for passing various liquids (oil, associated and distilled water) in polyethylene pipes, assembled by the author of the article. While working, methods of statistical and dynamic data processing were applied.

***Results.*** Based on the results of previous experiments, graphs were plotted for the change in the weight and volume of immersed granules over time. They have shown that polyethylene has a quadratic dependence, and diffusion for the three liquids studied in this work (distilled water, accompanying water and oil) is described by Fick's law. This indicates the fact that the rate of liquid diffusion through polyethylene is the key factor.

***Discussion and Conclusions.*** The obtained results have shown that the rate of liquid diffusion through polyethylene is the key factor. Immersion in oil has a greater impact than immersion in associated or distilled water due to the presence of salts. It has been found out that the relative change in the weight and thickness of the polyethylene pipe walls through which oil passes is greater than those through which the associated water passes. Moreover, the microscopic cross sections images in the samples before and after the tests have confirmed the obtained results.

**Keywords:** Polyethylene, associated water, solid materials, salts, distilled water.

**Acknowledgements.** The author would like to thank the reviewers and the editorial board of the journal for valuable comments.

**For citation.** Antypas IR. Polyethylene Resistance to Oil and Associated Water. *Advanced Engineering Research (Rostov-on-Don).* 2023;23(1):55–65. https://doi.org/10.23947/2687-1653-2023-23-1-55-65

*Научная статья*

## Устойчивость полиэтилена к нефти и сопутствующей воде

**И. Р. Антибас**
Донской государственный технический университет, Российская Федерация, г. Ростов-на-Дону, пл. Гагарина, 1
✉Imad.antypas@mail.ru

**Аннотация**

***Введение.*** Полиэтилен является наиболее широко применяемым материалом в различных областях народного хозяйства, а изделия из него обладают существенными достоинствами, такими как лёгкость, нерастворимость в органических растворах при вполне удовлетворительной прочности. Однако механизм его разрушения достаточно сложен и зависит от условий работы и контактирующих с ним веществ. Цель исследований

заключалась в изучении устойчивости полиэтилена к нефти и сопутствующей воде при статическом и динамическом режиме и комнатной температуре.

***Материалы и методы.*** Исследования проводились на лабораторном устройстве для пропускания различных жидкостей (нефть, сопутствующая и дистиллированная вода) в полиэтиленовых трубах, собранном авторами статьи. При работе были применены методы статистической и динамической обработки данных.

***Результаты исследования.*** Графики изменения веса и объёма погруженных гранул во времени, построенные по результатам проведенных экспериментов, показали, что для полиэтилена характерна квадратичная зависимость и диффузия для трех исследуемых в данной работе жидкостей (дистиллированная вода, сопутствующая вода и нефть) описывается законом Фика. Это указывает на тот факт, что скорость диффузии жидкости через полиэтилен является наиболее важным фактором.

***Обсуждение и заключения.*** Эксперименты и полученные результаты показали, что скорость диффузии жидкости через полиэтилен является наиболее важным фактором. Погружение в нефть оказывает большее влияние, чем погружение в сопутствующую или дистиллированную воду из-за присутствия солей. Было обнаружено, что относительное изменение веса и толщины стенок полиэтиленовых труб, по которым проходит нефть, больше тех, по которым проходит сопутствующая вода, а микроскопические изображения срезов в образцах до и после испытаний подтвердили полученные результаты.

**Ключевые слова:** полиэтилен, сопутствующая вода, твердые материалы, соли, дистиллированная вода.

**Благодарности.** Автор выражает признательность рецензентам и редакции журнала за ценные замечания.

**Для цитирования.** Антибас И.Р. Использование метода конечных элементов для моделирования резервуара высокого давления из полимера, армированного углеродным волокном. *Advanced Engineering Research (Rostov-on-Don).* 2023;23(1):55–65. https://doi.org/10.23947/2687-1653-2023-23-1-55-65

**Introduction.** Polyethylene is one of the main elements of the olefin family, which is usually characterized by a waxy appearance, chemical inertia and physical properties deterioration at high temperatures. Since polyethylene is a partially crystallized material and does not go into secondary chemical reactions with any liquids, it has no solvents, and its water absorption at ambient temperature is relatively low.

Polyethylene does not dissolve in organic solutions, but it expands at a temperature of more than 70 °C and dissolves in granular aromatic hydrocarbons, it is not affected by oil, fats, kerosene and other hydrocarbons. It is also resistant to aqueous solutions of acids, salts and alkalis [1–5].

Polyethylene is oxidized by nitric acid, which causes a deterioration in the characteristics of the products obtained from it. Oxidation occurs in the presence of ultraviolet rays at ambient temperature, causing final brittleness and deterioration of the mechanical and thermal insulation properties [6–8]. The scientific interest is focused at the practical interaction study of polyethylene and oil, which is a mixture of hydrocarbon materials consisting mainly of compounds containing carbon and hydrogen as well as some elements mixed with hydrocarbons, such as sulfur, nitrogen and oxygen, in addition to metal elements in simple proportions, such as iron, nickel, arsenic and vanadium. Along with them, chlorides salts of land-based minerals as well as their sulfates are present in oil. Moreover, oil contains water in certain percentages, depending on its type and production conditions, and this percentage can increase up to 30 % relative to the total volume of oil, since it is in the form of saturated solutions of sodium chloride, magnesium sulfate and calcium. Carbon dioxide and hydrogen sulfide gases dissolving in water increase its volume. Acid and oxygen, reacting with iron and manganese dissolved in the associated water, form insoluble products. The associated water contains a small percentage of organic chloride salts, not exceeding 50 parts per million [9, 10].

The impurities contained in crude oil (solid materials – salts – water – chemical additives) cause serious risks to the oil refining equipment, its operating time and efficiency. Polymer materials are known to be destroyed in a completely different way than metal materials; therefore, when producing various products from them, it is necessary to take into account their physico-chemical properties and electrochemical reactions.

Plastics cannot dissolve like metals, but they are damaged or destroyed due to swelling, that is, the so-called embrittlement occurs, in which they soften, harden and change colour, which leads to their mechanical properties deterioration.

There are several mechanisms of polymer materials destruction:

– structure swelling;

– dissolution;

– bonds are destroyed under heat, chemical reactions or free radical reactions. The surface layer embrittlement can occur by any one mechanism or by a combination of mechanisms [11–13].

Dissolution and swelling without breaking chemical bonds are the main causes of embrittlement upon contact with impurities, and this process is complex, since small amounts of polymer solution penetrate inside [14], forming a seeping layer with altered physical properties (Fig. 1).

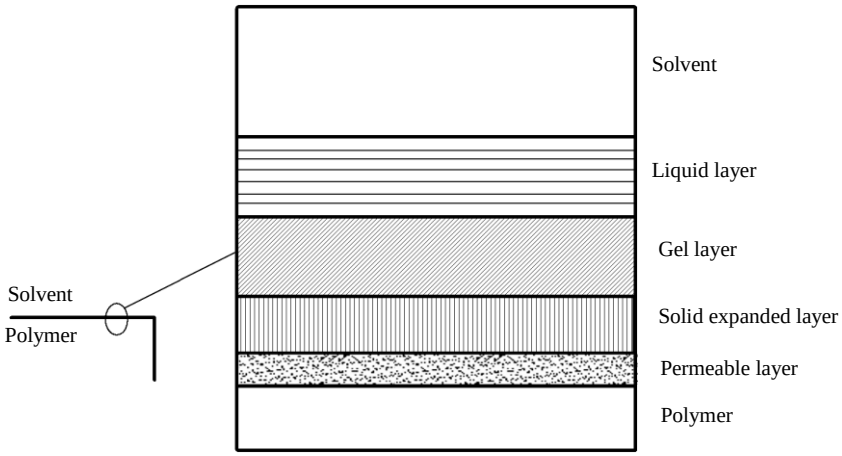


Fig. 1. Layer-structure of embrittlement process

The research objective is to study the polyethylene resistance to oil and associated water at room temperature, both at rest and in motion.

**Materials and research methods.** Table 1 shows the substances dissolved in oil after its extraction.

Table 1

Substances soluble and insoluble in oil after its extraction

| Soluble substances | | | Insoluble substances | |
|---|---|---|---|---|
| solid substances | | gases | metal substances | organic substances |
| positive electrolytes: $Mg^+$, $Fe^+$, $K^+$, $Na^+$, $Mn^+$ negative electrolytes: $Br^-$, $Cl^-$, $F^-$, $CO_3^{-2}$, $SO_4^{-2}$, $HCO_3^-$ | plants and animals | $O_2$, $H_2S$, $N_2$, $CO_2$ | $Fe(OH)_3$, $FeS_2$, $SCO_2$ sand with clay substance, sulfate compounds, carbonates, alkaline land-based minerals. | Compounds obtained as a result of the addition of demulsifiers, bacteria, aquatic plants as well as plant and animal residues. |

Table 2 shows the composition of the associated water used in the experiments.

Table 2

Composition of associated water used in experiments

| Analysis | Measured value | Measurement units |
|---|---|---|
| Density | 1.015 | gr/cm$^3$ |
| $Cl^-$ | 10,100 | ppm |
| $Na^+$ | 2,427 | |
| $Mg^+$, | 370 | |
| $Ca^{2+}$ | 1,270 | |
| Total stiffness $CaCO_3$ | 4,243 | |
| Alkalinity $(CaCO_3)_m$ | 530 | |
| $SO_4^{-2}$ | 1,093 | |
| $NO_3^-$ | 100 | |
| $NH_4^-$ | 13 | |
| $H_2S$ | 130 | |
| $PH$ | 8.5 | |

Petroleum alcohol was used as a cleaning agent. The experiments were carried out using granules and pipes made of high-pressure polyethylene HDPE of low density (Table 3).

Table 3

Technical characteristics of polyethylene granules and pipes used in the experiments

| | Granules | Pipes |
|---|---|---|
| Type | Low-density high-pressure polyethylene | |
| Density | 0.914 | 0.917 |
| Shore hardness | 44.6 | 46.7 |
| Elongation-to-cut ratio | absent | 4.42 |
| The degree of softening onset | 109-122 | 110-112 |

**Laboratory instruments.** Oil and associated water passed through polyethylene pipes in a laboratory device assembled by the author (Fig. 2). The complex of equipment included:

– sealed glass containers;

– scale with a sensitivity of ± 0.1 g, %;

– electronic micrometer with an accuracy of 1 micrometer;

electronic microscope connected to a computer

– An electron microscope connected to a computer.

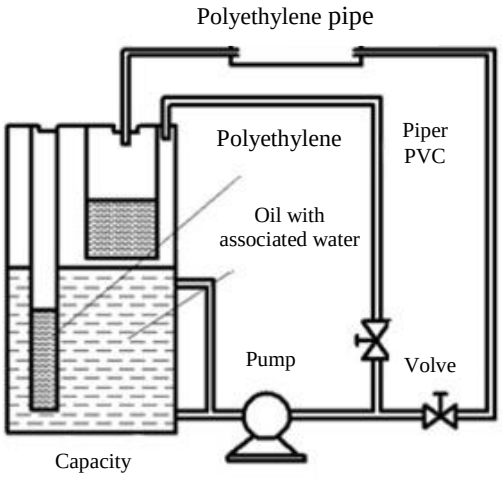


Fig. 2. Laboratory device for passing oil and associated water in polyethylene pipes

**Experiments.** In calm mode (immersion method), the sequence of actions when setting up the experiment was as follows:

– weight $W_1$ and volume $V_1$ were determined for several polyethylene granules samples, the characteristics of which are given in Table 3;

– the samples were completely immersed in oil, associated and distilled water in the sealed containers for certain periods of time;

– the taken samples were cleaned;

– the sample weight was determined as $W_2$ and its volume as $V_2$ during the experiment;

– the weight change was calculated as $\Delta W=W_2 - W_1$ and the volume change – as $\Delta V = V_2 - V_1$,

–the relative weight change as $\frac{\Delta W}{W_1}\cdot 100$ and the relative volume change as $\frac{\Delta V}{V_1}\cdot 100$ were calculated after each sample testing.

In dynamic mode:

– oil and associated water flowed in the polyethylene pipes at a constant speed at the ambient temperature, their weight as $W_1$ and the wall thickness were determined for specific periods of time;

– the pipes were cleaned after each experiment;

– their weight as $W_2$ was determined after the experiment $W_2$, and the wall thickness – after the experiment as $X_2$;

– the weight change was determined as $\Delta W = W_2 - W_1$, the volume change was as $\Delta V = V_2 - V_1$, the relative weight change was as $\frac{\Delta W}{W_1}\cdot 100$ and thickness change was as $\Delta X$ after the experiment.

**Results and discussion**

The weight and volume changes test results of particles immersed in oil, associated and distilled water were summarized in Tables (4–9). A graphical dependence was found for the relative weight and size changes of oil granules immersed in water, associated and distilled water (Fig. 3 and 4).

Table 4

Weight change of granules immersed in oil

| No. | 1 | | | 2 | | | 3 | | |
|---|---|---|---|---|---|---|---|---|---|
| Immersion time, days | $W_1$, gr | $W_2$, gr | $\Delta W$, % | $W_1$, gr | $W_2$, gr | $\Delta W$, % | $W_1$, gr | $W_2$, gr | $\Delta W$, % |
| 10 | 27.022 | 27.673 | 2.240 | 26.9611 | 27.5542 | 2.200 | 25.384 | 25.921 | 2.261 |
| 30 | 26.652 | 28.6376 | 7.450 | 26.4489 | 28.4589 | 7.600 | 26.577 | 28.613 | 7.661 |
| 60 | 25.839 | 28.2497 | 9.330 | 23.486 | 25.7346 | 9.574 | 25.266 | 25.266 | 9.396 |
| 90 | 26.863 | 29.6979 | 10.55 | 27.3432 | 30.1732 | 10.350 | 25.683 | 25.683 | 10.28 |

Table 5

Volume change of oil granules

| No. | 1 | | | 2 | | | 3 | | |
|---|---|---|---|---|---|---|---|---|---|
| Immersion time, days | $V_1$, $cm^3$ | $V_2$, $cm^3$ | $\Delta V$, % | $V_1$, $cm^3$ | $V_2$, $cm^3$ | $\Delta V$, % | $V_1$, $cm^3$ | $V_2$, $cm^3$ | $\Delta V$, % |
| 10 | 50.0 | 51.0 | 2.0 | 50.0 | 51.0 | 2.0 | 50.0 | 51.0 | 2.0 |
| 30 | 50.0 | 52.1 | 4.2 | 50.0 | 52.4 | 4.8 | 50.0 | 52.3 | 4.6 |
| 60 | 50.0 | 53.0 | 6.0 | 50.0 | 53.0 | 6.0 | 50.0 | 53.0 | 6.0 |
| 90 | 50.0 | 53.7 | 7.4 | 50.0 | 53.7 | 7.4 | 50.0 | 53.9 | 7.8 |

Table 6

Weight change of granules immersed in the associated water

| No. | 1 | | | 2 | | | 3 | | |
|---|---|---|---|---|---|---|---|---|---|
| Immersion time, days | $W_1$, gr | $W_2$, gr | $\Delta W$, % | $W_1$, gr | $W_2$, gr | $\Delta W$, % | $W_1$, gr | $W_2$, gr | $\Delta W$, % |
| 10 | 55.045 | 55.430 | 0.70 | 58.765 | 58.765 | 0.70 | 28.514 | 28.695 | 0.63 |
| 30 | 55.333 | 55.948 | 1.11 | 26.400 | 26.400 | 1.10 | 26.962 | 27.25 | 1.07 |
| 60 | 45.831 | 55.629 | 1.45 | 27.332 | 27.332 | 1.60 | 26.614 | 26.99 | 1.44 |
| 90 | 26.226 | 26.6452 | 1.595 | 27.0853 | 27.0853 | 1.650 | 26.8433 | 27.254 | 1.530 |

Table 7

Volume change of particles immersed in the associated water

| No. | 1 | | | 2 | | | 3 | | |
|---|---|---|---|---|---|---|---|---|---|
| Immersion time, days | $V_1$, $cm^3$ | $V_2$, $cm^3$ | $\Delta V$, % | $V_1$, $cm^3$ | $V_2$, $cm^3$ | $\Delta V$, % | $V_1$, $cm^3$ | $V_2$, $cm^3$ | $\Delta V$, % |
| 10 | 50.0 | 50.0 | 0.0 | 50.0 | 50.0 | 0.0 | 50.0 | 50.0 | 0.0 |
| 30 | 50.0 | 50.5 | 1.0 | 50.0 | 50.5 | 1.0 | 50.0 | 50.5 | 1.0 |
| 60 | 50.0 | 51.0 | 2.0 | 50.0 | 51.0 | 2.0 | 50.0 | 51.0 | 2.0 |
| 90 | 50.0 | 51.52 | 2.5 | 50.0 | 51.1 | 2.2 | 50.0 | 51.1 | 2.2 |

Table 8

Weight change of granules immersed in distilled water

| No. | 1 | | | 2 | | | 3 | | |
|---|---|---|---|---|---|---|---|---|---|
| Immersion time, days | $W_1$, gr | $W_2$, gr | $\Delta W$, % | $W_1$, gr | $W_2$, gr | $\Delta W$, % | $W_1$, gr | $W_2$, gr | $\Delta W$, % |
| 10 | 56.003 | 56.003 | 0.000 | 26.761 | 26.762 | 0.00 | 26.723 | 26.723 | 0.00 |
| 30 | 54.40 | 54.40 | 0.000 | 27.058 | 27.058 | 0.12 | 26.599 | 26.599 | 0.00 |
| 60 | 55.48 | 55.489 | 0.000 | 26.303 | 26.303 | 0.00 | 26.084 | 26.084 | 0.00 |
| 90 | 55.37 | 55.37 | 0.000 | 26.8300 | 26.8300 | 0.000 | 27.1665 | 27.1665 | 0.000 |

Table 9

Volume change of granules immersed in distilled water

| No. | 1 | | | 2 | | | 3 | | |
|---|---|---|---|---|---|---|---|---|---|
| Immersion time, days | $V_1$, $cm^3$ | $V_2$, $cm^3$ | $\Delta V$, % | $V_1$, $cm^3$ | $V_2$, $cm^3$ | $\Delta V$, % | $V_1$, $cm^3$ | $V_2$, $cm^3$ | $\Delta V$, % |
| 10 | 50.0 | 50.0 | 0.0 | 50.0 | 50.0 | 0.0 | 50.0 | 50.0 | 0.0 |
| 30 | 50.0 | 50.1 | 0.2 | 50.0 | 50.1 | 0.2 | 50.0 | 50.1 | 0.2 |
| 60 | 50.0 | 50.0 | 0.0 | 50.0 | 50.0 | 0.0 | 50.0 | 50.0 | 0.0 |
| 90 | 50.0 | 50.0 | 0.0 | 50.0 | 50.0 | 0.0 | 50.0 | 50.0 | 0.0 |

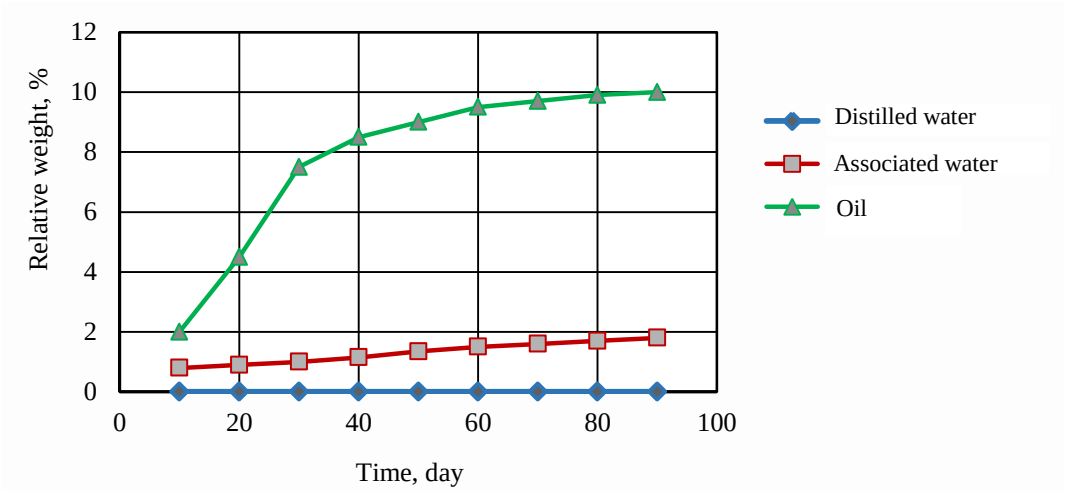


Fig. 3. Relative weight change of the immersed granules by time

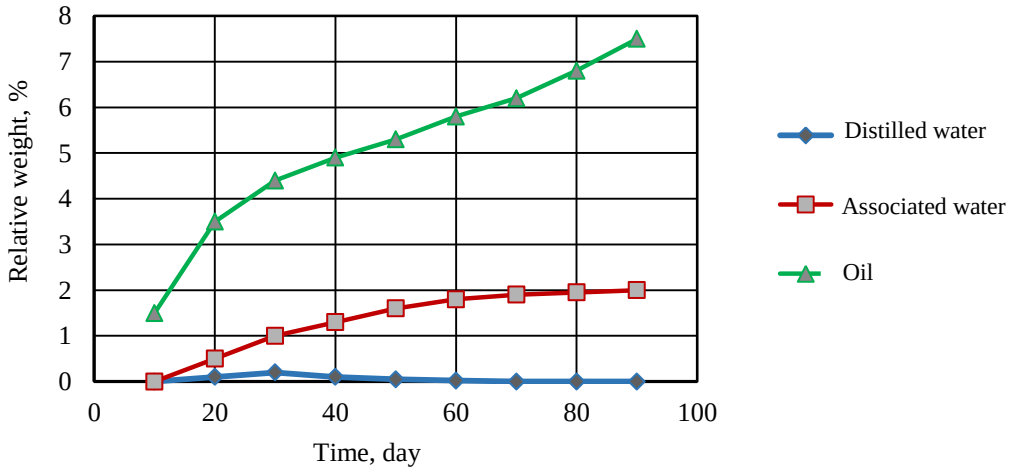


Fig. 4. Relative volume change of immersed granules by time

Figures 3 and 4 show that the time dependence of the relative weight and size changes of polyethylene granules has the character of a quadratic dependence and follows Fick's law in diffusion in the cases of three studied liquids (distilled water, associated water and oil), which indicates that the diffusion speed of liquid through polyethylene is the most important factor.

The relative weight change of granules immersed in the distilled water is not mentioned, but it is rarely noticeable in the associated water and increases more in the oil, as shown in Figure 4. This is due to the fact that salt diffusion significantly effects on the relative weight and volume between the granules immersed in the distilled water, on the one hand, and the granules immersed in the oil and related water, on the other hand.

The test results of the pipe weight and thickness changes, in which oil and associated water flow, are systematized in Tables 10 and 11. A graphical dependence of the pipe relative weight and thickness changes, through which the oil passes with the associated water flow shown in Figure 5 and 6, was obtained.

The sample cross section micrographs were taken before and after the tests with a 510-time increase and shown in Figure (7).

Table 10

Pipe weight and thickness changes through which oil flows

| Immersion time, days | | | 30 | | 60 | | 90 | |
|---|---|---|---|---|---|---|---|---|
| Pipe number | $W_1$ (gr) | $X_1$, mm | $W$, % | $\Delta X$ | $\Delta W$, % | $\Delta X$ | $W$, % | $\Delta X$ |
| 1 | 18.019 | 2.483 | 0.60 | 0.024 | 1.07 | 0.05 | 3.02 | 0.17 |
| 2 | 18.6440 | 2.485 | 0.90 | 0.032 | 1.12 | 0.07 | 3.01 | 0.19 |
| 3 | 18.6009 | 2.490 | 0.58 | 0.022 | 1.14 | 0.07 | 3.12 | 0.21 |
| 4 | 18.6441 | 2.483 | 0.91 | 0.032 | 1.12 | 0.096 | 3.00 | 0.19 |
| 5 | 18.5999 | 2.487 | 0.37 | 0.022 | 1.13 | 0.08 | 3.11 | 0.22 |

Table 11

Pipe weight and thickness changes through which the associated water flows

| Immersion time, days | | | 30 | | 60 | | 90 | |
|---|---|---|---|---|---|---|---|---|
| Pipe number | $W_1$ (gr) | $X_1$, mm | $W$, % | $\Delta X$ | $W$, % | $\Delta X$ | $W$, % | $\Delta X$ |
| 1 | 15.22 | 2.483 | 0.399 | 0.012 | 0.521 | 0.025 | 1.35 | 0.087 |
| 2 | 19.134 | 2.484 | 0.404 | 0.015 | 0.478 | 0.029 | 1.42 | 0.086 |
| 3 | 15.905 | 2.483 | 0.409 | 0.011 | 0.459 | 0.028 | 1.38 | 0.075 |
| 4 | 18.6009 | 2.400 | 0.39 | 0.013 | 0.469 | 0.027 | 1.40 | 0.080 |
| 5 | 18.019 | 2.483 | 0.38 | 0.012 | 0.498 | 0.027 | 1.39 | 0.079 |

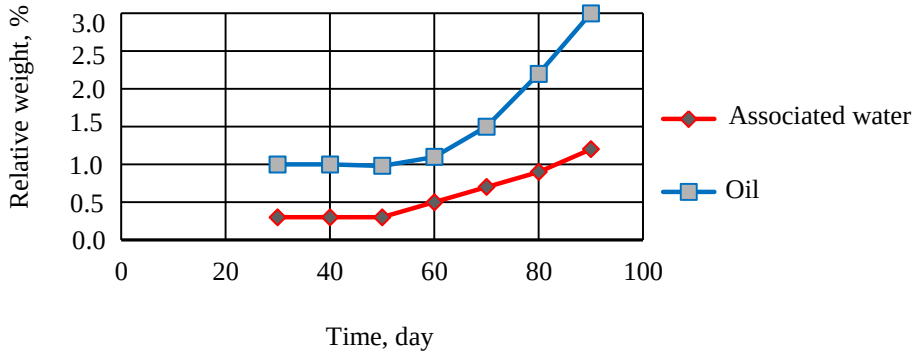


Fig. 5. Pipe relative weight change through which oil and associated water flow, over time

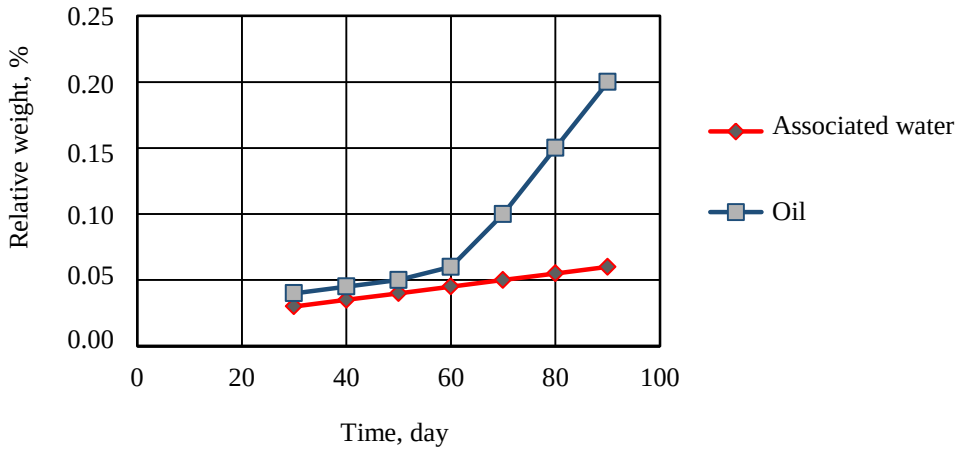


Fig. 6. Pipe relative thickness change in which oil and associated water flow, depending on time period

Due to Figures (6) and Table (12), it is noted that the relative change in the weight and thickness of the polyethylene pipe walls through which oil passes is greater than those through which the associated water passes, which indicates that polyethylene is more affected by oil.

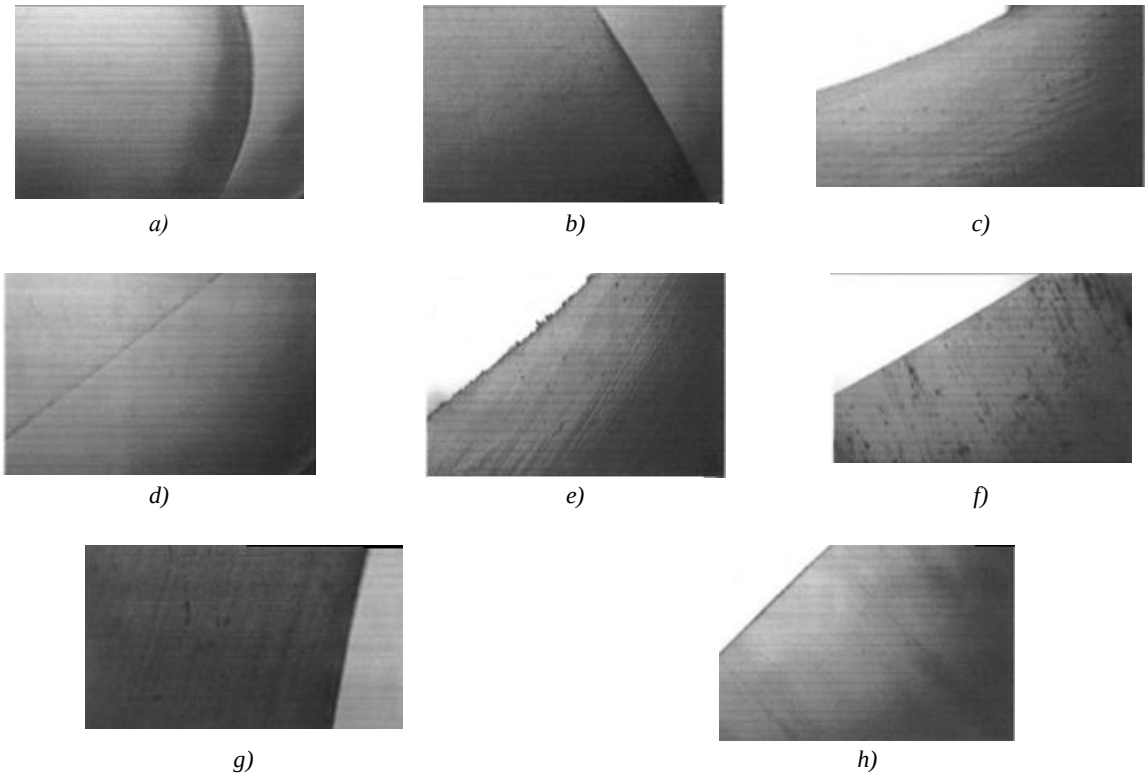

Fig. 7. Sample cross section micrographs before and after tests with a 510-time increase: *a* — cross section of a clean granule; *b* — cross section of an oil granule; *c* — cross section of a pipe with associated water in oil; *d* — cross section of a pipe immersed in oil; *e* — inner surface of the pipe with associated water; *g* — cross section of the pipe immersed in oil after 200 hours; *h* — inner surface of the pipe immersed in oil

Figure 7 shows cuts of pipe and granules samples before and after the tests, reflecting the surface colour and smoothness of the cross sections subjected to the tests, compared to the clean cross sections, which confirms the previous results obtained due to the basis of the graphs.

**Conclusions**

The experiments and the results obtained have shown that the liquid diffusion speed through polyethylene is the most significant factor. Immersion in oil has a greater impact than immersion in associated water and distilled water according to the presence of salts.

It has been found out that the relative change in the weight and thickness of the polyethylene pipe walls through which oil passes is greater than those through which the associated water passes, and the microscopic cross sections images in the samples before and after the tests have confirmed the obtained results.

**Reference**

1. Antypas I. The Influence of Polyethylene Processing on the Plastic Containers Blowing. *Journal of Physics: Conference Series*. 2020;1515:042042. 10.1088/1742-6596/1515/4/042042

2. Zakharyan EM, Petrukhina NN, Dzhabarov EG, et al. Pathways of Chemical Recycling of Polyvinyl Chloride. Part 2. *Russian Journal of Applied Chemistry*. 2020;93:1445–1490. 10.1134/S1070427220100018

3. Chinedu Nwapa, Okunwaye OJ, Okonkwo CL, et al. Mechanical Properties of High Density Polyethylene and Linear Low Density Polyethylene Blend. *SSRG International Journal of Polymer and Textile Engineering (SSRG-IJPTE)*. 2020;7:22–28. 10.14445/23942592/IJPTE-V7I1P103

4. Antypas IR. Improvement of Mechanical Behavior of Neoprene Rubber by means of Glass Fiber. *Journal of Physics: Conference Series*. 2021;1889:042007. http://dx.doi.org/10.1088/1742-6596/1889/4/042007

5. Wei-Li Wu, Yi-Wen Wang. High Density Polyethylene Film Toughened with Polypropylene and Linear Low Density Polyethylene. *Materials Letters*. 2019;257:126689. http://doi.org/10.1016/j.matlet.2019.126689

6. Chaudhary AK, Vijayakumar RP. Effect of Chemical Treatment on Biological Degradation of High-Density Polyethylene (HDPE). *Environment, Development and Sustainability*. 2020;22:1093–1104. https://doi.org/10.1007/s10668-018-0236-6

7. Lethola M, Miettinen IT, Lampola T, et al. Pipeline Materials Modify the Effectiveness of Disinfectants in Drinking Water Distribution Systems. *Water Research*. 2005;39:1962–1971. http://dx.doi.org/10.1016/j.watres.2005.03.009

8. Antypas IR, Savostina TP. Study of Mechanical Properties of Recycled Polyethylene of High and Low Density. *Materiale Plastice*. 2021;58:210–215. https://doi.org/10.37358/MP.21.4.5546

9. Zabolotnyi O, Zabolotnyi V, Koshevoy N. Oil Products Moisture Measurement Using Adaptive Capacitive Instrument Measuring Transducers. In book: Nechyporuk M, Pavlikov V, Kritskiy D. (eds.) *Integrated Computer Technologies in Mechanical Engineering*. 2021;188:81–91. http://dx.doi.org/10.1007/978-3-030-66717-7_7

10. Beglyarovas ÉS, Sokolova A, Bakshtanin M. Change of Indicators of Pollution of Surface Drain of Urban Territories when Carrying Out Construction Work on the Example of the Private Reservoirs of Rivers Likhoborka and Zhabenka. *Power Technology and Engineering*. 2021;55:1–5. http://dx.doi.org/10.1007/s10749-021-01316-0

11. Martins LS, Mulinari D, Zanini NC. Envelopes with Microplastics Generated from Recycled Plastic Bags for Crude Oil Sorption. *Polymer Engineering and Science*. 2021;61:2055–2065. http://dx.doi.org/10.1002/pen.25734

12. Ketan Patel, Samir H Chikali, Swaminathan Sivaram. Ultrahigh Molecular Weight Polyethylene: Catalysis, Structure, Properties, Processing and Applications. *Progress in Polymer Science*. 2021;109:101290. https://doi.org/10.1016/j.progpolymsci.2020.101290

13. Lethola M, Miettinen LT, Lampola T, et al. Pipeline Materials Modify the Effectiveness of Disinfectants in Drinking Water Distribution Systems. *Water Research*. 2005;39:1962–1971. http://dx.doi.org/10.1016/j.watres.2005.03.009

14. Reye JT, Moore EJ, Riga AT. *Dissolution and Swelling Characterization of Diverse Amorphous Polymers by Thermal Mechanical Analysis*. In: Proc. Annual Conference of the North American Thermal Analysis Society (NATAS), 2005. P. 1–22. https://www.researchgate.net/publication/343759376_Dissolution_and_Swelling_-_Characterization_of_Diverse_Amorphous_Polymers_by_Thermal_Mechanical_Analysis

*About the Author:*

**Imad Rizakalla Antipas,** associate professor of the Fundamentals of Machinery Design Department, Don State Technical University (1, Gagarin sq., Rostov-on-Don, 344003, RF), Cand.Sci. (Eng.), associate professor, ScopusID, ResearchID, ORCID, imad.antypas@mail.ru

**Received** 01.02.2023.

**Revised** 17.02.2023.

**Accepted** 20.02.2023.

*Conflict of interest statement*

The author does not have any conflict of interest.

*The author has read and approved the final manuscript.*

*Об авторе:*

**Имад Ризакалла Антибас,** доцент кафедры «Основы конструирования машин» Донского государственного технического университета (344003, РФ, г. Ростов-на-Дону, пл. Гагарина, 1), кандидат технических наук, доцент, ScopusID, ResearchID, ORCID, imad.antypas@mail.ru

**Поступила в редакцию** 01.02.2023.

**Поступила после рецензирования** 17.02.2023.

**Принята к публикации** 20.02.2023.

*Конфликт интересов*

Автор заявляет об отсутствии конфликта интересов.

*Автор прочитал и одобрил окончательный вариант рукописи.*

# INFORMATION TECHNOLOGY, COMPUTER SCIENCE AND MANAGEMENT
# ИНФОРМАТИКА, ВЫЧИСЛИТЕЛЬНАЯ ТЕХНИКА И УПРАВЛЕНИЕ



UDC 004.89
https://doi.org/10.23947/2687-1653-2023-23-1-66-75

*Original article*

## Machine Learning Model for Early Detection of COVID-19 by Heart Rhythm Abnormalities

**Maksim S Mezhov**[1] ✉, **Vyacheslav O Kozitsin**[1], **Iurii D Katser**[2]

[1] "Digital Technologies and Platforms" LLC, 53, Dubininskaya St., Moscow, Russian Federation

[2] Skolkovo Institute of Science and Technology, 30, Bolshoy Boulevard, Moscow, Russian Federation

✉ msmezhov@ya.ru

**Abstract**

***Introduction.*** Electronic devices capable of collecting individual telemetry data have opened up prospects for preclinical detection of COVID-19 signs. Known solutions involve the analysis of information that is difficult to obtain at the moment. We are talking, specifically, about the blood condition or a PCR test. This significantly limits the possibility of integrating algorithms with wrist gadgets. At the same time, the cardiovascular system as an object of observation is quite informative, the data collection is well developed. The article describes the problem of detecting covid anomalies in rhythm strips. The work aims at creating a mathematical model based on machine learning algorithms to automate the process of detecting covid abnormalities in the heart rhythm. The possibility of integrating the results obtained with fitness bracelets and smart watches is shown.

***Materials and Methods.*** The work involved an open technology stack: Python, Scikit-learn, Lightgbm. When assessing the quality of models for binary classification, metric $F_1$ was used. 229 cardiac rhythm strips (cardiointervalographies) of patients with COVID-19 were studied. The presence or absence of signs of an anomaly was determined taking into account the time of the rhythm strip and the intervals between heartbeats. Deviations that could indicate infection were shown graphically. Based on the exploratory analysis results, a list of signs indicating an anomaly was made.

***Results.*** As a result of the work done, a mathematical model was obtained that detected heart rate abnormalities specific to COVID-19 with an accuracy of 83 %. The basic features determining the predictive ability of the model were identified and ranked. They included the current value of the interval between heartbeats, the derivatives at the subsequent and previous points of measuring the duration of the heartbeat, the first derivative at the current point, and the deviation of the current value of the duration of the *RR*-interval from the median. The first indicator in this list was recognized as the most significant, the last — the least. For machine learning purposes, the potential of five algorithms was evaluated: IsolationForest, LGBMClassifier, RandomForestClassifier, ExtraTreesClassifier, SGDOneClassSVM. The normal and abnormal results of observations in isolation trees were visualized. A parameter was set that corresponded to the probability of regular observation outside the norm, and its value was selected — 0.11. Taking into account this indicator, a graph was constructed for the SGDOneClassSVM model. Based on the data set, using the cross-validation technique, the quality metric was calculated. The case in hand was a rhythm strip with a time series of observations taken in one continuous time interval from one person. A step-by-step process of obtaining averaged metric values for each model was described. In comparison, the highest indicator was recorded for the LGBMClassifier model, the lowest — for SGDOneClassSVM and IsolationForest.

***Discussion and Conclusions.*** The resulting mathematical model takes up little space in the memory of a mobile device, i.e., it does not impose significant requirements on computing resources. The solution has an acceptable detection quality for pre clinical screening of COVID-19-related cardiovascular disorders. The algorithm detects anomalies in 83 % of cases. Four minutes is enough to record a rhythm strip. The proposed scenario for using an integrated solution is concise and easy to implement. Widespread use of the development can contribute to the detection of COVID-19 at an early stage.

**Keywords:** COVID-19, causes of death in covid-positive patients, complications in the work of cardiovascular system, PCR test, preclinical monitoring of the cardiovascular system, built-in pulse rate sensors, rhythm strip, RR-interval, cardiac electrocardiogram, abnormal heartbeat, heartbeat with abnormal rhythm, machine learning, LGBMClassifier algorithm.

**Acknowledgements.** The authors would like to thank the management and moderators of the open All-Russian competition of professionals in the digital economy "Digital Breakthrough" for the data provided for the study.

**For citation.** Mezhov MS, Kozitsin VO, Katser IuD. Machine Learning Model for Early Detection of COVID-19 by Heart Rhythm Abnormalities. *Advanced Engineering Research (Rostov-on-Don).* 2023;23(1):66–75. https://doi.org/10.23947/2687-1653-2023-23-1-66-75

*Научная статья*

# Модель машинного обучения для обнаружения COVID-19 на ранней стадии по аномалиям в ритме сердца

**М.С. Межов[1], В.О. Козицин[1], Ю.Д. Кацер[2]**

[1]ООО «Цифровые технологии и платформы», Российская Федерация, Москва, ул. Дубининская, 53, стр. 6

[2]Сколковский институт науки и технологии, Российская Федерация, Москва, территория инновационного центра «Сколково», Большой бульвар, 30, стр. 1

✉ msmezhov@ya.ru

**Аннотация**

***Введение.*** Электронные устройства, способные собирать данные по телеметрии индивидуума, открыли перспективы доклинического выявления признаков COVID-19. Известные решения предполагают анализ информации, которую сложно получить в моменте. Речь идет, например, о состоянии крови или ПЦР-тесте. Это существенно ограничивает возможности интеграции алгоритмов с наручными гаджетами. При этом сердечно-сосудистая система как объект наблюдения достаточно информативна, съем данных хорошо проработан. В статье описана задача детекции ковидных аномалий в ритмограммах. Цель работы — создание математической модели на базе алгоритмов машинного обучения для автоматизации процесса выявления ковидных аномалий в ритме сердца. Показана возможность интеграции полученных результатов с фитнесс-браслетами и умными часами.

***Материалы и методы.*** В работе задействовали открытый стек технологий: Python, Scikit-learn, Lightgbm. При оценке качества моделей для бинарной классификации использовалась метрика $F_1$. Изучены 229 ритмограмм сердца (кардиоинтервалографий) пациентов с COVID-19. Наличие или отсутствие признаков аномалии определялось с учетом времени ритмограммы и интервалов между сердцебиениями. Графически показаны отклонения, которые могут свидетельствовать о заражении. По итогам разведочного анализа собран перечень признаков, указывающих на аномалию.

***Результаты исследования.*** В результате проделанной работы получена математическая модель, которая детектирует специфичные для COVID-19 аномалии сердечного ритма с точностью 83 %. Выявлены и ранжированы основные признаки, определяющие прогностическую способность модели. Это текущее значение интервала между ударами сердца, производные в последующей и предыдущей точках измерения продолжительности сердцебиения, первая производная в текущей точке и отклонение от медианы текущего значения длительности *RR*-интервала. Первый показатель в этом перечне признан наиболее значимым, последний — наименее. Для целей машинного обучения оценивался потенциал пяти алгоритмов: IsolationForest, LGBMClassifier, RandomForestClassifier, ExtraTreesClassifier, SGDOneClassSVM. Визуализированы нормальные и аномальные результаты наблюдений в изолирующих деревьях. Установлен параметр, который соответствует вероятности регулярного наблюдения за пределами нормы, и выбрано его значение — 0,11. С учетом данного показателя построен график для модели SGDOneClassSVM. По набору данных с применением техники перекрестной проверки рассчитана метрика качества. Речь идет о ритмограмме с временны́м рядом наблюдений, снятых за один непрерывный интервал времени у одного человека. Описан пошаговый процесс получения усредненных значений метрики для каждой модели. При сравнении самый высокий показатель зафиксирован у модели LGBMClassifier, наименьшие — у SGDOneClassSVM и IsolationForest.

***Обсуждение и заключения.*** Полученная математическая модель занимает мало места в памяти мобильного устройства, то есть не предъявляет значимых требований к вычислительным ресурсам. Решение обладает приемлемым качеством детекции для доклинического скрининга связанных с COVID-19 сердечно-сосудистых

нарушений. Алгоритм обнаруживает аномалии в 83 % случаев. Для записи ритмограммы достаточно 4 минут. Предлагаемый сценарий использования интегрированного решения лаконичен и легко реализуем. Широкое использование разработки может способствовать выявлению COVID-19 на ранней стадии.

**Ключевые слова:** COVID-19, причины смерти ковид-положительных пациентов, осложнения в работе сердечно-сосудистой системы, ПЦР-тест, доклинический контроль сердечно-сосудистой системы, встроенные датчики частоты пульса, ритмограмма, RR-интервал, электрокардиограмма сердца, аномальное по продолжительности сердцебиение, сердцебиение с аномальным ритмом, машинное обучение, алгоритм LGBMClassifier.

**Благодарности.** Авторы выражают благодарность руководству и модераторам открытого всероссийского соревнования профессионалов в сфере цифровой экономики «Цифровой прорыв» за предоставленные данные для исследования.

**Для цитирования.** Межов М.С., Козицин В.О., Кацер Ю.Д. Модель машинного обучения для обнаружения COVID-19 на ранней стадии по аномалиям в ритме сердца. *Advanced Engineering Research (Rostov-on-Don).* 2023;23(1):66–75. https://doi.org/10.23947/2687-1653-2023-23-1-66-75

**Introduction.** Investigation of the impact of COVID-19 on humans remains a challenge. Thus, in 2021–2022, more than 16,000 scientific papers were published on this topic. One of the main causes of death of covid-positive patients was complications in the cardiovascular system (hereinafter referred to as CVS) caused by exposure to coronavirus [1]. Two methods are mainly used for preclinical diagnosis of COVID-19: biochemical method based on polymerase chain reaction (PCR test) and blood analysis. Contacts with medical staff needed in this case (including visits to medical institutions) complicate regular operational control and increase the burden on the healthcare system. Thus, it seems relevant to use modern technologies of preclinical control of CVS for early detection of COVID-19 signs.

Wearable electronic devices can provide regular monitoring. The most common of them are fitness bracelets and smart watches with built-in heart rate sensors and the ability to perform measurements with high discreteness [2]. This approach opens up opportunities for analyzing data flows based on machine learning[1] [3].

The presented study aims at creating a trainable model capable of detecting covid anomalies based only on data on heart rhythm. A number of papers [4–6] consider similar problems, but the solutions are based on additional information about the state of the blood and other characteristics[2]. This significantly limits the possibilities of their integration with wearable devices, because at the moment, it is impossible to enter the results of a blood test or a smear for a PCR test into the model. The novelty of the proposed solution is in the fact that only heart rate data is used, which can be taken with a high frequency in a way convenient for a person and interpret the indicators in real time.

**Materials and Methods**

**Data characteristics.** 229 impersonal rhythm strips (cardiointervalographies) of patients with COVID-19 were used in the research. The information was obtained in 2021 as part of the open All-Russian competition "Digital Breakthrough" for professionals in the digital economy. A data fragment is presented in Table 1.

Table 1

A fragment of the data set

| Number of rhythm strip | Time in milliseconds | RR interval between heartbeats in milliseconds | Sign of covid anomaly* |
|---|---|---|---|
| 81 | 0 | 576 | 0 |
| 81 | 568 | 568 | 0 |
| 81 | 1,140 | 572 | 0 |
| … | … | … | … |
| 176 | 44,332 | 568 | 0 |
| 176 | 44,968 | 636 | 1 |
| 176 | 45,596 | 628 | 0 |
| *0 — no anomaly, 1 - there is an anomaly. | | | |

Figure 1 shows the relationship of the rhythm strip (RR interval) and the electrocardiogram of the heart (ECG).

[1] Permyakov SA, et al. Ehndogennye anomalii kardioritma u patsientov s COVID-19. In: Proc. VII All-Russian Conf. "Nelineinaya dinamika v kognitivnykh issledovaniyakh – 2021". Nizhny Novgorod: Institute of Applied Physics of RAS; 2021. P. 109–110. (In Russ.)

[2] Diagnosis of COVID-19 and Its Clinical Spectrum. Kaggle Inc. URL: https://www.kaggle.com/datasets/einsteindata4u/covid19 (accessed: 10.09.2022).

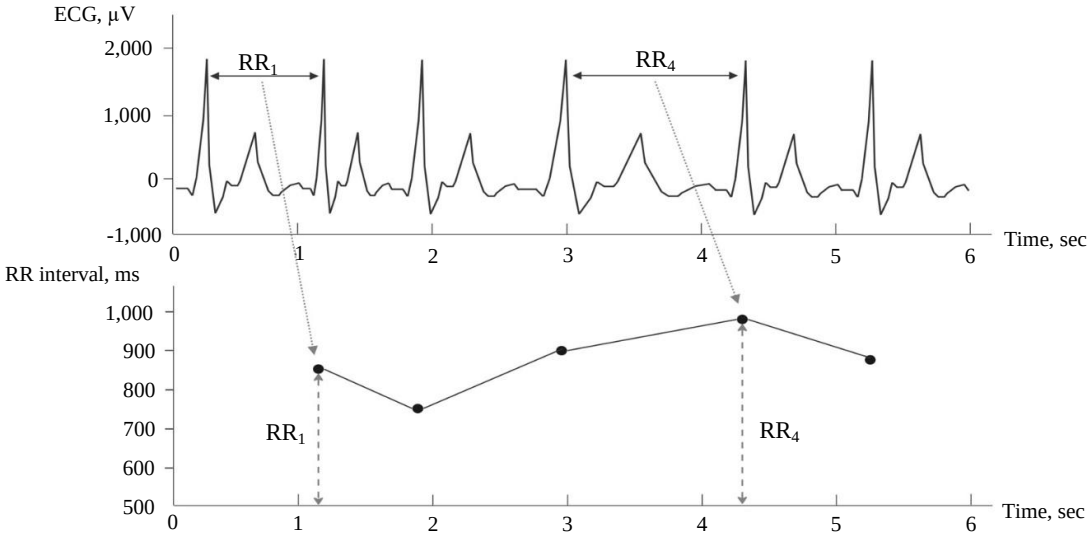


Fig. 1. Comparison of electrocardiogram and heart rhythm strip: horizontal axis shows the time in seconds, vertical axis for the ECG — microvolts

In all rhythm strips from this set, there are marked abnormal areas. In Figure 2, abnormal areas are highlighted with a red dotted line. The $x$-axis shows the duration of one measurement of the rhythm strip in milliseconds, the $y$-axis — the interval between adjacent heartbeats in milliseconds.

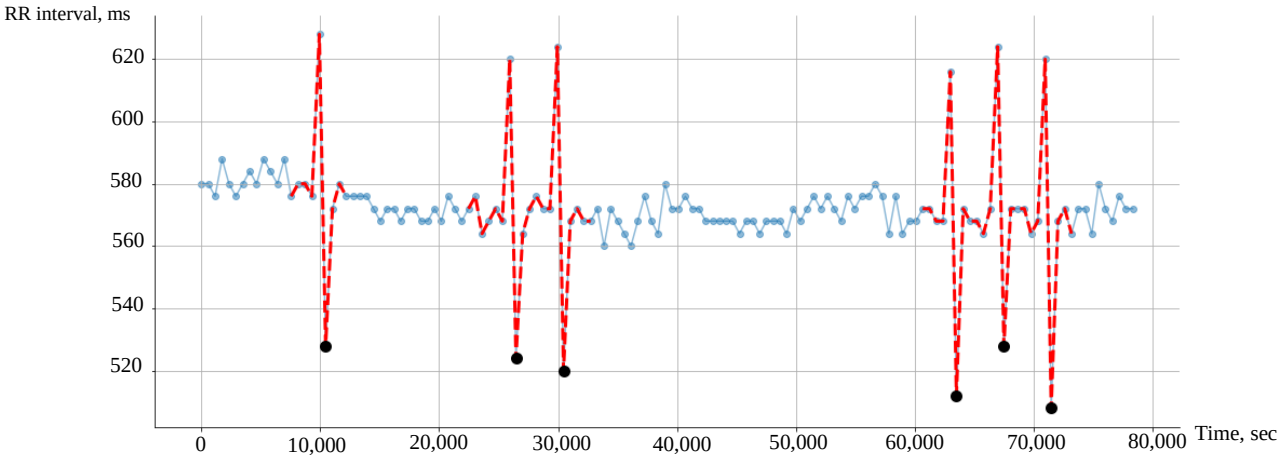


Fig. 2. Chart of rhythm strip No. 69: abnormal areas are highlighted with red dotted lines, abnormal points — with black bullet points

Each rhythm strip is presented by its own identifier. The duration of rhythm strips in the studied data set is different: 4 minutes on average, 31 minutes maximum. Each measurement inside one rhythm strip has a timestamp in milliseconds from the start of recording. The duration of the RR interval is also presented in milliseconds. Each specific value in the rhythm strip allows us to talk about the signs of an anomaly (0 — no, 1 — there is). 2.53 % of observations are marked with number 1. Thus, the data set has a strong class imbalance, which is typical for anomaly detection tasks.

In the data markup, there are various approaches to the allocation of abnormal areas. Groups of points in the vicinity of a characteristic peak and fall in the duration of the heart rhythm were distinguished as abnormal: 3rd, 4th, 6th measurements (Fig. 2). Not always the number of points in the neighborhood is marked the same — there may be a different number of abnormal points to the left and right of the peak. Moreover, rhythm strips with noisy indications were detected. This was the case when the connection with the gadget was lost, and measurements were taken when installing or removing the device. Sixteen rhythm strips with incorrect data had to be excluded from consideration, and the markup was redone:

– only one point stands out in the anomalous section, characterizing the anomalous fragment;

– abnormal points are indicated by black bullets (Fig. 2).

**Feature extraction.** In its pure form, only one signal was presented — the value of intervals between heartbeats. Therefore, to refine the model, additional features were prepared based on the available signal: deviation from the median value and derivatives in neighboring rhythm measurements. This list of features was selected after an

exploratory data analysis and visual identification of the pattern in places corresponding to abnormal areas. In Figure 2, they were marked with a red dotted line.

**Research Results**

**Metric for evaluating the quality of anomaly detection.** To assess the quality of the model in the binary classification problem, due to the imbalance of classes, metric $F_1$ [7] (1) was used. It provided evaluating how well a constructed model detected a rare class. In that context, a rare class referred to abnormal heartbeats in duration — heartbeats with an abnormal rhythm:

$$F_1 = 2 \times \frac{\text{accuracy} \times \text{completeness}}{(\text{accuracy} + \text{completeness})}. \quad (1)$$

Here:

– accuracy — the proportion of abnormal heartbeats correctly detected by the model from the total number of heartbeats that the model identified as abnormal;

– completeness (or in other words, sensitivity) — the proportion of heartbeats that the model correctly detected as abnormal from the total number of abnormal heartbeats in the entire data set.

**Machine learning algorithms.** As part of the study, five machine learning algorithms described below were applied.

1. IsolationForest — an algorithm with uncontrolled self-learning based on extremely randomized decision trees [8].

2. Light Gradient Boosting Machine Classifier (LGBMClassifier) — an algorithm for gradient boosting over decision trees [9]. To increase the operation speed, two techniques were used: Gradient-based One-Side Sampling and Exclusive Feature Bundling[3].

3. RandomForestClassifier is based on decision trees and implements multiple selection of a random subset of features. They are used to build simpler estimators — decision trees. The results are aggregated to obtain a final prediction [10].

4. ExtraTreesClassifier is similar to RandomForestClassifier, however, it additionally implements a random selection of the boundary along which nodes branch in decision trees [11].

5. SGDOneClassSVM[4] — a linear version of One-Class Support Vector Machine using Stochastic Gradient Descent.

IsolationForest and SGDOneClassSVM were chosen due to their wide use in anomaly detection tasks [12, 13]. LGBMClassifier, RandomForestClassifier and ExtraTreesClassifier perform well enough in different tasks, therefore, they were also used to compare the results [12, 13].

The specific feature of the IsolationForest and SGDOneClassSVM algorithms is that they do not require a clear marking of anomalous observations at the input, while it is mandatory for the rest of the algorithms used in the study.

IsolationForest is based on the assumption that when constructing isolating trees, abnormal observations can be isolated (separated) in fewer operations than normal observation instances. For each observation, the algorithm calculates the anomaly score by the formula:

$$s(x, n) = 2^{-\frac{E(h(x))}{c(n)}}, \quad (2)$$

where $h(x)$ — number of edges up to instance $x$ in each isolating decision tree; $E(h(x))$ — average value $h(x)$ on the entire set of isolating trees; $c(n)$ — normalizing constant for a data set of size $n$ (3).

$$c(n) = 2H(n-1) - \frac{2(n-1)}{n}, \quad (3)$$

$$H(k) = \ln(k) + \gamma. \quad (4)$$

In equation (4) $\gamma$ — Euler's constant equal to 0.57721…

If observation $x$ has an anomaly estimation value $s$, close to 1, then it is considered anomalous. If $s$ is close to 0.5, then the observation has no obvious signs of an anomaly. If $s$ is close to 0, then the observation can be considered normal (Fig. 3).

[3] LightGBM: A Highly Efficient Gradient Boosting Decision Tree. www.microsoft.com URL: https://www.microsoft.com/en-us/research/wp-content/uploads/2017/11/lightgbm.pdf (accessed: 10.09.2022).

[4] Online One-Class SVM. Scikit-learn developers (BSD License). scikit-learn.org URL: https://scikit-learn.org/stable/modules/sgd.html#online-one-class-svm (accessed: 10.09.2022).

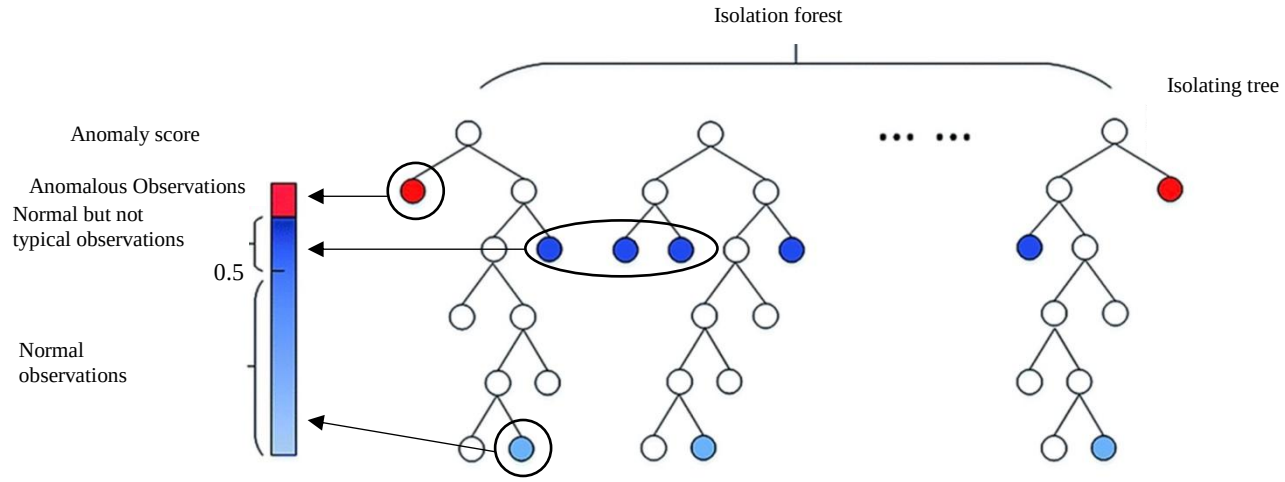


Fig. 3. Normal and anomalous observations in isolating trees (the authors' figure)

SGDOneClassSVM is based on the opposite approach to IsolationForest. The algorithm determines the boundaries of normal observations and compares all new observations to the boundaries of this norm to identify an anomaly.

**Feature Significance.** An assessment of the degree of impact of features on the predictive ability of the model is shown in Figure 4.

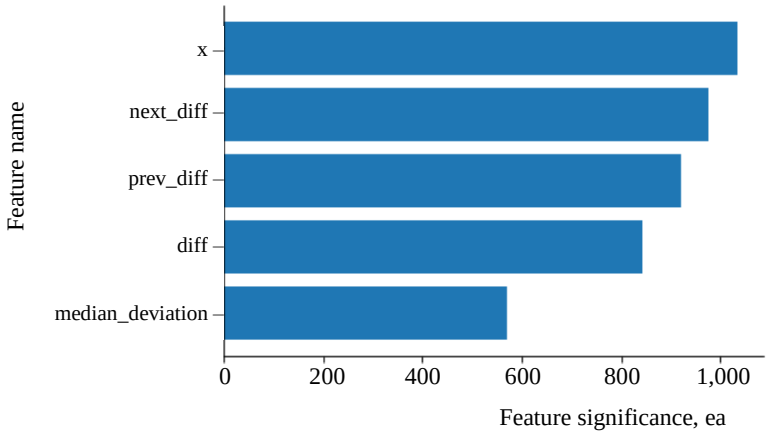


Fig. 4. Feature significance diagram: *x* — current value of the interval; next_diff — derivative at the next point of measuring the heartbeat duration; prev_diff — derivative at the previous point of measuring the heartbeat duration; diff — the first derivative at the current point; median_deviation — deviation of the current value of the RR interval duration from the median

To calculate the numerical significance estimate, a mechanism built into LGBMClassifier was used, which returns an array of numerical estimates for each feature via the *feature_importances_* property of the trained model. Significance in models based on gradient boosting over decision trees is usually calculated on the Gini-impurity Index[5] [14], used in the process of determining the branching points when training the model:

$$Gini(d) = 1 - \sum_{i=1}^{k} p_i^2 \,. \quad (5)$$

Here, $d$ — a set of observations that match the conditions at the considered branching point, $d \in D$; $k$ — number of classes presented in the entire training dataset $D$; $p_i$ — probability of observations belonging to class $i$ at the considered branching point of the decision tree.

The following features were the most significant: the current value of interval ($x$), the derivative at the next (next_diff) and previous (prev_diff) points of measuring the heartbeat duration (Fig. 4). A complete list of the features used is given in Table 2.

[5] Karabiber F. Gini Impurity. learndatasci.com URL: https://www.learndatasci.com/glossary/gini-impurity/ (accessed: 10.09.2022).

Table 2

List of features used

| No. | Feature | Description |
|---|---|---|
| 1 | *x* | RR interval at the current measuring point |
| 2 | next_diff | First derivative at the next point |
| 3 | prev_diff | First derivative at the previous point |
| 4 | diff | First derivative at the current point |
| 5 | median_deviation | Deviation of the current value of the RR interval duration from the median within one rhythm strip |

**Comparison of models.** For effectiveness of SGDOneClassSVMmodel, it is important to select parameter *nu*, which corresponds to the probability of detecting regular observation outside the norm. In other words, *nu* determines the upper bound of the error rate when training the model, and the lower bound of the support vector fraction[6]. To select *nu* taking into account the available data nature, the quality metric was additionally assessed at different values of the specified parameter (Fig. 5). As a result, *nu* equal to 0.11 was selected.

.

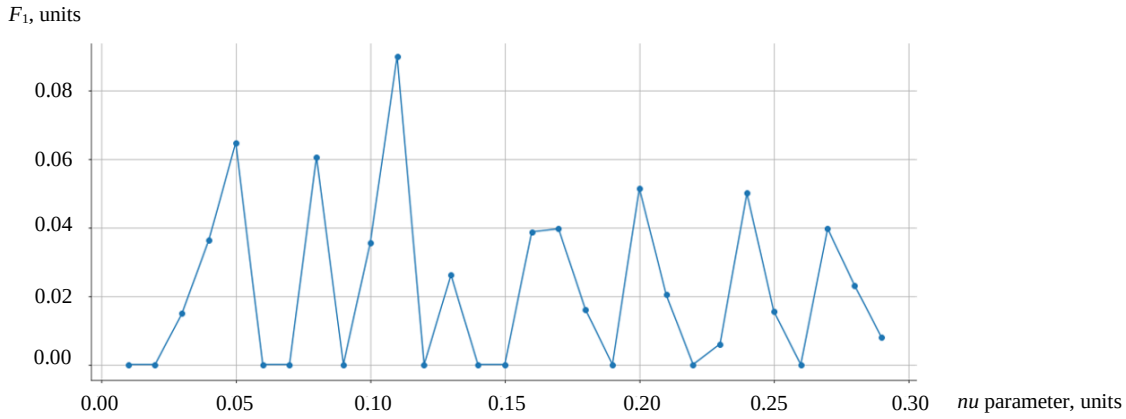


Fig. 5. Estimate of parameter *nu* (on the horizontal axis) for *SGDOneClassSVM* model.
On the vertical axis — values of metric $F_1$

To calculate the quality metric on various models, the entire data set was used through the cross-validation technique. Within one rhythm strip, we had a time series of observations taken in one continuous period of time from one person, therefore, they should be considered as dependent [15]. The following strategy was used to divide the data into training and test sets. The selected data set consisted of 213 rhythm strips marked with a unique identifier (*id*). This made it possible to allocate rhythm strips for training and testing models. A set of rhythm strips for the test could be randomly selected by identifiers. The approach used in the presented work is described below.

I. Five actions were performed in the data partitioning cycle.

1. The initial number for generating pseudo-random numbers was fixed (seed) —np.random.seed(fold), where fold — number of the current data partition.

2. 42 random integer values were generated in the range from 1 to 213. This was how we got random numbers of rhythm strip identifiers for the test data set.

3. The numbers of rhythm strip identifiers that remained after the selection of identifiers for the test were entered in a separate list. They were used for a training set.

4. Models were trained on rhythm strips from the training set, and prediction quality metrics were evaluated on rhythm strips from the test set.

5. The quality metric value was recorded for each model calculated on the test set of rhythm strips at the current data split.

[6] SGDOneClassSVM documentation. Scikit-learn developers (BSD License). scikit-learn.org URL: https://scikit-learn.org/stable/modules/generated/sklearn.linear_model.SGDOneClassSVM.html#sklearn.linear_model.SGDOneClassSVM (accessed: 10.09.2022).

II. Steps 1–5 were repeated for each data split number.

III. The obtained values of the quality metric were averaged for each of the models.

A comparative assessment of the average prediction quality metric for each model is given in Table 3.

Table 3

Evaluation of quality metric $F_1$

| Model | Metric $F_1$* |
|---|---|
| LGBMClassifier | 0.8328 |
| RandomForestClassifier | 0.7638 |
| ExtraTreesClassifier | 0.7369 |
| SGDOneClassSVM | 0.0169 |
| IsolationForest | < 1e-4 |
| * Average value for the selected cross-validation strategy on five partitions. | |

**Discussion and Conclusions.** A mathematical model for detecting anomalies in the heart rhythm with an accuracy of 83 % has been developed. According to quality metric $F_1$, the model based on LGBMClassifier algorithm turned out to be the best. IsolationForest and SGDOneClassSVM showed weak results on current data.

The proposed model can be implemented as a component of the software part of wearable personal smart devices. The proposed scenario for using the solution is as follows:

– the recording of the rhythm strip is activated on a personal wearable device through the user interface;

– upon completion, the record is submitted to the developed model for analysis;

– based on the results of data analysis, the mathematical model issues a notification about the presence or absence of anomalies on the screen of the wearable device.

Note that an average of 4 minutes is probably enough to record one rhythm strip. During this time, it is possible to detect covid anomalies in the heart rhythm.

The model occupies 493 kilobytes in the memory of the wearable device, which is quite suitable for practical use. The solution relies only on information about the heart rate and does not involve factors inaccessible to mobile personal gadgets.

Improving the accuracy of anomaly detection involves additional research. They should focus on the development of unique features that are detected by the initial heart rate signal. However, the current solution already makes it possible to quickly and easily assess the probability of COVID-19 at an early stage. This, along with the implementation of medical recommendations, can further contribute to reducing the risk of mortality from the negative impact of coronavirus infection on the cardiovascular system.

**References**

1. Tursunova ND, Shafigulina IS, Grebennikova IV, et al. Patogeneticheskie aspekty vliyaniya COVID-19 na serdechno-sosudistuyu sistemu cheloveka. *European Journal of Natural History.* 2022;1:73–77. (In Russ.)

2. Molodchenkov AI, Grigoriev OG, Sharafutdinov YaN. Automatic Calculation of Disease Risk Factors Values Using Artificial Intelligence Methods and Internet of Things Technology. *Journal of Information Technologies and Computing Systems.* 2021;1:83–96. https://doi.org/10.14357/20718632210109

3. Polevaya SA, Eremin EV, Bulanov NA, et al. Event-Related Telemetry of Heart Rhythm for Personalized Remote Monitoring of Cognitive Functions and Stress under Conditions of Everyday Activity. *Modern Technologies in Medicine*. 2019;11:109–115. http://dx.doi.org/10.17691/stm2019.11.1.13

4. Kouame Amos Brou, Ivan Smirnov, Mabouh Moise Hermann. Comparison of Machine Learning Models for Coronavirus Prediction. *Advanced Engineering Research (Russia).* 2022;22:67–75. https://doi.org/10.23947/2687-1653-2022-22-1-67-75

5. Ashish Bhargava, Elisa Akagi Fukushima, Miriam Levine, et al. Predictors for Severe COVID-19 Infection. *Clinical Infectious Diseases.* 2020;71:1962–1968. https://doi.org/10.1093/cid/ciaa674

6. Krasyukova YuI, Vakhrusheva TA, Pei He Su. Machine Learning Model for Determining the Probability of Covid-19 Disease by Primary Signs. *Intellektual'nye resursy — regional'nomu razvitiyu*. 2021;2:67–71.

7. Alaa Tharwat. Classification Assessment Methods. *Applied Computing and Informatics.* 2021;17:174. https://doi.org/10.1016/j.aci.2018.08.003

8. Yupeng Xu, Hao Dong, Mingzhu Zhou, et al. Improved Isolation Forest Algorithm for Anomaly Test Data Detection. *Journal of Computer and Communications.* 2021;9:49–51. https://doi.org/10.4236/jcc.2021.98004

9. Bruce P, Bruce A, Gedeck P. *Practical Statistics for Data Scientists,* 2nd ed. Boston: O'Reilly Media; 2020. 342 p.

10. Breiman L. Random Forests. *Machine Learning.* 2001;45:5–32. https://doi.org/10.1023/A:1010933404324

11. Geurts P, Ernst D, Wehenkel L Extremely Randomized Trees. *Machine Learning.* 2006;63:3–42. https://doi.org/10.1007/s10994-006-6226-1

12. Kaur H, Singh G, Minhas J. A Review of Machine Learning Based Anomaly Detection Techniques. *International Journal of Computer Applications Technology and Research.* 2013;2:185–187. http://dx.doi.org/10.7753/IJCATR0202.1020

13. Katser ID, Kozitsin VO, Maksimov IV. NPP Equipment Fault Detection Methods. *Proc. of Universities. Nuclear Power Engineering*. 2019;4:5–27. https://doi.org/10.26583/npe.2019.4.01

14. Daniya T, Geetha M, Suresh Kumar K Dr. Classification and Regression Trees with Gini Index. *Advances in Mathematics Scientific Journal*. 2020;9:8237–8247. http://dx.doi.org/10.37418/amsj.9.10.53

15. Valliappa Lakshmanan, Sara Robinson, Michael Munn. *Machine Learning Design Patterns: Solutions to Common Challenges in Data Preparation, Model Building, and MLOps,* 1st ed. Boston: O'Reilly Media; 2020. 408 p.

*About the Authors:*

**Maksim S Mezhov,** leading expert, "Digital Technologies and Platforms" LLC (53, Dubininskaya St., Moscow, 115054, RF), ORCID, msmezhov@ya.ru

**Vyacheslav O Kozitsin,** leading expert, "Digital Technologies and Platforms" LLC (53, Dubininskaya St., Moscow, 115054, RF), ORCID, Vyacheslav.Kozitsin@skoltech.ru

**Iurii D Katser,** postgraduate, Skolkovo Institute of Science and Technology (30, Bolshoy Boulevard, Moscow, 121205, RF), ScopusID, ORCID, Iurii.katser@skoltech.ru

*Claimed contributorship:*

MS Mezhov: basic concept formulation; research objectives and tasks; data collection; model development; calculations and analysis of the results. VO Kozitsin: text preparation; formulation of conclusions; pre-processing of data; the text revision. IuD Katser: control of the study; revision of the text; correction of the conclusions.

**Received** 09.12.2022.
**Revised** 25.01.2023.
**Accepted** 25.01.2023.

*Conflict of interest statement*

The authors do not have any conflict of interest.

*All authors have read and approved the final manuscript.*

*Об авторах:*

**Максим Сергеевич Межов,** ведущий эксперт ООО «Цифровые технологии и платформы» (115054, РФ, Москва, ул. Дубининская, 53, стр. 6), ORCID, msmezhov@ya.ru

**Вячеслав Олегович Козицин,** ведущий эксперт ООО «Цифровые технологии и платформы» (115054, РФ, Москва, ул. Дубининская, 53, стр. 6), ORCID, Vyacheslav.Kozitsin@skoltech.ru

**Юрий Дмитриевич Кацер,** аспирант сколковского института науки и технологии (121205, РФ, Москва, территория инновационного центра «Сколково», Большой бульвар, 30, стр. 1), ScopusID, ORCID, Iurii.katser@skoltech.ru

*Заявленный вклад соавторов*

М.С. Межов — формирование основной концепции, цели и задач исследования, сбор данных, разработка моделей, расчеты и анализ результатов. В.О. Козицин — подготовка текста, формулирование выводов, предварительная обработка данных и доработка текста. Ю.Д. Кацер — контроль проведения исследования, доработка текста и корректировка выводов.

**Поступила в редакцию** 09.12.2022.
**Поступила после рецензирования** 25.01.2023.
**Принята к публикации** 25.01.2023.

*Конфликт интересов*

Авторы заявляют об отсутствии конфликта интересов.

*Все авторы прочитали и одобрили окончательный вариант рукописи.*

# INFORMATION TECHNOLOGY, COMPUTER SCIENCE AND MANAGEMENT
# ИНФОРМАТИКА, ВЫЧИСЛИТЕЛЬНАЯ ТЕХНИКА И УПРАВЛЕНИЕ



UDC 004.4
https://doi.org/10.23947/2687-1653-2023-23-1-76-84

*Original article*

## Data Warehouse Failover Cluster for Analytical Queries in Banking

**Victor V Sivov** ✉, **Vladimir A Bogatyrev**
ITMO University,49, Kronverksky Pr., St. Petersburg, Russian Federation

✉ v.sivov777@gmail.com

**Abstract**

***Introduction.*** The banking sector assigns high priority to data storage, as it is a critical aspect of business operations. The volume of data in this area is steadily growing. With the increasing volume of data that needs to be stored, processed and analyzed, it is critically important to select a suitable data storage solution and develop the required architecture. The presented research is aimed at filling the gap in the existing knowledge of the data base management system (DBMS) suitable for the banking sector, as well as to suggest ways for a fault-tolerant data storage cluster. The purpose of the work is to analyze the key DBMS for analytical queries, determine the priorities of the DBMS for the banking sector, and develop a fault-tolerant data storage cluster. To meet the performance and scalability requirements, a data storage solution with a fault-tolerant architecture that meets the requirements of the banking sector has been proposed.

***Materials and Methods.*** Domain analysis allowed us to create a set of characteristics that a DBMS for analytical queries (OnLine Analytical processing — OLAP) should correspond to, compare some popular DBMS OLAP, and offer a fault-tolerant cluster configuration written in xml, supported by the ClickHouse DBMS. Automation was done using Ansible Playbook. It was integrated with the Gitlab version control system and Jinja templates. Thus, rapid deployment of the configuration on all nodes of the cluster was achieved.

***Results.*** For OLAP databases, criteria were developed and several popular systems were compared. As a result, a reliable cluster configuration that met the requirements of analytical queries has been proposed for the banking industry. To increase the reliability and scalability of the DBMS, the deployment process was automated. Detailed diagrams of the cluster configuration were also provided.

***Discussion and Conclusions.*** The compiled criteria for the DBMS OLAP allowed us to determine the need for this solution in the organization. Comparison of popular DBMS can be used by organizations to minimize costs when selecting a solution. The proposed configuration of the data warehouse cluster for analytical queries in the banking sector will improve the reliability of the DBMS and meet the requirements for subsequent scalability. Automation of cluster deployment by the mechanism of templating configuration files in Ansible Playbook provides configuring a ready-made cluster on new servers in minutes.

**Keywords:** DBMS, OLAP, data warehouse, ClickHouse, failover cluster.

**Acknowledgements.** The author would like to thank V.A. Bogatyrev, Dr.Sci. (Engineering), professor of the Computer Engineering Department of ITMO University, Honorary Worker of Science and Technology of the Russian Federation, who conducted expert interviews together with the authors of the article.

**For citation.** Sivov VV, Bogatyrev VA. Data Warehouse Failover Cluster for Analytical Queries in Banking. *Advanced Engineering Research (Rostov-on-Don)*. 2023;23(1):76–84. https://doi.org/10.23947/2687-1653-2023-23-1-76-84

*Научная статья*

# Отказоустойчивый кластер хранилища данных для аналитических запросов в банковской сфере

**В.В. Сивов** ✉, **В.А. Богатырев**
Санкт-Петербургский национальный исследовательский университет информационных технологий, механики и оптики, Российская Федерация, г. Санкт-Петербург, Кронверкский пр., д. 49
✉ v.sivov777@gmail.com

**Аннотация**

***Введение.*** Банковский сектор придает большое значение хранению данных, поскольку это критически важный аспект бизнес-операций. Объем данных в данной сфере неуклонно растет. С увеличением объемов данных, которые необходимо хранить, обрабатывать и анализировать, крайне важно выбрать подходящее решение для хранения данных и разработать необходимую архитектуру. Представленное исследование направлено на то, чтобы заполнить пробел в существующих знаниях СУБД, подходящих для банковского сектора, а также предложить способы для отказоустойчивого кластера хранения данных. Цель работы — анализ ключевых СУБД для аналитических запросов, определение приоритетов СУБД для банковского сектора и разработка отказоустойчивого кластера хранения данных. Для выполнения требований к производительности и масштабируемости предложено решение для хранения данных с отказоустойчивой архитектурой, отвечающее требованиям банковского сектора.

***Материалы и методы.*** Анализ предметной области позволил создать набор характеристик, которым должна соответствовать СУБД для аналитических запросов (OLAP), выполнить сравнение некоторых популярных OLAP СУБД и предложить отказоустойчивую кластерную конфигурацию, написанную на языке xml, поддерживаемую СУБД ClickHouse. Автоматизация выполнена с помощью Ansible Playbooks. Он интегрирован с системой управления версиями Gitlab и шаблонами Jinja. Таким образом достигается быстрое развертывание конфигурации на всех нодах кластера.

***Результаты исследования.*** Для баз данных OLAP были разработаны критерии, проведен сравнительный анализ нескольких популярных систем. В результате была предложена надежная кластерная конфигурация в банковской индустрии, которая удовлетворяет требованиям аналитических запросов. Для увеличения надежности и масштабируемости СУБД процесс развертывания был автоматизирован. Также приведены детальные схемы конфигурации кластера.

***Обсуждение и заключения.*** Составленные критерии для OLAP СУБД позволяют определить необходимость данного решения в организации. Сравнение популярных СУБД может быть использовано организациями для минимизации затрат при выборе решения. Предлагаемая конфигурация кластера хранилища данных для аналитических запросов в банковской сфере позволит повысить надежность СУБД и удовлетворить требования к последующей масштабируемости. Автоматизация развертывания кластера путем механизма шаблонизации конфигурационных файлов в Ansible Playbooks позволяет настроить готовый кластер на новых серверах за минуты.

**Ключевые слова:** СУБД, OLAP, хранилище данных, ClickHouse, отказоустойчивый кластер.

**Благодарности.** Автор выражает благодарность В.А. Богатыреву, доктору технических наук, профессору кафедры вычислительной техники Университета ИТМО, почетному работнику науки и техники РФ, проводившему экспертные интервью совместно с автором статьи.

**Для цитирования.** Сивов В.В., Богатырев В.А. Отказоустойчивый кластер хранилища данных для аналитических запросов в банковской сфере. *Advanced Engineering Research (Rostov-on-Don).* 2023;23(1):76–84. https://doi.org/10.23947/2687-1653-2023-23-1-76-84

**Introduction**. Data storage in the banking sector is one of the key business factors. To ensure the security of customer information and transactions, it is required to take measures of protection, distribution and creation of backups. For operational analysis, employees should be able to make operational analytical requests to the data warehouse, while not interfering with the work of other processes within the organization and without causing a heavy load on the storage itself. Databases and Data Warehouse are information systems in which data is stored, but they are also used to solve various tasks. The article describes what such systems do, what the main differences between them are, and why their effective use is essential for business development.

Many organizations make mistakes in designing the architecture of databases and data warehouses, losing sight of aspects of information security, scalability and fault tolerance. The urgency of this problem is due to the intensive development of systems in banks, the expansion of their fields of application and the increase in the amount of data in need of constant analysis. For operational analysis of a large amount of data, a storage is needed that must meet all reliability and security requirements.

Effective decision-making processes in business depend on high-quality information. In today's competitive business environment, flexible access to a data warehouse is required, organized in such a way as to increase business productivity, provide fast, accurate and up-to-date data understanding. The data warehouse architecture is designed to meet such requirements and is the basis of these processes [1–5].

The objective of the work is to determine the priority DBMS for performing analytical queries in the banking sector and design a fault-tolerant data warehouse cluster. This solution will significantly increase the speed of execution of analytical queries, solve problems with scalability and reliability of the data warehouse.

**Materials and Methods.** The database stores real-time information about one specific part of the business. Its main task is to process daily transactions. Databases use Online Transaction Processing (OLTP) to quickly delete, insert, replace and update a large number of short online transactions.

Data warehouse is a system that collects data from lots of different sources within an organization for reporting and analysis, using operational analytical processing (OLAP) to quickly analyze large amounts of data. This system focuses on reading, rather than changing historical data from lots of different sources, therefore, compliance with ACID (Atomic, Consistent, Isolated and Durable) requirements is less strict. Data warehouses perform complex functions of aggregation, analysis and comparison of data to support management decision-making in companies.

A warehouse in the banking sector may contain:

– user account information (personal data, addresses, phone numbers);

– information about banking products and services (loans, deposits, plastic cards, mobile banking, etc.);

– data on transactions (including card transactions) in minimal detail for the last three years;

– information about accounts, balances on them, etc.

To meet the needs for OLAP, there are separate types of database management systems (DBMS) [3–6]. Each of the systems has its own characteristics in the construction of architecture.

To perform an effective analysis of compliance with these requirements, warehouses must:

– have a high capacity capable of accommodating huge amounts of data (billions or trillions of rows);

– be organized as wide tables with multiple columns;

– perform queries with a small number of columns;

– have a high query execution speed (in milliseconds or seconds);

– provide for most of the read-only requests;

– support fast bulk data loading when updating (more than 1,000 rows at a time) and adding, but without changing them;

– have high throughput to process a single request (up to billions of rows);

– have high reliability;

– ensure data security and consistency.

For the OLAP scenario of work in the banking sector, it is preferable to use column-based analytical databases, since they can store a lot of columns in a table, which will not affect the speed of reading data. Column-based DBMS provide strong compression of data in columns, since data in one column of the table is usually of the same type, which cannot be said about a row. They also enable to get a tenfold increase in query execution speed on lower-power equipment. At the same time, thanks to compression, the data will occupy 5-10 times less space on the disk than in the case of traditional DBMS [7–11].

During the requirements analysis, the following column DBMS were selected: ClickHouse, Vertica, Amazon Redshift.

ClickHouse is the preferred solution due to the following advantages: open source; it is possible to define some or all structures that will be stored only in memory; high speed; good data compression; http and command line interface; cluster can be scaled horizontally; high availability; ease of installation and configuration. Installation is carried out on the organization's servers in an isolated segment, which meets the security requirements for sensitive data in the banking sector. The DBMS is also included in the register of domestic software; therefore, it provides implementing this software product in state-owned companies.

Amazon Redshift solution is provided only as a cloud service. For organizations from the banking sector that cannot place their data in the clouds for a number of security-related reasons, this product loses its appeal.

Vertica is an alternative version of ClickHouse with a paid license for large clusters and the installability on the company's local servers.

The implementation of the distributed data warehouse architecture is presented below. To increase fault tolerance and performance, the implementation of a distributed ClickHouse failover cluster with three shards and two replicas is proposed.

Sharding (horizontal scaling) makes it possible to write and store parts of data in a distributed cluster, process and read them in parallel on all nodes of the cluster, increasing data throughput.

Replication is copying data to multiple servers; thus, each bit of data can be found on multiple nodes.

Scalability is determined by sharding or segmentation of data. The reliability of the data warehouse is determined by data replication [12–16].

Sharding and replication are completely independent, different processes are responsible for them. It is required to localize small data sets on one shard and ensure a fairly even distribution across different shards in the cluster. To do this, it is recommended to take the hash function value from a field in the table as a sharding key.

Sharding and replication are completely independent, different processes are responsible for them. It is required to localize small data sets on one shard and ensure a fairly even distribution across different shards in the cluster. To do this, it is recommended to take the hash function value from a field in the table as a sharding key.

Depending on the number of available resources and servers, it is proposed to implement this configuration on 3 or 6 nodes. For a production environment, it is recommended to use a cluster of 6 nodes. It should be noted that replication

does not depend on sharding mechanisms and works at the level of individual tables, and also, since the replication coefficient is 2, each shard is represented in 2 nodes [17–19]. Configuration options are described below.

The logical topology diagram is as follows:

3(Shard) × 2(Replicas) = Clickhouse Cluster of 6 nodes.

The probability of trouble-free operation of a system with 2 replicas and 3 shards on 6 nodes is equal to:

$$P_c = [1 - (1 - p)^2]^3.$$

The probability of trouble-free operation is an objective possibility that the system will work for time *t* without restorations [7, 13].

Thus, a table containing 30 million rows will be distributed evenly across 3 nodes of the cluster. The remaining 3 nodes will store replicas of the data. When one of the cluster nodes is disabled, data will be taken from another available node that contains its replica, thereby achieving reliability [20]. A cluster of 6 nodes is shown in Figure 1.

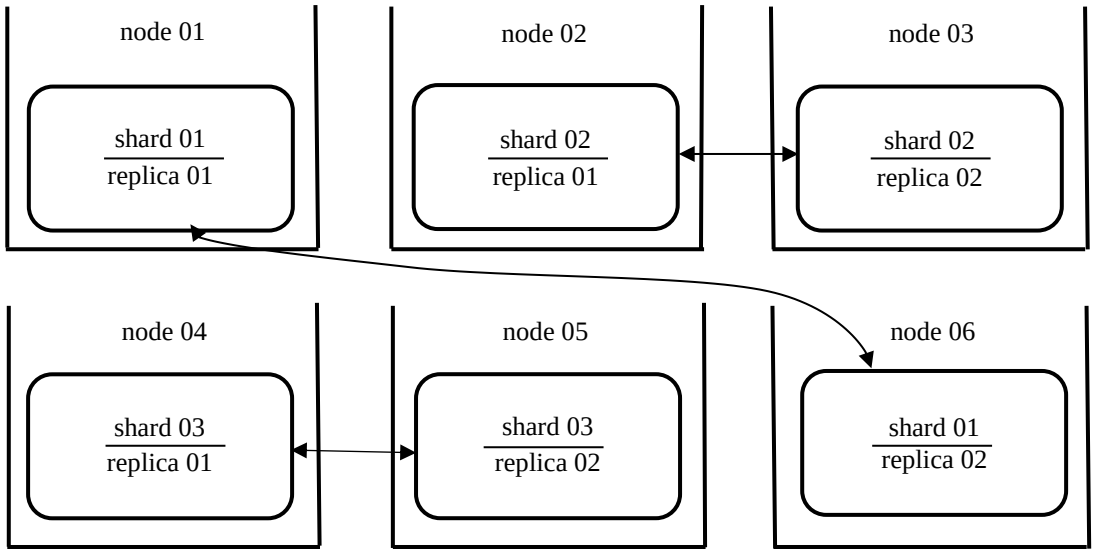


Fig. 1. Fault-tolerant cluster of 6 nodes (the authors' figure)

To replicate data and execute distributed DDL queries, we need to use +1 node with ZooKeeper installed. You can also use ClickHouse Keeper, compatible with ZooKeeper, which does not require installation on a separate server.

An example of a fragment of the configuration file is shown in Figure 2, from which it can be seen that the shard has replication configured for the 1st and 6th nodes.

```
<yandex>
    <remote_servers>
        <cluster_1>

            <shard>
                <weight>1</weight>
                <internal_replication>true</internal_replication>
                <replica>
                    <host>{{ node1 }}</host>
                    <port>9000</port>
                </replica>
                <replica>
                    <host>{{ node6 }}</host>
                    <port>9000</port>
                </replica>
            </shard>
```

Fig. 2. Fragment of the configuration file for 6 nodes (the authors' figure)

An option of the cluster configuration of 3 nodes with cyclic replication is shown in Figure 3.

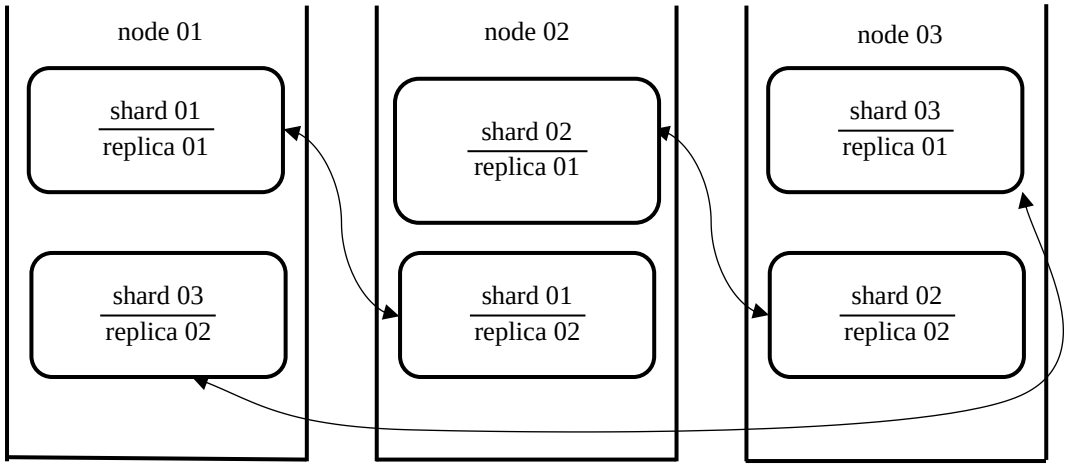


Fig. 3. Fault-tolerant cluster of 3 nodes (the authors' figure)

This implementation requires two different segments located on each node. The main problem arises due to the fact that each shard has the same table name, ClickHouse cannot distinguish one shard/replica from another when they are located on the same server.

To solve this problem, it is needed:

– to place each shard in a separate database (schema);

– to set default_database for each shard;

– to set internal_replication parameter of each shard to true;

– to use an empty database parameter in a distributed table DDL script.

For this topology in an industrial environment, 6 server nodes are required, where each server stores data from only one segment, a security trapdoor for a separate database is not required. To save resources in the development or testing area, a configuration with 3 nodes can be used.

Automation is performed using Ansible Playbooks and integrated with Gitlab version control system. Thus, rapid deployment of the configuration on all nodes of the cluster is provided. When changing the configuration, it can be applied to all nodes with a single command or deploy a new DBMS cluster in a few minutes [21].

**Research Results.** The fault-tolerant cluster of the analytical DBMS provides redundancy for important system components, which allows for continuous operation even in case of errors in individual cluster nodes. This is done through load balancing, data replication between cluster nodes, and high reliability of the components used in the cluster. The result is an increase in the availability and reliability of the analytical DBMS, which is business-critical when analytical queries play a key role. The fault-tolerant cluster configuration of the data warehouse for analytical queries in the banking sector, taking into account the automation of the deployment process, enables to increase the reliability of the analytical data warehouse and meet the requirements for scalability. The developed task of automating cluster deployment using the mechanism of templating configuration files in Ansible Playbooks provides for the configuration of a ready-made cluster on new servers in a few minutes. The tasks of the template include operations to install the required packages, create the needed configuration and launch the cluster.

An example of configuration files for automatic deployment of a DBMS cluster is shown in Figure 4. The j2 extension says that they are created using the Jinja template engine. Purpose-built placeholders in the template provide writing code similar to Python syntax. Parameters are passed to the template for automatic insertion into the final document, thereby achieving automatic assembly into development, testing and industrial operation zones, which does not require manual modification of configuration files.

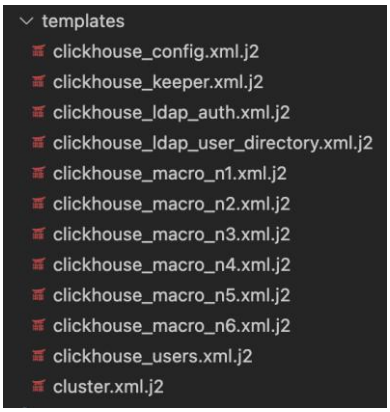


Fig. 4. Configuration files

Description of configuration files:

clickhouse_config.xml.j2 — general cluster configuration;

clickhouse_keeper.xml.j2 — zookeeper configuration, which is responsible for node synchronization and replication;

clickhouse_ldap_auth.xml.j2 — LDAP connection configuration for data security;

clickhouse_ldap_user_directory.xml.j2 — role-based configuration by access groups to ensure data security;

clickhouse_macro_n1(6).xml.j2 — macro files (each node has its own);

clickhouse_users.xml.j2 — configuration file for creating local users needed for administration;

cluster.xml.j2 — cluster configuration file.

To test the reliability of this configuration, an experiment was conducted during which data was loaded into a DBMS cluster with a replication factor equal to 2. The dwh schemas and cluster_test_data tables were created on each of the nodes of the DBMS cluster, and a distributed table was created on the dwh cluster.cluster_test_data_distributed. The rows of the dwh.test_data_distributed table distributed across the cluster were 27,547,855. The rows of the dwh.cluster_test_data table with each of the cluster nodes are listed below:

9,186,544 rows — 1st node;

9,182,959 rows — 2nd node;

9,182,959 rows — 3rd node;

9,178,352 rows — 4th node;

9,178,352 rows — 5th node;

9,186,544 rows — 6th node.

Conspicuously, the table was distributed over the entire cluster. According to the configuration shown in Figure 1, the replication factor was 2, which means that each data block would be presented on 2 nodes. This can be seen from the number of rows on the nodes: the sixth node stored a copy of the first, the third — a copy of the second, the fifth — a copy of the fourth.

The fault tolerance of this configuration can be checked by alternately disabling nodes in the cluster. To do this, you can turn off the node or stop services on one of the nodes with the systemctl stop clickhouse-server command. During the experiment, DBMS services were stopped on cluster nodes.

With simultaneous disconnection of the 3rd, 4th, 6th or 1st, 2nd, 5th nodes that contained replicas, users continued to receive data from the dwh.cluster_test_data_distributed table, and the number of rows was equal to 27,547,855. When one of the nodes was disabled, the data continued to be displayed, and the number of rows was equal to 27,547,855. When the nodes containing the replica and the original data were disconnected at the same time, data loss occurred. This configuration can be scaled to 12 nodes, then the replication coefficient will be 3, and the sharding coefficient will be 6.

**Discussion and Conclusions.** The proposed solution can increase the speed of execution of analytical queries, solve problems with the scalability and reliability of data storage in banking organizations. The authors have automated cluster deployment by using templates in Ansible Playbooks, which provides setting up a ready-made cluster on new

servers in minutes. This configuration can be scaled by increasing the number of nodes and adding them to the configuration files.

A set of characteristics that DBMS OLAP should correspond to was indicated, DBMS comparison was performed, a fault-tolerant cluster configuration of a data warehouse for analytical queries in the banking sector was proposed, automation of the configuration deployment process was performed. A similar solution is applicable for deployment on FreeBSD, Linux, macOS. The cluster configuration diagrams are given. This configuration can solve the problem of reliability and scalability, which is often found in organizations.

**References**

1. Sivov VV. *Data Security in the Business Analytics System*. In: Proc. IV All-Russian Sci.-Pract. Conference with international participation "Information Systems and Technologies in Modeling and Control". 2019. P. 142–145.

2. Solomon Negash, Paul Gray. Business Intelligence. In: *Handbook on Decision Support Systems 2*. Springer, Berlin, Heidelberg; 2008. P. 175–193.

3. Imhoff C, Galemmo N, Geiger JG. *Mastering Data Warehouse Design: Relational and Dimensional Techniques.* John Wiley & Sons; 2003. 456 p.

4. Hugh J Watson. Tutorial: Business Intelligence – Past, Present, and Future. *Communications of the Association for Information Systems*. 2009;25:39. https://doi.org/10.17705/1CAIS.02539

5. Roscoe Hightower, Mohammad Shariat. Conceptualizing Business Intelligence Architecture. *Marketing Management Journal.* 2007;17:40–46.

6. Inmon WH. *Building the Data Warehouse*, 4th ed. John Wiley & Sons; 2005. 576 p.

7. Bogatyrev VA, Bogatyrev SV, Bogatyrev AV. Timely Redundant Service of Requests by a Sequence of Cluster. *CEUR Workshop Proceedings.* 2020;2590:1–12.

8. Henning Baars, Hans-George Kemper. Management Support with Structured and Unstructured Data — An Integrated Business Intelligence Framework. *Information Systems Management*. 2008;25:132–148.

9. Rachmiel AG, Morgan NP, Danielewski D. *Batch Management of Metadata in a Business Intelligence Architecture.* U.S. Patent No. 8,073,863 B2. 2011.

10. Dehne F, Eavis T, Rau-Chaplin A. The cgmCUBE Project: Optimizing Parallel Data Cube Generation for ROLAP. *Distributed and Parallel Databases.* 2006;19:29–62.

11. Bogatyrev V, Bogatyrev S, Bogatyrev A. Timely Redundant Service of Requests by a Sequence of Cluster. *CEUR Workshop Proceedings.* 2020;2590:1–12.

12. Milenin EI, Sivov VV. Simulation Model of Information Interaction of Measuring Devices in an Automated Environmental Monitoring System Based on IoT Technologies. *CEUR Workshop Proceedings.* 2021;2834:484–492.

13. Bogatyrev VA, Bogatyrev SV, Golubev IYu. Optimization and the Process of Task Distribution between Computer System Clusters. *Automatic Control and Computer Sciences.* 2012;46:103–111.

14. Cuzzocrea A, Il-Yeol Song, Davis KC. *Analytics over Large-Scale Multidimensional Data: The Big Data Revolution!* In: Proc. DOLAP 2011, ACM 14th International Workshop on Data Warehousing and OLAP. 2011. P. 101–104. http://dx.doi.org/10.1145/2064676.2064695

15. Sivov VV. *Sravnenie klyuchevykh programmnykh produktov dlya biznes-analitiki v bankovskoi sfere.* In: Proc. VI Int. Sci.-Pract. Conf. "Informatsionnye sistemy i tekhnologii v modelirovanii i upravlenii". 2021. P. 281–287. (In Russ.)

16. Cuzzocrea A, Bertino E. Privacy Preserving OLAP over Distributed XML Data: A Theoretically-Sound Secure-Multiparty-Computation Approach. *Journal of Computer and System Sciences.* 2011;77:965–987. http://dx.doi.org/10.1016/j.jcss.2011.02.004

17. Cattell R. Scalable SQL and NoSQL Data Stores. *ACM SIGMOD Record.* 2010;12:12–27. https://doi.org/10.1145/1978915.1978919

18. Turban E, Sharda R, Delen D, et al. *Decision Support and Business Intelligence Systems*, 9th ed. Pearson College Div; 2010. 696 p.

19. Olszak CM, Ziemba E. Approach to Building and Implementing Business Intelligence Systems. *Interdisciplinary Journal of Information, Knowledge, and Management.* 2007;2:135–148. http://dx.doi.org/10.28945/105

20. Sarawagi S, Agrawal R, Megiddo N. *Discovery-Driven Exploration of OLAP Data Cubes.* In: Proc. Int. Conf. on Extending Database Technology – EDBT' 1998. Berlin: Springer, Berlin, Heidelberg; 1998. P. 168–182.

21. Anandarajan M, Anandarajan A, Srinivasan CA. (eds.) *Business Intelligence Techniques. A Perspective from Accounting and Finance.* Berlin: Springer-Verlag Berlin; 2004. 268 p.

*About the Authors:*

**Victor V Sivov,** postgraduate of the Computer Science Department, ITMO University (49, Kronverksky Pr., St. Petersburg, 197101, RF), ORCID, v.sivov777@gmail.com

**Vladimir A Bogatyrev,** professor of the Computer Science Department, ITMO University (49, Kronverksky Pr., St. Petersburg, 197101, RF), professor of the Information Systems Security Department, State University of Aerospace Instrumentation (67, Bolshaya Morskaya St., Saint Petersburg, 190000, RF), Dr.Sci. (Eng.), ORCID, ScopusID

*Claimed contributorship:*

VV Sivov: basic concept formulation; research objectives and tasks; computational analysis; analysis of the research results; formulation of conclusions. VA Bogatyrev: academic advising; analysis of research results; revision of the text; correction of the conclusions.

**Received** 01.02.2023.
**Revised** 17.02.2023.
**Accepted** 20.02.2023.

*Conflict of interest statement*

The authors do not have any conflict of interest.

*All authors have read and approved the final manuscript.*

*Об авторах:*

**Виктор Валерьевич Сивов**, аспирант кафедры «Вычислительная техника» Санкт-Петербургского национального исследовательского университета информационных технологий, механики и оптики (197101, РФ, г. Санкт-Петербург, Кронверкский проспект, д. 49), ORCID, v.sivov777@gmail.com

**Владимир Анатольевич Богатырев,** доктор технических наук, профессор кафедры «Вычислительная техника» Санкт-Петербургского национального исследовательского университета информационных технологий, механики и оптики (197101, РФ, г. Санкт-Петербург, Кронверкский проспект, д. 49), профессор кафедры «Информационная безопасность» Санкт-Петербургского государственного университета аэрокосмического приборостроения (190000, РФ, г. Санкт-Петербург, ул. Большая Морская, д. 67, лит. А), ORCID, ScopusID

*Заявленный вклад соавторов:*

В.В. Сивов — формирование основной концепции, цели и задачи исследования, проведение расчетов, подготовка текста, анализ результатов исследований, формирование выводов. В.А. Богатырев — научное руководство, анализ результатов исследований, доработка текста, корректировка выводов.

**Поступила в редакцию** 01.02.2023.
**Поступила после рецензирования** 17.02.2023.
**Принята к публикации** 20.02.2023.

*Конфликт интересов*

Авторы заявляют об отсутствии конфликта интересов.

*Все авторы прочитали и одобрили окончательный вариант рукописи.*

# INFORMATION TECHNOLOGY, COMPUTER SCIENCE AND MANAGEMENT
# ИНФОРМАТИКА, ВЫЧИСЛИТЕЛЬНАЯ ТЕХНИКА И УПРАВЛЕНИЕ



UDC 519.873+ 519.876.2
https://doi.org/10.23947/2687-1653-2023-23-1-85-94

*Original article*

## Two-Criteria Technique for the Resource-Saving Computing in the Fog and Edge Network Tiers

**Anna B Klimenko**
Institute of IT and Security Technologies, RSUH, 25, Kirovogradskaya St., Moscow, Russian Federation
✉ Anna_klimenko@mail.ru

**Abstract**

***Introduction.*** At present, the concepts of fog and edge computing are used in a wide range of applications of various kinds. One of the key problems in the organization of computing in groups of mobile devices that make up the edge/fog layer is the mission assurance based on battery power availability. In this context, a lot of developments aimed at energy saving of device systems have been presented to date. However, one important aspect remains beyond the consideration of the problem of resource saving, namely, the issue of saving the residual resource of a computing device. The aim of this research is to formalize the workload distribution problem as two-criteria optimization problem, and to develop the basic solution technique.

***Materials and Methods.*** Within the framework of this article, an approach to resource saving is proposed. It is based on the evaluation of two device criteria: battery life and residual resource of a computing device. The residual resource of a computing device can be estimated using the probability of failure-free operation of the device, or as the reciprocal of the failure rate, taking into account that the exponential law of failure distribution is used in the simulation. From this, a model of the problem of two-criteria optimization is formulated, taking into account the dynamics of the network topology in the process of performing a user mission. The topology dynamics is reflected in the model as a sequence of topologies, each of which corresponds to a certain period of time of the system operation.

***Results.*** Based on the proposed model of the two-criteria optimization problem, a method was proposed for resource saving in the edge and foggy layers of the network. It reflected the specifics of the dynamic layers of the network, and also took into account the importance of the criteria for estimating the consumption of device resources. An experiment was conducted to evaluate the impact of the method of distributing tasks over a network cluster on the probability of failure-free operation of devices and on the average residual resource.

***Discussion and Conclusions.*** The conducted experiment has demonstrated the feasibility of using the developed method, since the distribution of tasks among executing devices had a significant impact (up to 25 % according to the results of the experimen t) on the average residual resource of a computing device.

**Keywords:** resource saving, calculation planning, fog computing, edge computing, optimization.

**Acknowledgements.** The author would like to thank the management of the Institute of IT and Security Technologies, Russian State University for the Humanities, for the assistance provided during the preparation of the project.

**For citation.** Klimenko AB. Two-Criteria Technique for the Resource-Saving Computing in the Fog and Edge Network Tiers. *Advanced Engineering Research (Rostov-on-Don).* 2023;23(1):85–94. https://doi.org/10.23947/2687-1653-2023-23-1-85-94

*Научная статья*

# Двухкритериальный метод обеспечения ресурсосбережения в краевом и туманном слоях сети

**А.Б. Клименко**

Институт информационных наук и технологий безопасности РГГУ, Российская Федерация, г. Москва, ул. Кировоградская, д. 25

✉ Anna_klimenko@mail.ru

**Аннотация**

***Введение.*** В настоящее время концепции туманных и краевых вычислений используются широким кругом приложений самой различной направленности. Одной из ключевых проблем организации вычислений в группах мобильных устройств, составляющих краевой/туманный слой, является обеспечение выполнения миссии на основе наличия заряда батареи. В связи с этим к настоящему времени представлено немало разработок, направленных на энергосбережение систем устройств. Однако очень важный аспект остается за рамками рассмотрения проблемы ресурсосбережения, а именно — вопрос сбережения остаточного ресурса вычислительного устройства. Целью данного исследования является формализация задачи распределения нагрузки как двухкритериальной задачи оптимизации и выбор базового метода ее решения.

***Материалы и методы.*** В рамках данной статьи предлагается подход к ресурсосбережению на основе оценивания двух критериев устройств: ресурса батареи и остаточного ресурса вычислительного устройства. Остаточный ресурс вычислительного устройства может быть оценен при помощи значений вероятности безотказной работы устройства или как величина, обратная интенсивности отказов с учетом того, что при моделировании используется экспоненциальный закон распределения отказов. На основе этого сформулирована модель задачи двухкритериальной оптимизации с учетом динамики топологии сети в процессе выполнения пользовательской миссии. Динамика топологии отражена в модели как последовательность топологий, каждая из которых соответствует определенному отрезку времени функционирования системы.

***Результаты исследования.*** На основании представленной модели задачи двухкритериальной оптимизации предложен метод обеспечения ресурсосбережения в краевом и туманном слое сети, отражающий специфику динамических слоев сети, а также учитывающий важность критериев оценивания расхода ресурсов устройств. Проведен эксперимент, позволяющий оценить влияние способа распределения задач по сетевому кластеру на вероятность безотказной работы устройств и на средний остаточный ресурс.

***Обсуждение и заключения***. Проведенный эксперимент демонстрирует целесообразность применения разработанного метода, поскольку распределение задач по исполняющим устройствам оказывает существенное влияние (до 25 % по итогам эксперимента) на средний остаточный ресурс вычислительного устройства.

**Ключевые слова:** ресурсосбережение, планирование вычислений, туманные вычисления, краевые вычисления, оптимизация.

**Благодарности.** Автор выражает признательность руководству Института информационных наук и технологий безопасности Российского государственного гуманитарного университета за помощь, оказанную в процессе подготовки проекта.

**Для цитирования.** Клименко А.Б. Двухкритериальный метод обеспечения ресурсосбережения в краевом и туманном слоях сети. *Advanced Engineering Research (Rostov-on-Don).* 2023;23(1):85–94. https://doi.org/10.23947/2687-1653-2023-23-1-85-94

**Introduction.** Currently, applications using edge and fog network segments are widely used [1–5]. Distributed computing performed on the nodes of these segments has significant difference from distributed computing performed

in cloud structures, namely, relatively high topology dynamics and, in addition, the presence of certain distances between the nodes used. This results in the need to take this parameter into account when modeling the time of information exchanges between executable tasks. The existence of topology dynamics is explained by the fact that network edge devices are, as a rule, user devices (including all kinds of sensors, smartphones, laptops, etc.) that belong to certain people and can be moved, turned off, access to data/resources may be prohibited. At the same time, all of them depend on the presence of a battery charge (power source) [6, 7]. The fog layer of the network is less dynamic. However, it is also characterized by all of the above to one degree or another: the occurrence of a certain distance between nodes with the presence of transit sections of the network, the possible mobility of the nodes themselves, e.g., in case of data processing by groups of mobile devices. An interesting example in this sense are groups of low-orbit satellites that are currently used for data processing, but the nodes are displaced relative to the Earth's surface at a fairly high speed (access time is on the order of several minutes) and, therefore, the question arises about the routing and transmission of processing results to ground stations [8].

As part of the issues of resource saving of devices used in the dynamic layers of the network, a number of works have been published [9–11], in which attention is focused on energy saving. As a rule, the model assumes the dependence of the consumed energy of the device on its workload [12]. At the same time, such an important factor as saving the residual computing resource of the device remained outside the focus of research [13].

The residual computing resource of a device is a value that is closely related to such reliability characteristics as the probability of failure-free operation and gamma-percentage time to failure. Also, the average residual life, taking into account the use of the exponential law of failure rate distribution, is characterized by the following expression:

$$R(\tau) = \frac{1}{P(\tau)} \int_{\tau}^{\infty} P(x)dx , \quad (1)$$

where $P(x)$ — probability of faultless operation (PFO) of the object during time $x$.

For the exponential resource distribution law, the PFO is defined as:

$$P(x) = e^{-\lambda x} , \quad (2)$$

where $\lambda$ — hazard rate, $\lambda > 0$.

Then, according to formula (1), the average residual life is determined from the following formula:

$$R(\tau) = R = \frac{1}{\lambda} . \quad (3)$$

At the same time, there are works devoted to the relationship between the values of PFO, gamma-percentage time to failure, and the average residual resource on the temperature of the computing element of the device, which, in turn, is described as a function of the device load [14–16]. The problem of device resource saving can also be posed as the problem of maximizing the average residual resource of the device.

Thus, the problem of resource saving is considered in recent works either as a task of minimizing the power consumption of devices, or as a task of saving the residual computing resource.

However, under present-day conditions, it is reasonable to talk about two-criteria optimization of resource consumption of devices for the following reasons:

– electricity is a renewable but critical resource for the mission of the device, whether it is a sensor of an information and control system or a controlled mobile device;

– residual computing resource determines the duration of the device's expedient operation, and the operation time, respectively, is the sum of the missions performed by the device.

Therefore, the objective of this study was to develop a resource saving method for devices of dynamic network layers, within which the assessment would be carried out on the basis of two criteria — power consumption and computing resource consumption of the device.

**Materials and Methods.** Let us define the concept of "mission of a group of devices" as a predetermined sequence of solving by a group of devices a complex of computational tasks related to information exchanges. The mission of a group of devices can be described by an acyclic graph, whose vertices will be weighted by the complexity of the tasks, and the arcs, respectively, will determine the limits of the sequence and the amount of data transmitted by the tasks. Let the mission be described by graph $W = \{w_l, z_l, I\}$, where $w_l$ — complexity of the task, $z_l$ — proportion of the task completed by the time of the topology change, $I$ — matrix of data volumes transferred between tasks. A group of devices in a dynamic network layer is described by a set of graphs, each of which defines the topology of the network at time $t_i$. We assume that the mission execution time includes a certain time interval with discrete instants of time $[t_0, t_1, \ldots t_k]$, each of which corresponds to the topology graph $G_i=\{<p_{ij}, e_{ij}, R_{ij}>, H\}$, $j=1\ldots m$, $p_{ij}$ — performance of the $j$-th node of the $i$-th topology, $e_{ij}$ — energy resource of the $j$-th node of the $i$-th topology, $R_{ij}$ — average residual computing resource of the $j$-th node of the $i$-th topology, $m$ — number of devices in a group, $H$ — matrix of network connections between nodes. We also assume that at each subsequent time $t_{i+1}$, for graphs $G_{i+1}$ and $G_i$, the following is true: at least one of the vertices belonging to $G_i$, will be contained in $G_{i+1}$, which is required to continue the mission.

We also assume that if the topology graph changes at time $t_{i+1}$, it is possible to reassign tasks that were performed in the $i$- th topology on the nodes that ceased to exist at $i+1$ time, to any of the available topology nodes $i+1$. At the same time, we make the assumption that the tasks transferred to new nodes start to be executed at the same place where their execution was interrupted.

Estimation of the residual computational resource will be implemented as follows: to estimate the PFO of the device of the fog layer, we will use the expressions proposed in [17, 18]:

$$\lambda = \lambda_0 \cdot 2^{\frac{kD}{10}}, \tag{4}$$

where $D$ — calculator load (in fractions).

$$D = \frac{w_i}{p_j \cdot t_{constra\,int}}, \tag{5}$$

where $w_i$ — complexity of the work performed.

Accordingly, PFO (t) can be estimated, as well as the average residual resource:

$$P(t) = e^{-\lambda t} = e^{-\lambda_0 \cdot t \cdot 2^{kD/10}} = e^{-\lambda_0 \cdot t \cdot 2^{kw/10\, pt_{constra\,int}}}, \tag{6}$$

where $t_{constraint}$ — time limit for which the task must be completed by the node to meet the mission time limit $t_m$.

When estimating the residual energy resource, we also assume that the energy consumption is proportional to the workload of the computing node, and there are no more energy costs:

$$E_{jm} = E_{j0} - \xi D, \tag{7}$$

where $E_{j0}$ — initial level of energy available, $E_{jm}$ — residual level, $\xi$ — coefficient expressing the relationship between the load of the computing element and its energy consumption.

The result of the operation of the two-criteria method for ensuring resource saving will be a sequence of distributions of still unsolved mission tasks over time $[t_0, t_{i-1}]$ by topology $G_i$ taking into account the fact that some of the tasks that are in the process of being solved on the nodes inherited from topology $G_{i-1}$, remain at their places and are not transferred: $A = \{A_i\}$;

$$A_i = \begin{vmatrix} t_{11} & \dots & \dots \\ \dots & t_{lj} & \dots \\ \dots & \dots & t_{lk} \end{vmatrix}. \quad (8)$$

Matrix $A$ describes the distribution of unsolved problems for which $z_l<1$. At the same time, the number of nodes corresponds to new topology $G_i$. Nodes inherited from $G_{i-1}$, are renumbered and occupy indices starting from 1.

Since the mission may involve more than one topology, we will decompose the problem as follows: we will use the "greedy" policy and assume that a satisfying solution (minimization of resource consumption, estimated by two chosen criteria) can be obtained, if for each topology, we choose the best solution.

That is, the task model will have the following form: $\forall g_l, z_l < 1, t_i > 0$ to get such $A_i$, that $R(t_m)$ $R_j(t_m) \to \max, e_j(t_m) \to \max$, при $\max(A_{ijk}) \le t_m$.

Consider the possible priority of the formulated objective functions. For each individual topology, it is required to minimize both the power consumption and the consumption of computing resources. In some special cases, the coincidence of optimization goals for two criteria can be achieved. Specifically, the task is distributed to the node in such a way that it will provide it with the minimum workload of the computational element and at the same time the minimum power consumption.

However, this situation is not always possible. For example, there is a node loaded less than other calculations, but at the same time its energy resource is almost exhausted. By assigning a task to it, we jeopardize the mission (or it is necessary to change topologies as the supply of electricity runs out), and by assigning a task to a more loaded node, we worsen the value of the residual computing resource criterion. The opposite situation can also occur: a node with a large residual power resource may have a low residual computing resource as a result of participating in previous device missions.

Therefore, it is advisable to rank the objective function (OF) in terms of importance, on the basis of which to select a further solution method.

For critical missions, the battery life of the device plays a leading role [19–21]. Accordingly, the OF that determines the residual computing resource can be reduced to an additional constraint. Uncompleted mission tasks will be redistributed depending on the remaining battery charge.

It should be noted that the above is also true for missions that do not have critical execution. In the event that the device loses battery power without completing the mission, it may be lost. Then the optimization of the computing resource will become meaningless.

On the other hand, by reducing the residual computational resource to a limitation, the solution may not be obtained at all due to the lack of available nodes whose characteristics would satisfy it.

**Research Results.** Multicriteria optimization problems, as a rule, are reduced to solving one or more single-criteria problems. In this case, it is more expedient to leave one OF, and present the second one as a constraint.

For the system under consideration, the fulfillment of the mission is critical for each node; therefore, we transform the OF for energy consumption into a restriction, the implementation of which will cut off unacceptable options for distributing tasks among the nodes. Further, within the framework of the resulting set of nodes, the distribution will occur with minimization of the consumption of the residual computing resource.

Let us describe the main stages of the two-criteria method for ensuring resource saving as the basic result of the study:

– on the existing $G_i$-topology, select nodes that have sufficient energy resources to complete the mission without changing the topology;

– distribute mission tasks among selected nodes in such a way as to minimize the consumption of computing resources for idle nodes, to which unsolved tasks will be attached.

It is possible to rank the nodes obtained at the first step of the method in descending order of the availability of an energy resource. But then, by distributing tasks primarily among nodes with the maximum amount of energy resource, there may be a deterioration in the values of the residual computing resource criterion.

Let us illustrate the dependence of the PFO values of devices on the selection of a node for solving the problem (in this experiment, we compare the states of the nodes under the transmission of incoming data and during their processing).

The topology is shown in Figure 1.

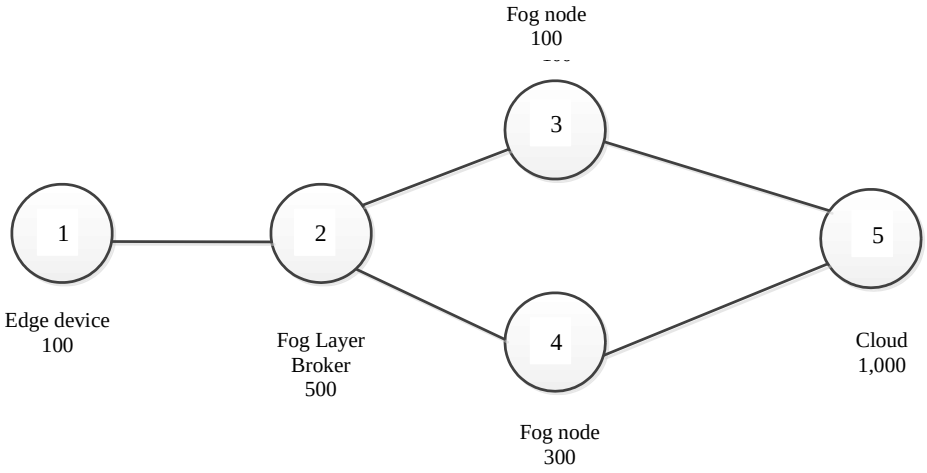


Fig. 1. Experimental fragment of network topology

The experiment was carried out for 10-time intervals, each of which was 100 hours with the following parameter values: Wreceive (amount of data received by the task) — 500 units, Wsend (amount of data sent by the task) — 100 units, Wprocess (data processing complexity) — 150 units, Tdecl (time allotted for solving the task) — 50 units.

The following are graphs of PFO nodes depending on whether the node processes data or only transmits it (Fig. 2–5).

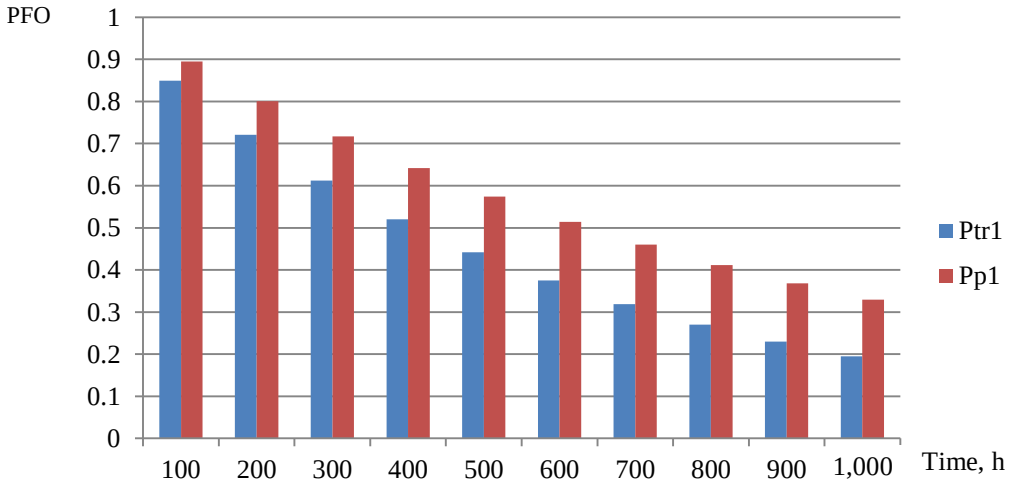


Fig. 2. Comparison of PFO values for node 1 under data processing (Pp1) and when transferring data (Ptr1)

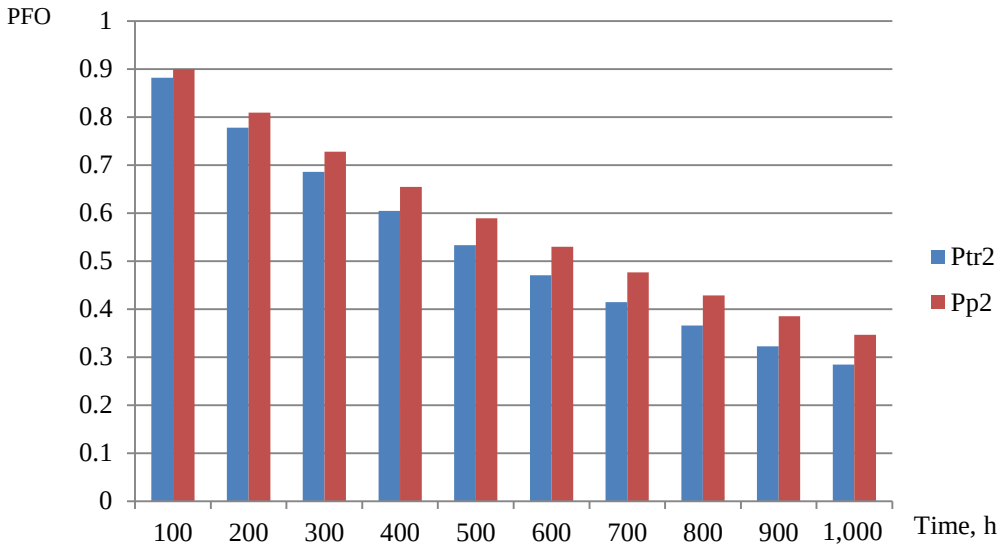


Fig. 3. Comparison of PFO values for node 2 under data processing (Pp2) and when transferring data (Ptr2)

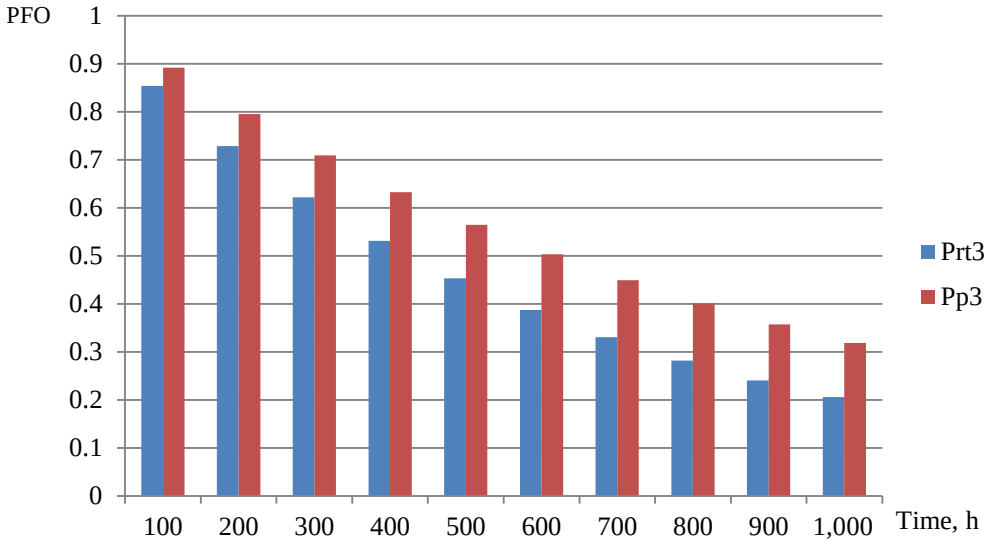


Fig. 4. Comparison of PFO values for node 3 under data processing (Pp3) and when transferring data (Ptr3)

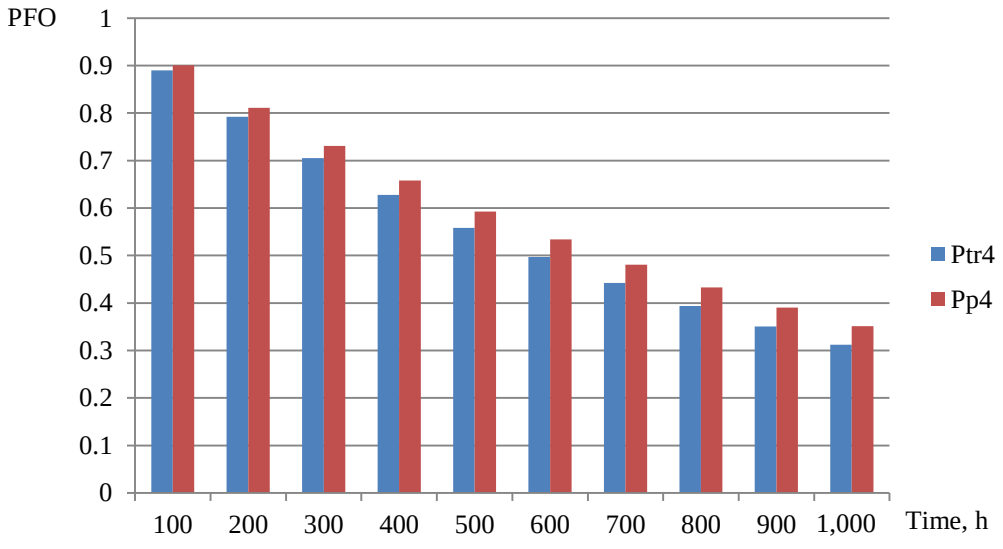


Fig. 5. Comparison of PFO values for node 4 under data processing (Pp4) and when transferring data (Ptr4)

Further, Figure 6 shows comparison of differences in the values of the average residual computing resource.

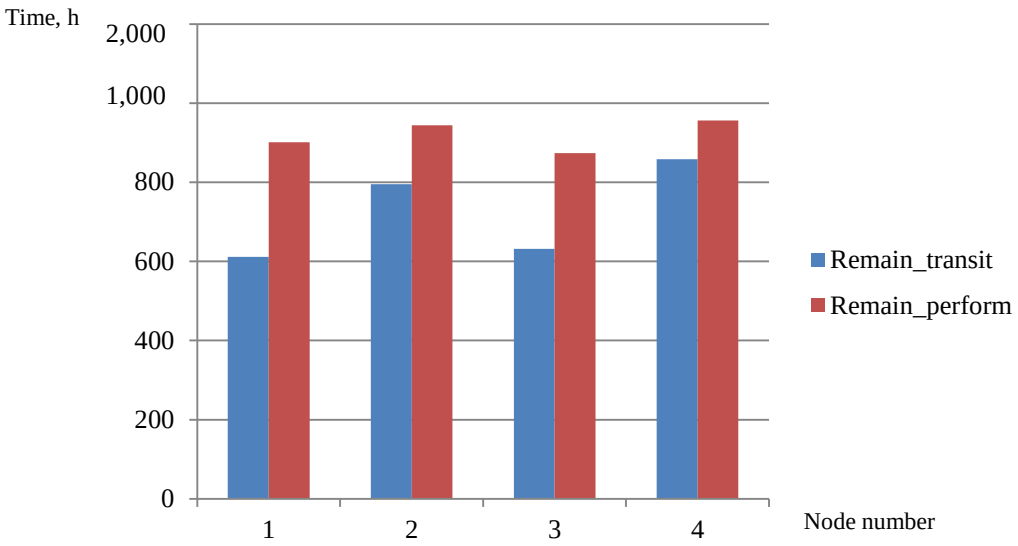


Fig. 6. Comparison of average residual resource values for nodes 1–4 during data transit (Remain_transit) and under data processing (Remain_perform)

**Discussion and Conclusions.** The article proposes a two-criteria method for ensuring resource saving in the edge and fog layers of the network. It differs from those previously presented in the subject area of organizing distributed computing in the dynamic layers of the network in the following. The proposed method takes into account both the state of the battery of the device (which is critical for the mission) and the residual resource of the computing device (what affects the duration of the appropriate use of the device outside the mission).

The developed method is based on the formulated problem of two-criteria optimization, which is then proposed to be reduced to a single-criteria one through converting the objective function of the energy resource balance into a constraint.

The nodes that are not suitable for the battery level are cut off in advance. Then there is a distribution of tasks according to the criterion of the residual computing resource.

The conducted experiment makes it possible to compare the results of task distribution over nodes in the presence of information interactions between tasks. It is clearly shown that the method of task distribution affects significantly the value of the residual resource of a computing device (up to 25 %). Thus, it is possible to improve the resource consumption indicators of devices involved in calculations in the edge and fog layers of the network.

**References**

1. Mehbub Alam, Nurzaman Ahmed, Rakesh Matam, et al. *L3Fog: Fog Node Selection and Task Offloading Framework for Mobile IoT*. In: Proc. IEEE Conference on Computer Communications Workshops — IEEE INFOCOM 2022. P. 1–6. 10.1109/INFOCOMWKSHPS54753.2022.9798118

2. Abdelfettah Maatoug, Ghalem Belalem, Saïd Mahmoudi. A Location-Based Fog Computing Optimization of Energy Management in Smart Buildings: DEVS Modeling and Design of Connected Objects. *Frontiers of Computer Science*. 2023;17:172501. https://doi.org/10.1007/s11704-021-0375-z

3. Abohamama AS, Amir el Ghamry, Eslam Hamouda. Real-Time Task Scheduling Algorithm for IoT-Based Applications in the Cloud–Fog Environment. *Journal of Network and Systems Management*. 2022;30(4):54. https://doi.org/10.1007/s10922-022-09664-6

4. Saad Ahmad Khan, Muhammad Abdullah, Waheed Iqbal, et al. Efficient Job Placement Using Two-Way Offloading Technique over Fog-Cloud Architectures. *Cluster Computing*. 2022;154:1–19. 10.1007/s10586-022-03750-9

5. Rajasi Gore, Shashwati Banerjea, Neeraj Tyagi. A Heterogeneous Soft-Hard Fusion Framework on Fog Based Private SaS Model for Smart Monitoring of Public Restrooms. *Journal of Ambient Intelligence and Humanized Computing.* 2022. Vol. 63. https://doi.org/10.1007/s12652-022-04401-y

6. Haibo Wang, Hongli Xu, He Huang, et al. Robust Task Offloading in Dynamic Edge Computing. *IEEE Transactions on Mobile Computing*. 2021;22:500–514. https://doi.org/10.1109/TMC.2021.3068748

7. Enlu Liu, Xiaoheng Deng, Zhi Cao, et al. *Design and Evaluation of a Prediction-Based Dynamic Edge Computing System.* In: Proc. 2018 IEEE Global Communications Conference (GLOBECOM). https://doi.org/10.1109/GLOCOM.2018.8647199

8. Fraire JA, Gerstacker C, Hermanns H, et al. On the Scalability of Battery-Aware Contact Plan Design for LEO Satellite Constellations. *International Journal of Satellite Communications and Networking*. 2020;39:193–204. https://doi.org/10.1002/sat.1374

9. Yung-Ting Chuang, Chiu-Shun Hsiang. A Popularity-Aware and Energy-Efficient Offloading Mechanism in Fog Computing. *The Journal of Supercomputing.* 2022;78:1–24. https://doi.org/10.1007/s11227-022-04626-w

10. Ida Syafiza Binti, Taizir EH El-Gorashi, Mohamed OI Musa, et al. Energy Efficient Fog Based Healthcare Monitoring Infrastructure. *IEEE Access.* 2020;8:197828–197852. https://doi.org/10.1109/ACCESS.2020.3033555

11. Fatemah S Behbehani, Taisir El-Gorashi, Jaafar MH Elmirghani. Power Minimization in Vehicular Cloud Architecture. arXiv:2102.09011 2021. https://doi.org/10.48550/arXiv.2102.09011

12. Shilpa B Kodli, Sujatha Terdal. Survey on Energy Efficient-Load Balancing in Cloud. *International Journal of Computer Applications.* 2022;184(25):15–24. http://dx.doi.org/10.5120/ijca2022922301

13. Fudukhin AV. Prognozirovanie nadezhnosti ehlektronnykh ustroistv posle dlitel'nogo khraneniya. *Mathematical Machines and Systems.* 2004;4:164–170. (In Russ.)

14. Klimenko AB, Melnik EV. A Method of Improving the Reliability of the Nodes Containing Ledger Replicas. In book: Silhavy R, Silhavy P, Prokopova Z. (eds.) *Software Engineering Application in Informatics.* 2021. P. 584–592. https://doi.org/10.1007/978-3-030-90318-3_47

15. Klimenko A, Melnik E. Information and Control Systems with Distributed Ledger Usage: A Reliability Issue. In book: Radek Silhavy (ed.) *Artificial Intelligence in Intelligent Systems. Springer*; 2021. P. 133–144. https://doi.org/10.1007/978-3-030-77445-5_12

16. Melnik E, Safronenkova I, Kapustyan S. *The Efficiency Improvement of Robots Group Operation by Means of Workload Relocation.* In: Proc. Int. Conf. on Interactive Collaborative Robotics. 2021;450:126–137. https://doi.org/10.1007/978-3-030-87725-5_11

17. Melnik EV, Gorelova GV. About Effect of Processor Computational Load Balancing in Highly Reliable Distributed Information and Control Systems, Research Planning. *Mechatronics, Automation, Control*. 2012;11:29–35.

18. Kalyaev IA, Melnik EV. *Detsentralizovannye sistemy komp'yuternogo upravleniya*. Rostov-on-Don: Izdatel'stvo YuNTS RAN; 2011. 196 p. (In Russ.)

19. Preedipat Sattayasoonthorn, Jackrit Suthakorn. *Battery Management for Rescue Robot Operation*. In: Proc. 2016 IEEE Int. Conf. on Robotics and Biomimetics (ROBIO). 2016. P. 1227–1232. https://doi.org/10.1109/ROBIO.2016.7866493

20. Vinay Jadhav, Surendra Bhosale. *Battery Management System for Drones.* In: Proc. Int. Conf. on Electrical Electronics and Data Communication. 2022. URL: https://www.researchgate.net/publication/362889754_Battery_Management_System_for_Drones (accessed: 10.12.2022).

21. Wei Liu, Tobias Placke, Chau KT. Overview of Batteries and Battery Management for Electric Vehicles. *Energy Reports*. 2022;8:4058–4084. https://doi.org/10.1016/j.egyr.2022.03.016

*About the Author:*

**Anna B Klimenko,** associated professor of the Fundamental and Applied Mathematics Department, Institute of IT and Security Technologies, RSUH (25, Kirovogradskaya St., Moscow, 117534, RF), Cand.Sci. (Engineering), ScopusID, ORCID, anna_klimenko@mail.ru

**Received** 15.12.2022.

**Revised** 20.01.2023.

**Accepted** 20.01.2023.

*Conflict of interest statement*

The author does not have any conflict of interest.

*The author has read and approved the final manuscript*.

*Об авторе:*

**Анна Борисовна Клименко,** доцент кафедры «Фундаментальная и прикладная математика» Института информационных наук и технологий безопасности Российского государственного гуманитарного университета (117534, Москва, ул. Кировоградская, д. 25 корп. 2), кандидат технических наук, ScopusID, ORCID, anna_klimenko@mail.ru

**Поступила в редакцию** 15.12.2022.

**Поступила после рецензирования** 20.01.2023

**Принята к публикации** 20.01.2023.

*Конфликт интересов*

Автор заявляет об отсутствии конфликта интересов.

*Автор прочитал и одобрил окончательный вариант рукописи.*

# INFORMATION TECHNOLOGY, COMPUTER SCIENCE AND MANAGEMENT
# ИНФОРМАТИКА, ВЫЧИСЛИТЕЛЬНАЯ ТЕХНИКА И УПРАВЛЕНИЕ



УДК 004.942
https://doi.org/10.23947/2687-1653-2023-23-1-95-106

*Original article*

## Mathematical Model of the pH Control System in an In Vitro Model of the Gastrointestinal Tract of Poultry

**Danila Yu Donskoy**[1], **Alexandr D Lukyanov**[1], **Vladimir Filipović** [2], **Tamara B Asten**[1]

[1] Don State Technical University, 1, Gagarin sq., Rostov-on-Don, Russian Federation
[2] University of Novi Sad, 1, Bul. cara Lazara, Novi Sad, Republic of Serbia
✉ dand22@bk.ru

**Abstract**

***Introduction.*** Essential nonlinearity of the chemical reactions of acids and bases determines the control algorithms in the mode of acidification or alkalization, that is, periodic dosing of a minimum volume of acid or alkali. Such regulation may be ineffective, specifically, it allows insufficient or excessive concentration of the controlled substance. The article discusses the problem of precise regulation of the hydrogen index in mini-bioreactors. It is proposed to use a digital model of the acidity control system to select the concentrations of topped-up solutions, determine the regulation methodology, and improve accuracy. The objective of the work is the assurance of required accuracy of pH regulation in an in vitro mini-model of the gastrointestinal tract of a static type.

***Materials and Methods.*** The initial block diagram of the model included accumulators and flows. It was the base for the main differential equations characterizing the change in volume and acidity. To correct the acidity readings of the resulting solution by temperature, a static model based on the polynomial approximation of experimental data using the least squares method was created. The structural elements of the mathematical model were investigated in the Matlab Simulink application package. To validate the adequacy of the mathematical model, transient characteristics were determined on a real system of in vitro modeling of the artificial gastrointestinal tract of poultry.

***Results.*** Within the framework of this work, the authors created and analyzed a nonlinear mathematical model of pH changes in a bioreactor taking into account external control actions. The flows of hydrochloric acid solution, alkali solution and drain from the reactor were presented as elements of a differential equation describing the accumulation of liquid in the reactor. To improve the accuracy, the solution was modified taking into account the temperature dependence of the hydrogen index. A dosing mathematical model based on a regulator with alkali and acid channels was proposed. The data obtained made it possible to generate a combined model of the pH regulation process in the bioreactor. The adequacy of the solution was confirmed empirically. The models of pH regulator, regulation of the volume of contents in the reactor and chemical reactions were shown in the form of structural diagrams. The transients of a mathematical model and a real control system were compared. It was established that the transient characteristics of the mathematical model and the real system were identical in terms of regulation time. The relative error of regulation of the real system was 0.35 %, and the mathematical model — 0.1 %, which corresponded to the required accuracy of regulation ± 0.1 pH. The influence of the studied flows on the neutralization reaction was shown in the form of graphs.

***Discussion and Conclusions.*** The proposed mathematical model will provide selecting optimal methods and algorithms for regulating acidity, which will accelerate the creation of a regulator for the nonlinear process of regulating the hydrogen index. In the future, these developments can be integrated into a comprehensive digital model of the entire artificial gastrointestinal tract of poultry to optimize control algorithms (dosing, mixing, periodicity, etc.), as well as approximation to objects in vivo.

**Keywords:** mathematical modeling, acidity, pH, in vitro modeling, in vivo modeling, control system, acidity regulation algorithm, digital model.

**Acknowledgements.** Appreciation is expressed for the financial support of research within the framework of Grant No. 075-15-2022-285 dated June 9, 2022, “Veterinary probiotic drugs for targeted modulation of animal health”.

**For citation.** Donskoy DYu, Lukyanov AD, Filipović V. Mathematical Model of the pH Control System in an In Vitro Model of the Gastrointestinal Tract of Poultry. *Advanced Engineering Research (Rostov-on-Don).* 2023;23(1):95–106. https://doi.org/10.23947/2687-1653-2023-23-1-95-106

*Научная статья*

# Математическая модель системы управления pH в in vitro модели желудочно-кишечного тракта домашней птицы

**Д.Ю. Донской**[1] ✉, **А.Д. Лукьянов**[1], **В. Филипович** [2], **Т.Б. Астен**[1]

[1] Донской государственный технический университет, Российская Федерация, г. Ростов-на-Дону, пл. Гагарина, 1

[2] Университет Нови-Сада, Республика Сербия, г. Нови-Сад, бул. Цара Лазара, 1

✉ dand22@bk.ru

**Аннотация**

***Введение.*** Существенная нелинейность химических реакций кислот и оснований определяет алгоритмы управления в режиме подкисления или подщелачивания, то есть периодической дозации минимального объема кислоты или щелочи. Такое регулирование может быть малоэффективным, т. е. допускает недостаточную или избыточную концентрацию контролируемого вещества. Статья посвящена проблеме точного регулирования водородного показателя в мини-биореакторах. Предлагается использовать цифровую модель системы управления кислотностью для подбора концентраций доливаемых растворов, определения методики регулирования и повышения точности. Цель работы — обеспечение требуемой точности регулирования pH в in vitro мини-модели желудочно-кишечного тракта статического типа.

***Материалы и методы.*** Исходная структурная схема модели включает накопители и потоки. Она представляет собой базу для основных дифференциальных уравнений, характеризующих изменение объема и кислотности. Для корректировки показаний кислотности результирующего раствора по температуре создана статическая модель, основанная на полиномиальной аппроксимации экспериментальных данных методом наименьших квадратов. В прикладном пакете MATLAB Simulink исследованы структурные элементы математической модели. На реальной системе in vitro моделирования искусственного желудочно-кишечного тракта домашней птицы определены переходные характеристики для подтверждения адекватности математической модели.

***Результаты исследования.*** В рамках данной работы авторы создали и проанализировали нелинейную математическую модель изменения pH в биореакторе с учетом внешних управляющих воздействий. Потоки раствора соляной кислоты, раствора щелочи и слива раствора из реактора представлены как элементы дифференциального уравнения, описывающего накопление жидкости в реакторе. Для повышения точности решение доработали с учетом температурной зависимости водородного показателя. Предложена математическая модель дозирования на основе регулятора с каналами щелочи и кислоты. Полученные данные позволили генерировать объединенную модель процесса регулирования pH в биореакторе. Адекватность решения подтвердили опытным путем. В виде структурных схем показаны модели: регулятора pH, регулирования объема содержимого в реакторе и химических реакций. Сравниваются переходные процессы математической модели и реальной системы управления. Установлено, что переходные характеристики математической модели и реальной системы идентичны по времени регулирования. Относительная погрешность регулирования реальной системы составила 0,35 %, а математической модели — 0,1 %, что соответствует требуемой точности регулирования ±0,1 pH. В виде графиков показано влияние исследованных потоков на реакцию нейтрализации.

***Обсуждение и заключения.*** Предлагаемая математическая модель позволит подобрать оптимальные методы и алгоритмы регулирования кислотности, что ускорит создание регулятора нелинейного процесса регулирования водородного показателя. В будущем эти наработки можно интегрировать в комплексную цифровую модель всего искусственного желудочно-кишечного тракта домашней птицы для оптимизации алгоритмов управления (дозации, перемешивания, периодичности и т. п.), а также аппроксимации к объектам in vivo.

**Ключевые слова:** математическое моделирование, кислотность, pH, моделирование in vitro, моделирование in vivo, система управления, алгоритм регулирования кислотности, цифровая модель.

**Благодарности.** Авторы выражают благодарность за финансовую поддержку исследований в рамках гранта Министерства науки и высшего образования Российской Федерации № 075-15-2022-285 от 9 июня 2022 г. «Ветеринарные пробиотические препараты направленного модулирования здоровья животных».

**Для цитирования.** Донской Д.Ю., Лукьянов А.Д., Филипович В. Математическая модель системы управления pH в in vitro модели желудочно-кишечного тракта домашней птицы. *Advanced Engineering Research (Rostov-on-Don).* 2023;23(1):95–106. https://doi.org/10.23947/2687-1653-2023-23-1-95-106

**Introduction.** Since the early 1980s, the scientific community studying the physiology and functional features of human internal organs has come to understand that in the near future, the focus of experimental techniques will shift from “in vivo” practices to “in vitro” systems [1]. The development of systems for hardware simulation of physiological processes will be of primary relevance, including for the following reasons: reduction of costs and time for conducting research; possibility of simultaneous conducting of the same type of experiments; and, what is not unimportant – increasing the ethics of research, reducing the need for experiments on living beings. By the beginning of the XXI century, a whole scientific direction was formed, engaged in the development of techniques and equipment for “in vitro” modeling and research [1].

Currently, in vitro models of the gastrointestinal tract are divided into two classes: static and dynamic. Static installations allow you to simulate the processes of digestion when using liquid nutrient media [2]. Dynamic models, unlike static ones, allow modeling peristaltic movements in the gastrointestinal tract, and are used when working with content nutrient media.

From the point of view of the simulated volume, the gastrointestinal tract models (regardless of the previous classification) are divided into micro- (up to 50 ml), mini- (from 50 to 400 ml) and macro-systems (over 400 ml) [3]. Microfluidic systems should be mentioned separately [4], but they go far beyond the scope of this work.

Patent analysis makes it possible to determine that the first is a patent for an invention “In vitro model of an in vivo digestive tract”[1]. This system is dynamic and precedes the market entry of the first TIM-2-type systems [5]. The development of this approach occurred in the models DGM [6], TIM-2 [5], HGS [7], etc. Static models, such as: DIDGI [8], SIMGI [9], SHIME [10], ARCOL [11], etc., moved away from complex modeling of peristalsis, and focused on more accurate modeling of the actual digestive processes. One of the reasons for this is the technical complexity and high cost of implementing systems with dynamic content compression. Another reason was the development of mathematical modeling methods and microcontroller control systems, which made it possible to control the medium in a test tube (reactor) with high accuracy and stability [4].

In this paper, we consider the solution to a particular problem of mathematical modeling of the pH regulation process for an in vitro mini-model of the gastrointestinal tract (gastrointestinal tract) of a static type [12]. The importance of precise control of the acidity of the chyme is determined by rather strict requirements for the conditions of in vitro experiments. Ensuring plausible conditions for the course of digestive processes, as well as the requirements for repeatability of experiments, require automatic pH control in the bioreactor with an accuracy not worse than ±0.1 units.[2] At the same time, the pH range can be from slightly alkaline (7.9 pH, oral cavity) up to strongly acidic (1.3 pH, stomach).

The objective of this work is to ensure the required accuracy of pH adjustment in an in vitro mini-model of the gastrointestinal tract (gastrointestinal tract) of a static type.

To achieve this goal, the following tasks will be solved in the work:

– development of mathematical model of nonlinear pH change in a bioreactor taking into account external control actions;

– study of a mathematical model by simulation methods;

[1] US5525305A. In vitro model of an in vivo digestive tract. URL: https://patents.google.com/patent/US5525305A/en

[2] No. 075-15-2019-1880. Veterinarnye probioticheskie preparaty napravlennogo modulirovaniya zdorov'ya zhivotnykh. URL: https://probioticdonstu.com/itno-2021-ru/ (In Russ.)

– refinement of the mathematical model in order to increase its accuracy by taking into account the temperature dependence of the hydrogen index;

– development of a mathematical model of the dosing process based on a two-channel competitive regulator (via alkali and acid channels);

– development of a unified mathematical model of the pH regulation process in a bioreactor;

– conducting experimental studies to confirm the adequacy of the combined mathematical model and determine the achieved accuracy of regulation.

**Materials and Methods.** To simulate the neutralization reaction, we will use the method of accumulators and flows [13]. The method is based on the use of fundamental or local conservation laws (accumulators) and mathematical description of patterns that change the amount of accumulated feature (flows).

The block diagram of the model is described in the figure, and contains two drives:

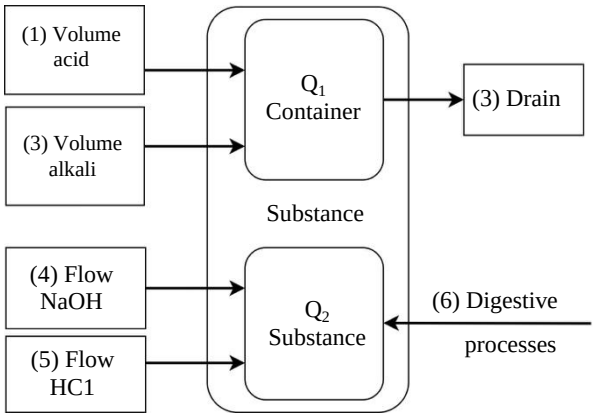


Fig. 1. Block diagram of the model

The reactor as a physical object simultaneously acts as a storage of the amount of liquid (Q1) and a storage of the amount of hydrogen ions (Q2). This is a container in which a controlled digestion process takes place, accompanied by a change in pH and a change in fluid volume.

There are three threads acting on the first drive:

– the first stream is the volume of acid topped up;

– the second stream is the volume of added alkali;

– the third stream is the volume poured out of the reactor.

The second drive is also affected by three threads:

– the fourth flow is the supply of sodium hydroxide by a pump [2];

– the fifth stream is the intake of hydrochloric acid. [2];

– the sixth stream is a potential change in pH during digestion. However, from a methodological point of view, it is a disturbing effect, and is not discussed in this paper.

Now, let us consider the mathematical implementation of the model for describing physico-chemical processes.

The volume of liquid in the reactor is described by the following equation:

$$V = S \cdot h. \quad (1)$$

Therefore, the change in the volume of liquid in the reactor:

$$dV = S \cdot dh. \quad (2)$$

For convenience, let us call the streams:

– the hydrochloric acid solution flow: q1=G1;

– the flow of the alkali solution (sodium hydroxide): q2= G2;

– the discharge flow of the solution from the reactor: q2 = G3.

Thus, the differential equation describing the accumulation of liquid in the reactor:

$$\frac{dh}{dt} = \frac{1}{S}\left(G_1 + G_2 - G_3\right). \tag{3}$$

To determine the dynamics of changes in the concentration of the solution in the reactor, it is required to find the differential of the amount of substance according to the following formula:

$$v = V \cdot C, \tag{4}$$

where V is the volume of the substance, l; C is the molar concentration, mol/l.

From (4) and (1), we obtain:

$$\frac{dv}{dt} = \frac{d}{dt}\left(S \cdot h \cdot C\right) = S \cdot \left(C \cdot \frac{dh}{dt} + h \cdot \frac{dC}{dt}\right). \tag{5}$$

The change in the concentration of the solution is influenced by the flows of alkali and acid with a certain concentration, then:

$$S \cdot \left(C \cdot \frac{dh}{dt} + h \cdot \frac{dC}{dt}\right) = \left(G_1 \cdot C_{NaOH} - G_2 \cdot C_{HCl}\right). \tag{6}$$

From equality (6), we express the change in concentration and simplify the expression:

$$\frac{dC}{dt} = \frac{1}{S \cdot h}\left(G_1(C_{NaOH} - C) + G_2(C - C_{HCl})\right). \tag{7}$$

Thus, the system of differential equations describing the dynamics of changes in the volume and concentration of the solution in the bioreactor is presented in formula 8:

$$\begin{cases} \frac{dh}{dt} = \frac{1}{S}(G_1 + G_2 - G_3), \\ \frac{dC}{dt} = \frac{1}{S \cdot h}\left(G_1(C_{NaOH} - C) + G_2(C - C_{HCl})\right). \end{cases} \tag{8}$$

To obtain the concentration of H ([H+]) cations from the solution of the system of equations (8), let us recall the basics of chemistry. The concentrations of hydrogen ions ([H+]) and hydroxide ions ([OH-]) in distilled water at 25 °C are equal and amount to 10-7 mol/l, this directly follows from the definition of the ionic product of water, which is presented below [11]:

$$K = \left[H^+\right] \times \left[OH^-\right] = 10^{-14}\,\text{mol}^2/l^2\,(\text{at } 25\,^\circ C). \tag{9}$$

It is also worth considering that:

$$T = [OH^-] - [H^+] = [Na^+] - [Cl^-]. \tag{10}$$

Now we find [H+] (denoted as $C_H$) through the square root of the previous expressions, taking into account the concentration of the solution according to equation (4) of our mathematical model [14]:

$$\begin{cases} C_H = \frac{T}{2}\left(\sqrt{1 + \frac{i \cdot K}{T^2}} - 1\right), T > 0, \\ C_H = \sqrt{K}, T = 0, \\ C_H = -\frac{T}{2}\left(\sqrt{1 + \frac{i \cdot K}{T^2}} + 1\right), T < 0. \end{cases} \tag{11}$$

Where ions i = 4.

To create a control system with feedback on acidity in the form of a hydrogen index (pH), it is necessary to calculate a negative decimal logarithm from the concentration calculated according to equations (7). Thus, we get the acidity of the solution under normal conditions, that is, at 25 °C.

But the contents of the bioreactor are not always in normal conditions. For example, to create an artificial environment characteristic of the in vivo environment of the gastrointestinal tract of poultry, a temperature of 42°C is maintained in the reactor[3]. Therefore, experimentally and on the basis of available research[4] a matrix of changes in the pH of buffer solutions depending on temperature was obtained on high-precision pH meters, and the readings were obtained using a measuring system with thermal compensation for the electrode used[5] [13].

Based on these data, a static model was constructed, it was obtained by polynomial approximation by the least squares method. A visual representation of the pH dependence on temperature is shown in Figure 2: [14–16].

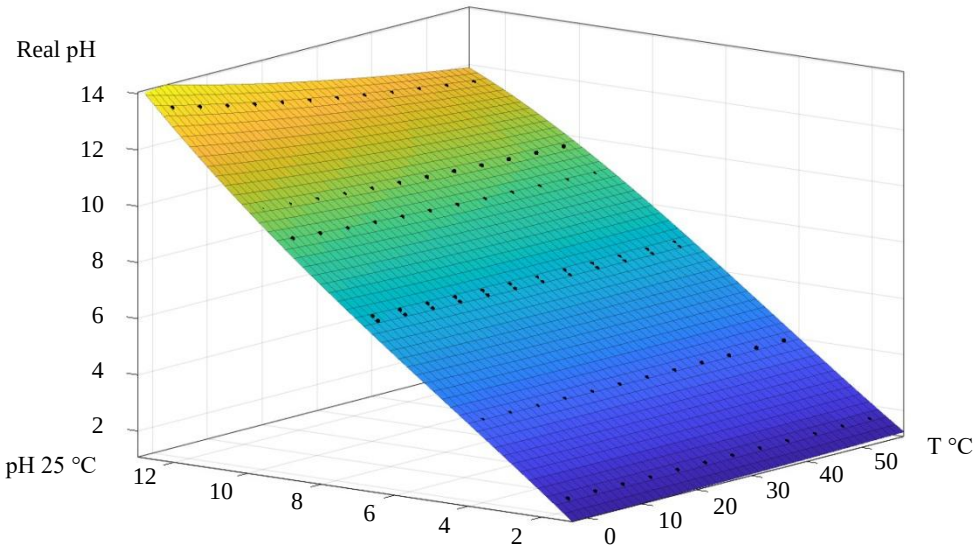


Fig. 2. A surface describing the dependence of pH on temperature (12)

$$F(x) = p00 + p10 \cdot x + p01 \cdot y + p20 \cdot x^2 + p11 \cdot x \cdot y + p02 \cdot y^2 + \\ + p30 \cdot x^3 + p21 \cdot x^2 \cdot y + p12 \cdot x \cdot y^2. \quad (12)$$

The coefficients of the equation are presented in Table 1.

Table 1

Coefficients of the equation (11)

| Coefficient | Value |
|---|---|
| p00 | 0.154 |
| p10 | -0.00511 |
| p01 | 0.899 |
| p20 | $-2.998 \cdot 10^{-6}$ |
| p11 | 0.00333 |
| p02 | 0.0130 |
| p30 | $-3.226 \cdot 10^{-7}$ |
| p21 | $1.588 \cdot 10^{-5}$ |
| p12 | $-4.98 \cdot 10^{-4}$ |

To determine the transients in the system, we will build a mathematical model in the MATLAB Simulink application package (Fig. 3):

[3] Automatic Temperature Compensation in pH Measurement. https://www.horiba.com/esp/water-quality/support/technical-tips/bench-meters/automatic-temperature-compensation-in-ph-measurement/?utm_source=uhw&utm_medium=301&utm_campaign=uhw-redirect
[4] Ibid.
[5] Gnaiger E. pH measurement and temperature dependence of pH. URL: https://www.bioblast.at/images/archive/b/be/20190329092613!MiPNet08.16_pH-Calibration.pdf

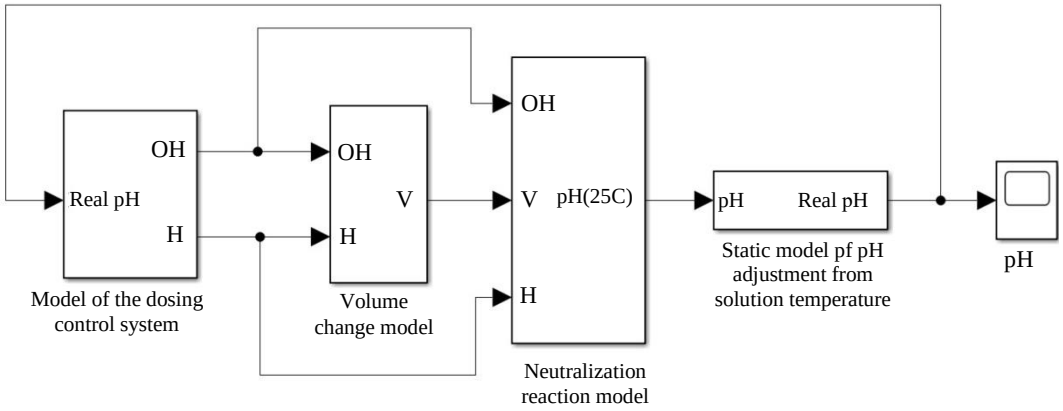


Fig. 3. General structure of the mathematical model in MATLAB Simulink

Let us consider the created system by blocks. The first block is a block of a two-channel acidity regulator with feedback. Noise has been introduced into the feedback circuit to simulate random events of a real system for measuring acidity and measuring instrument errors.

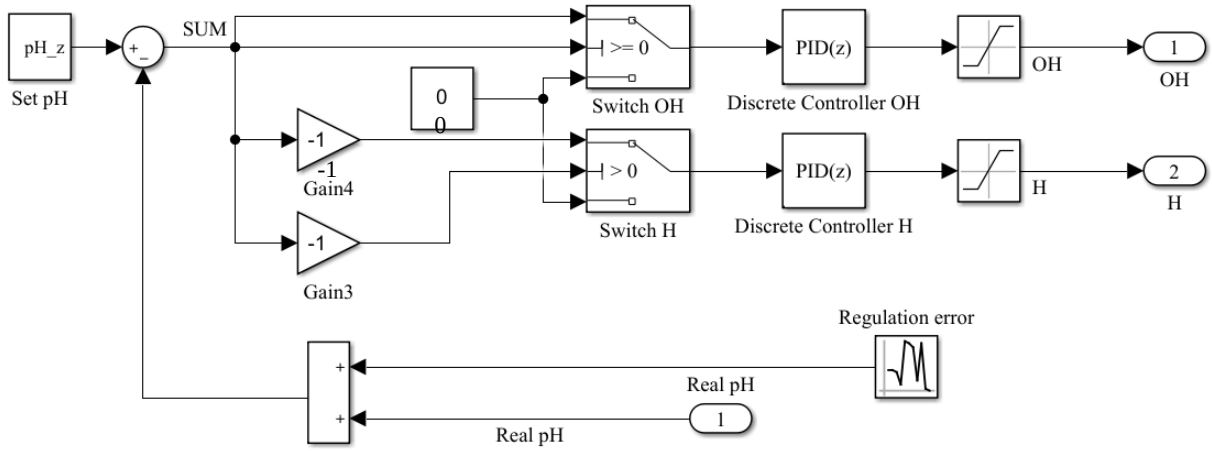


Fig. 4. Structure of the pH regulator, block “Model of the dosing control system”

The second unit is a system for monitoring the volume of solution in the reactor. The “Drain volume controller” function simulates the activation of pumping. If the volume of the solution approaches the maximum volume of the reactor, the function gradually resets the solution to the required volume.

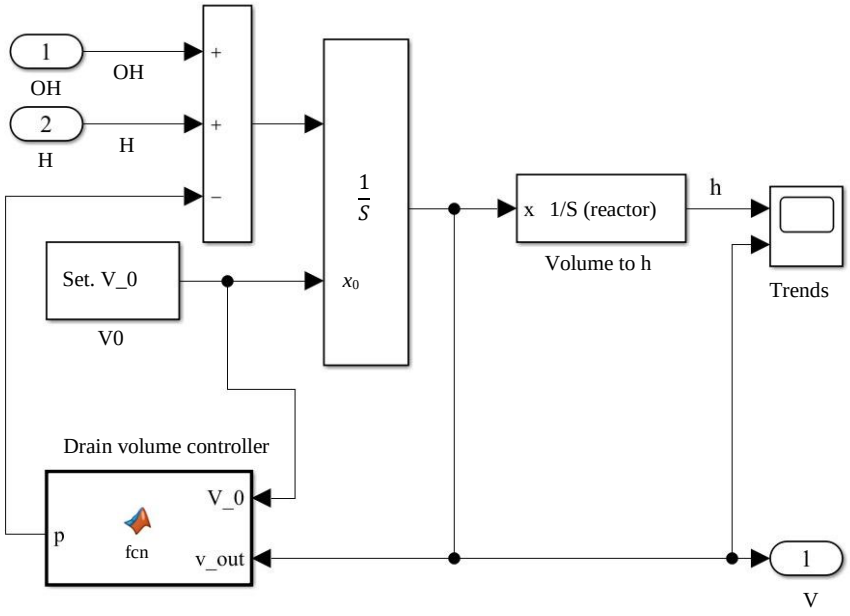


Fig. 5. Structure of the reactor content volume control model, block “Volume change model”

The third block is the main one. It implements the calculation of the chemical reaction of acid and alkali when added to the reactor and calculates the pH of the final solution under normal conditions. The function called “Neutralization” calculates the concentration of hydrogen ions in a solution [12]. And the “Concentration in pH” block implements the conversion of concentration into a hydrogen pH indicator.

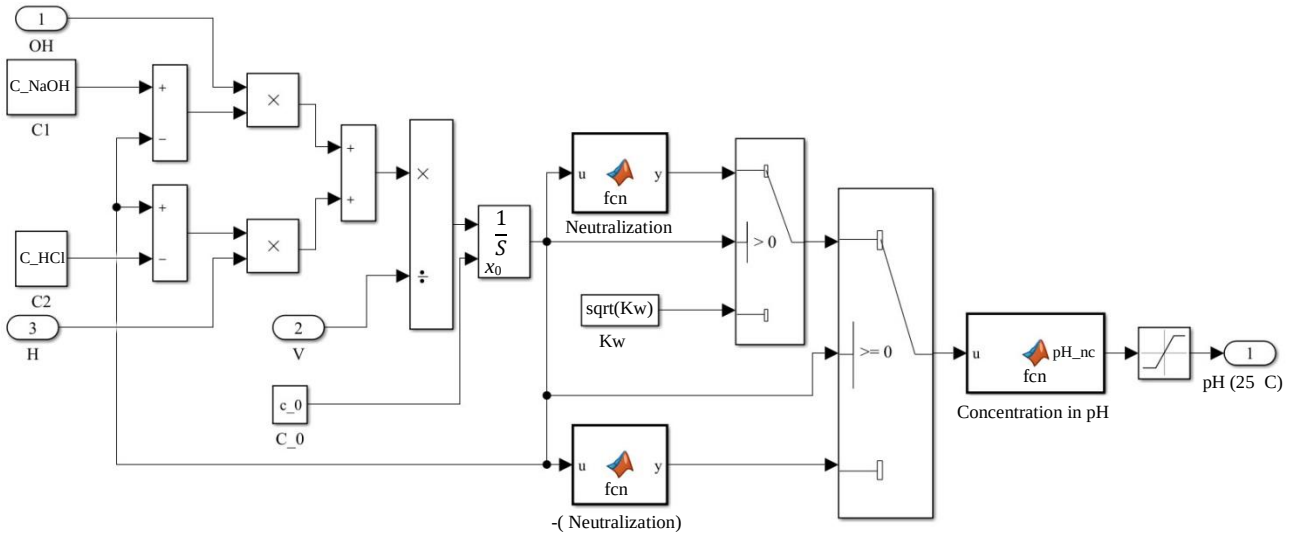


Fig. 6. Structure of the model describing the neutralization reaction

The fourth block enables to take into account the temperature changes of the solution with the function of the statistical model in the “Temperature correction” block.

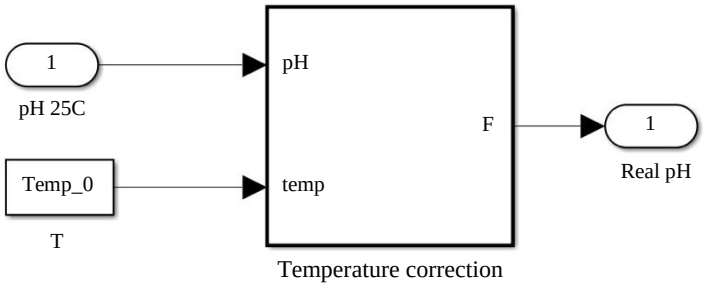


Fig. 7. Structure of the model describing the change in acidity from temperature, block “Static model of pH adjustment from solution temperature”

To determine the adequacy of the transient characteristics of the resulting mathematical model, experiments were conducted on a simulation model. The real model is represented by an automated control system for the artificial gastrointestinal tract of poultry with one control unit and a bioreactor. Figure 8 shows the experimental equipment and its description.

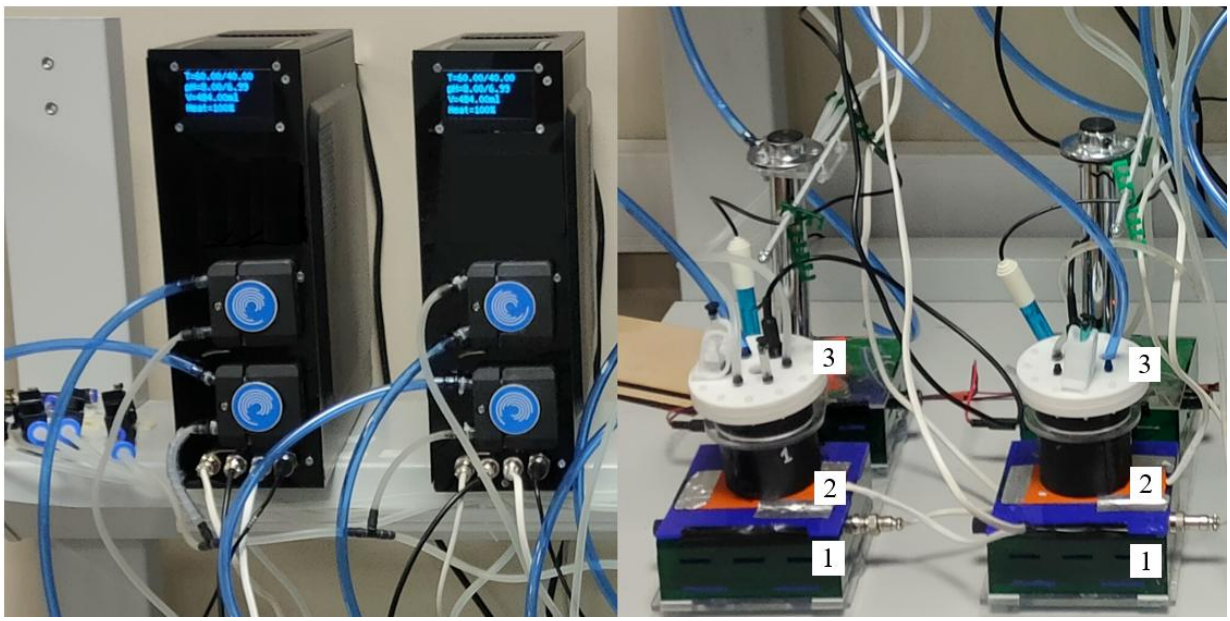


*a*) *b*)

Fig. 8. Research equipment and its description:
*a* — bioreactor environment control units; *b* — elements of bioreactor. 1 — controlled agitators; 2 — heaters; 3 — ports with sensors and a system for topping/draining solutions

The methodology of the experiment is as follows. The mathematical model takes into account the characteristics of a real system, such as:

– set acidity;
– reactor parameters (base area and height of the bioreactor);
– concentrations of added substances (acids and alkalis);
– initial concentration of the solution;
– initial volume of the solution;
– the temperature of the solution throughout the experiment;
– discreteness of the control process [14].

The mathematical model is an ideal system in which mixing of solutions in the reactor occurs instantly and uniformly. In real conditions, this is impossible, therefore, forced mixing is needed for the uniform dissolution of the added acid or alkali. In the simulation model, this problem is solved by a magnetic stirrer controlled via a SCADA system.

Unfortunately, this type of mixing device induces electromagnetic interference on the pH electrode. To eliminate interference, the mixing device was switched off for a short time, and the discreteness of measurements and the operation of the regulator was 20 seconds, which is due to the experimentally established time of normalization of the pH readings of the electrode in the reactor (according to the documentation of the electrode, sampling can reach 1-2 minutes).[6,7] The regulator of the real system is limited in the maximum volume of the dosed acid or alkali in order to ensure safety, which was taken into account in the model regulator.

**Experimental Results.** Figure 10 shows a comparison of the transition process of a mathematical model and a real control system. The pH electrode is a sensitive element that is susceptible to receiving external electromagnetic interference.

One of the experiments was carried out at a given acidity of the solution in the range of 2.15 ± 0.05 pH. The acidity of the initial solution was 6.2 pH. The temperature of the solution in the reactor: 22.25 °C. Solutions of 0.1 mol/liter NaOH and 0.1 mol/liter HCl were used to change the acidity. The dosing algorithm consisted in discrete proportional regulation.

[6] ph-4502c pH meter calibration notes. URL: https://tlfong01.blog/2019/04/26/ph-4502c-ph-meter-calibration-notes/ (accessed: 30.11.2022).
[7] EZO™ pH Circuit Datasheet. URL:https://files.atlas-scientific.com/pH_EZO_Datasheet.pdf (accessed: 30.11.2022).

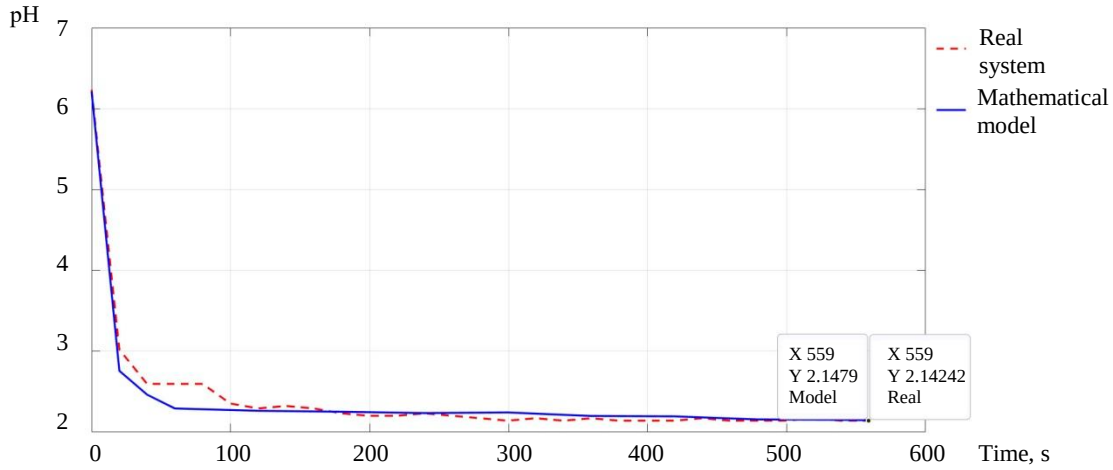


Fig. 8. Transient characteristics of a mathematical model and a real system when regulating from 6.2 to 2.15 pH

Figure 11 shows the flow integrals from differential equation (7).

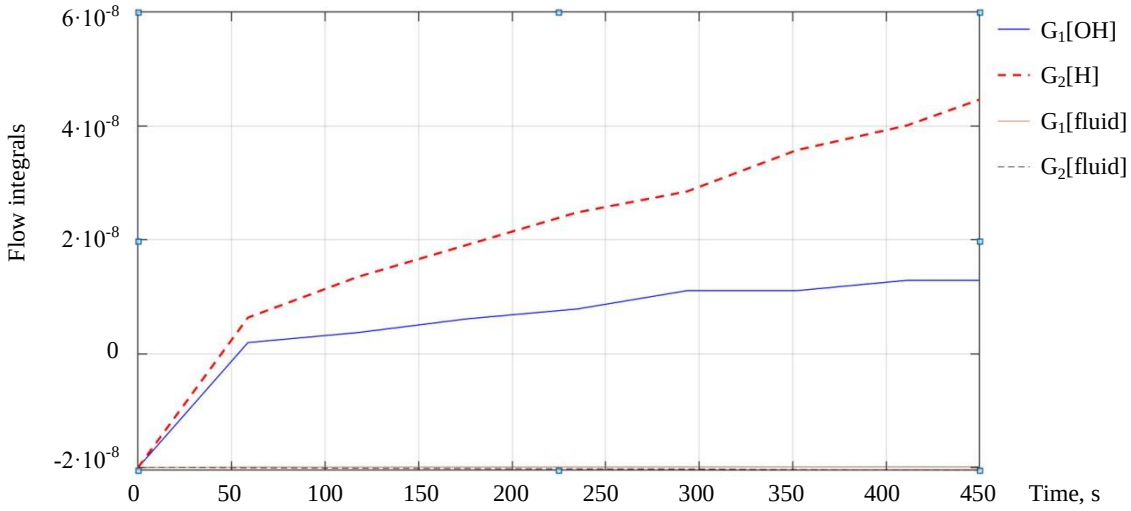


Fig. 9. The effect of each flow on the neutralization reaction during experiments

**Discussion and Conclusions**. Analysis of the simulation results have shown that flows with a solution concentration in the reactor do not make a significant contribution to the regulation of the entire system, therefore, they can be neglected for simplification. Then the system of differential equations of the digital model (8) will take the following form:

$$\begin{cases} \dfrac{dh}{dt} = \dfrac{1}{S}\left(G_1 + G_2 - G_3\right), \\ \dfrac{dC}{dt} = \dfrac{1}{S \cdot h}\left(G_1 \cdot C_{NaOH} - G_2 \cdot C_{HCl}\right). \end{cases} \quad (13)$$

According to the results of the experiments, taking into account the concentration of the solution in the reactor, the relative error of the steady-state acidity of the solution for the mathematical model was 0.1 %, and for a real system with the same algorithm 0.35 %.

Thus, taking into account the error of the electrode readings and the neglect of the mixing process of solutions in the mathematical model, the absolute error of the control results is within acceptable limits and does not exceed ± 0.1 pH of the set value. This means that the developed mathematical model adequately describes the neutralization reaction curve, and in the future, it will allow choosing optimal control algorithms, which would be a laborious process on a real system.

The developed model solves the problem and is a mathematical tool for the development of methods and algorithms for pH regulation, taking into account the temperature of the contents of the mini-reactor, the initial concentration of the main solution and the concentrations of top-up solutions, which will improve existing control algorithms.

**References**

1. Verhoeckx K, Cotter P, Lopez-Exposito I, et al. (eds.) *The Impact of Food Bioactives on Health. In Vitro and Ex Vivo Models.* Cham, Heidelberg, New York, Dordrecht, London: Springer Open; 2015. 342 p. URL: https://www.ncbi.nlm.nih.gov/books/NBK500148/ (accessed: 28.09.2022).

2. Alegría A, Garcia-Llatas G, Cilla A. Static Digestion Models: General Introduction. In book: *The Impact of Food Bioactives on Health. In Vitro and Ex Vivo Models.* Cham, Heidelberg, New York, Dordrecht, London: Springer Open; 2015. P. 3–12. URL: https://link.springer.com/chapter/10.1007/978-3-319-16104-4_1 (accessed: 28.09.2022).

3. Dupont D, Alric M, Blanquet-Diot S, et al. Can Dynamic *In Vitro* Digestion Systems Mimic the Physiological Reality? *Critical Reviews in Food Science and Nutrition*. 2019;59:1546–1562. URL: https://doi.org/10.1080/10408398.2017.1421900 (accessed: 28.09.2022).

4. Steinway SN, Saleh J, Bon-Kyoung Koo, et al. Human Microphysiological Models of Intestinal Tissue and Gut Microbiome. *Frontiers in Bioengineering and Biotechnology.* 2020;8:725. URL: https://www.frontiersin.org/articles/10.3389/fbioe.2020.00725 (accessed: 28.09.2022).

5. Venema K. The TNO In Vitro Model of the Colon (TIM-2). In book: *The Impact of Food Bioactives on Health. In Vitro and Ex Vivo Models.* Cham, Heidelberg, New York, Dordrecht, London: Springer Open; 2015. P. 293–304. URL: https://link.springer.com/chapter/10.1007/978-3-319-16104-4_26 (accessed: 28.09.2022).

6. Mandalari G, Chessa S, Bisignano C, et al. The Effect of Sundried Raisins (Vitis vinifera L.) on the In Vitro Composition of the Gut Microbiota. *Food & Function.* 2016;7:4048–4060. URL: http://dx.doi.org/10.1039/C6FO01137C (accessed: 28.09.2022).

7. Ferrua M, Singh R. Human Gastric Simulator (Riddet Model). In book: *The Impact of Food Bioactives on Health. In Vitro and Ex Vivo Models*. Cham, Heidelberg, New York, Dordrecht, London: Springer Open; 2015. P. 61–71. 10.1007/978-3-319-16104-4_7

8. Ménard O, Picque D, Dupont D. The DIDGI®system. In book: *The Impact of Food Bioactives on Health. In Vitro and Ex Vivo Models.* Cham, Heidelberg, New York, Dordrecht, London: Springer Open; 2015. P. 73–81. 10.1007/978-3-319-16104-4_8

9. Barroso E, Cueva C, Peláez C, et al. The Computer-Controlled Multicompartmental Dynamic Model of the Gastrointestinal System SIMGI. In book: *The Impact of Food Bioactives on Health. In Vitro and Ex Vivo Models.* Cham, Heidelberg, New York, Dordrecht, London: Springer Open; 2015. P. 319–327. 10.1007/978-3-319-16104-4_28

10. Van de Wiele T, Van den Abbeele P, Ossieur W, et al. The Simulator of the Human Intestinal Microbial Ecosystem (SHIME®). In book: *The Impact of Food Bioactives on Health. In Vitro and Ex Vivo Models.* Cham, Heidelberg, New York, Dordrecht, London: Springer Open; 2015. P. 305–317. https://doi.org/10.1007/978-3-319-16104-4_27

11. González C, González D, Zúñiga RN, et al. Simulation of Human Small Intestinal Digestion of Starch Using an In Vitro System Based on a Dialysis Membrane Process. Foods. 2020;9(7):913. https://doi.org/10.3390/foods9070913

12. Donskoy D, Katin O, Alekseenko L. Development and Implementation of the GIT-Modelling Bioreactor System: The Way to Reducing a Carbon Footprint. *E3S Web of Conferences.* 2021;279:01030. https://doi.org/10.1051/e3sconf/202127901030

13. Asuero AG, Michałowski T. Comprehensive Formulation of Titration Curves for Complex AcidBase Systems and Its Analytical Implications. *Critical Reviews in Analytical Chemistry.* 2011;41:151–187. 10.1080/10408347.2011.559440

14. Garcia C, Juliani R. Modelling and Simulation of pH Neutralization Plant Including the Process Instrumentation. In book: Michalowski T (ed.). *Applications of MATLAB in Science and Engineering.* 2011. P. 485–510. http://dx.doi.org/10.5772/1534

15. Egger L, Ménard O, Abbühl L, et al. Higher Microbial Diversity in Raw than in Pasteurized Milk Raclette-Type Cheese Enhances Peptide and Metabolite Diversity after *In Vitro* Digestion. *Food Chemistry*. 2021;340:128154. https://doi.org/10.1016/j.foodchem.2020.128154

16. Chistyakov VA, Lukyanov AD, Donskoy DYu, et al. Modeling and Analysis of Energy Efficiency of Methods for Maintaining Temperature Conditions in Microbioreactors. *IOP Conference Series: Materials Science and Engineering.* 2020;900:012015. 10.1088/1757-899X/900/1/012015

*About the Authors:*

**Danila Yu Donskoy,** postgraduate of the Production Automation Department, Don State Technical University (1, Gagarin sq., Rostov-on-Don, 344000, RF), ScopusID, ORCID, dand22@bk.ru

**Alexandr D Lukyanov,** Head of the Production Automation Department, Don State Technical University (1, Gagarin sq., Rostov-on-Don, 344000, RF), Cand.Sci. (Eng.), associate professor, ScopusID, ORCID, lex1998@rambler.ru

**Vladimir Filipović,** senior research fellow, faculty of Technology, University of Novi Sad (1, Bul. cara Lazara, Novi Sad, 21000, Serbia), ScopusID, ORCID

**Tamara B Asten,** professor of the World Languages and Cultures Department, Don State Technical University (1, Gagarin sq., Rostov-on-Don, 344000, RF), Dr.Sci. (Philology), ORCID, tamara@mail.ru

*Claimed contributorship:*

DYu Donskoy: basic concept formulation; research objectives and tasks; calculation analysis; conducting experiments; preparing text; forming conclusions. AD Lukyanov: academic advising; correction of the mathematical model; analysis of research results; text editing; correction of conclusions. V Filipović: academic advising; correction of the mathematical model. TB Asten: editing and partial translation of the text.

**Received** 09.01.2023.
**Revised** 01.02.2023.
**Accepted** 02.02.2023.

*Conflict of interest statement*
The authors do not have any conflict of interest.

*All authors have read and approved the final manuscript.*

*Об авторах:*
**Данила Юрьевич Донской,** ассистент кафедры «Автоматизация производственных процессов» Донского государственного технического университета (344003, РФ, г. Ростов-на-Дону, пл. Гагарина, 1), ScopusID, ORCID, dand22@bk.ru

**Александр Дмитриевич Лукьянов,** заведующий кафедрой «Автоматизация производственных процессов» Донского государственного технического университета (344003, РФ, г. Ростов-на-Дону, пл. Гагарина, 1), кандидат технических наук, доцент, ScopusID, ORCID, lex1998@rambler.ru

**Владимир Филипович,** доктор кафедры «Химическая инженерия» Университета Нови-Сада (21000, Республика Сербия, г. Нови-Сад, бул. Цара Лазара, 1), ScopusID, ORCID

**Тамара Борисовна Астен,** профессор кафедры «Мировые языки и культуры» Донского государственного технического университета (344003, РФ, г. Ростов-на-Дону, пл. Гагарина, 1), доктор филологических наук, ORCID, tamara@mail.ru.

*Заявленный вклад соавторов*
Д. Ю. Донской — формирование основной концепции, цели и задач исследования, расчеты, проведение экспериментов, подготовка текста, формулирование выводов. А. Д. Лукьянов — научное руководство, корректировка математической модели, анализ результатов исследований, редактирование текста, корректировка выводов. В. Филипович — научное руководство, корректировка математической модели. Т. Б. Астен — редактирование и частичный перевод текста.

**Поступила в редакцию** 09.01.2023.
**Поступила после рецензирования** 01.02.2023.
**Принята к публикации** 02.02.2023.

*Конфликт интересов*
Авторы заявляют об отсутствии конфликта интересов.

*Все авторы прочитали и одобрили окончательный вариант рукописи.*